Nuclear Localization of α-Synuclein and its Interaction with Histones

Doctoral thesis

to obtain a doctorate (PhD)

from the Faculty of Medicine

of the University of Bonn

Angela Rollar

from Bad Kreuznach, Germany

2026

Written with authorization of
the Faculty of Medicine of the University of Bonn

First reviewer: Priv. Doz. Dr. Dan Ehninger

Second reviewer: Prof. Dr. Harald Neumann

Day of oral examination: 24.04.2026

From the German Center of Neurodegenerative Disease

Table of contents

List of abbreviations

AAV	adeno-associated virus
ABC	avidin-biotin complex
AMC	7-amino-4-methylcoumarin
ANOVA	analysis of variance
αS^{TRE}-AAV	AAV encoding αSyn under the TRE-promoter
αSyn	alpha-synuclein
αSyn-AAV	AAV encoding αSyn
ATP13A2	ATPase cation transporting 13A2
BCA	bicinchoninic acid
BRCA1	breast cancer 1 gene
BSA	bovine serum albumin
°C	degrees Celcius
Ca^{2+} /CAMKII	Ca^{2+} /calmodulin-dependent protein kinase II
CHCHD2	coiled-coil-helix-coiled-coil-helix domain containing 2
Co-IP	Co-Immunoprecipitation
CTCF	corrected total cell fluorescence
DAB	3, 3'-diaminobenzidine
DAPI	4′,6-diamidino-2-phenylindole
DJ1	Parkinson disease protein 7
DLB	dementia with Lewy bodies
DMnX	dorsal motor nucleus of the vagus nerve
DNA	deoxyribonucleic acid
DNMT1	DNA methyltransferase 1
DTT	dithiothreitol
EDTA	ethylenediaminetetraacetic acid
ER	endoplasmatic reticulum
ERK	extracellular-signal-regulated kinase
FACS	fluorescence-activated cell sorting
GBA	glucocerebrosidase
GC	guanine cytosine

gc / ml	genomic copies per mililiter
GDNF	glial cell line-derived neurotrophic factor
GFP	green fluorescent protein
GFP-AAV	AAV encoding GFP
GWAS	genome-wide association study
h	hour(s)
HDAC	histone deacetyltransferase
IF	immunofluorescence
IHC	immunohistochemistry
IP	immunoprecipitation
ITR	inverted terminal repeat
KAT	lysine acetyltransferases
KTKEGV	lysine-threonine-lysine-glutamic acid-glycine-valine
LB	Lewy body
LRRK2	leucine-rich repeat kinase 2
LSM	laser-scanning microscope
M	molar (mol/L)
mM	milimolar
µl	microliter
µm	micrometer
MAPK	mitogen-activated protein kinase
MES	2-(N-morpholino)ethanesulfonic acid
MG-132	N-benzyloxycarbonyl-L-leucyl-L-leucyl-L-leucinal
min	minute(s)
MPTP	1-methyl-4-phenyl-1,2,3,6-tetrahydropyridine
MRI	magnetic resonance imaging
MSA	multiple systems atrophy
n	number of biological replicates
NAC	non-amyloid-β component of Alzheimer's disease amyloid
nm	nanometer
NLS	nuclear localization signal
NOTCH1	gene encoding neurogenic locus notch homolog protein 1

NRS	normal rabbit serum
6-OHDA	6-hydroxydopamine
PRKN	E3 ubiquitin protein ligase parkin
pA	polyadenylation signal sequence
PBS	phosphate-buffered saline
PCR	polymerase chain reaction
PD	Pakinson's disease
PFA	paraformaldehyde
PFF	preformed fibril
PGC-1α	Pparg coactivator 1 alpha
pH	potential hydrogen
PINK	gene encoding PTEN-induced putative kinase 1
PLA	proximity-ligation assay
PQ	paraquat
RAS	rat sarcoma virus proteins
RNA	ribonucleic acid
ROS	reactive oxygen species
rtTA	reverse tetracycline transactivator
SDS	sodium dodecyl sulfate
SEM	standard error of the mean
SN	substantia nigra
SNARE	soluble N-ethylmaleimide-sensitive factor attachment protein receptors
SNCA	gene encoding α-synuclein
SNpc	substantia nigra pars compacta
SUMO	small ubiquitin-like modifier
TBS	tris-buffered saline
TH	tyrosine hydroxylase
TRE	tetracycline response element
TRIM28	tripartite motif-containing 28
UPS	ubiquitin-proteasome system
VPS35	vacuolar protein sorting ortholog 35

x	times
x g	times the force of gravity
w / v	weight per volume
WB	western blot
WPRE	woodchuck hepatitis virus post-transcriptional regulatory element

1. Introduction

1.1 Parkinson's disease

Parkinson's disease (PD) is a progressive neurodegenerative disorder with a significant global burden, affecting more than 10 million individuals worldwide as of 2021 (Luo et al. 2024). First described by James Parkinson in his monograph "*An essay on the shaking palsy*" in 1817 (Parkinson 2002), PD is now recognized as a multifaceted disorder characterized by a wide range of motor and non-motor symptoms. The primary motor symptoms defining PD include tremor, rigidity, bradykinesia, shuffling gait, and postural instability (Lang and Lozano 1998; Bloem et al. 2021). These symptoms are primarily attributed to the progressive degeneration of dopaminergic neurons in the substantia nigra pars compacta (SNpc), resulting in dopamine depletion within nigrostriatal projections and striatal terminals and ultimately disrupting basal ganglia circuity involved in movement regulation (Poewe et al. 2017; Kalia and Lang 2015; Panicker et al. 2021). Besides the loss of nigral dopaminergic neurons, the second pathological hallmark of PD is the formation of α-Synuclein (αSyn) aggregates in the form of intraneuronal inclusions called Lewy bodies (LBs) and Lewy neurites (Dickson et al. 2009). In addition to motor symptoms, clinical manifestations of PD include a variety of non-motor symptoms, such as disturbances in the sleep-wake cycle, cognitive decline, mood disorders, autonomic dysfunction, sensory abnormalities, and pain. It is conceivable that some of these non-motor abnormalities may be a consequence of the progressive accumulation of Lewy inclusions (Pellicano et al. 2007; Jellinger 2011; Adler and Beach 2016). Notably, some non-motor symptoms may precede motor manifestations by over a decade, providing a potential opportunity to use their appearance for early (pre-motor abnormalities) diagnosis and early protective intervention (Chaudhuri and Schapira 2009; Savica et al. 2010).

Currently, there is no treatment capable of halting or slowing the progression of PD. Therapeutic strategies primarily focus on symptomatic management aimed at addressing, in particular, the dopamine deficiency due to neuronal loss in the SNpc. Pharmacological treatments, such as levodopa preparations, monoamine oxidase-B inhibitors, and dopamine agonists, seek to restore dopaminergic signaling (Fox et al. 2018; Livingston and Monroe-Duprey 2024). While effective at early disease stages, these treatments often lead to complications such as dyskinesias and wearing-off phenomenon after prolonged

use (Armstrong and Okun 2020). Advanced device-aided therapeutic options, including deep brain stimulation, MRI-guided focused ultrasound lesioning, and enteral dopaminergic suspension systems, offer partial solutions for managing refractory motor fluctuations; however, they are invasive and do not address the non-motor symptoms (Bloem et al. 2021; Zhang et al. 2022). As the disease progresses, both motor and non-motor impairments worsen, profoundly diminishing patients' quality of life (Poewe et al. 2017; Hinnell et al. 2012).

Epidemiologically, PD is the fastest-growing neurological disorder globally, with its prevalence having more than tripled between 1990 and 2021 (Luo et al. 2024). This trend is expected to accelerate, primarily because PD is an age-related disorder (it is quite rare before the age of 60-65), and increased life expectancy in future years will likely increase aging populations (Dorsey et al. 2018; Deliz et al. 2024). These projections emphasize the urgency of advancing our understanding of the mechanisms underlying neurodegeneration and αSyn pathology as well as developing effective new strategies for symptomatic and disease-modifying interventions.

1.2 Causes and modifying factors

PD is considered a multifactorial disorder that, in the vast majority of cases, arises from the interplay between genetic, environmental, and epigenetic influences. Varying modifying factors are thought to collectively contribute to disease onset, progression, and clinical manifestation.

1.2.1 Genetic factors

Although most cases of PD are sporadic, approximately 5-10 % of PD cases are linked to monogenic mutations (Lesage and Brice 2009; Pitz et al. 2024). Mutations in genes such as *LRRK2*, *CHCHD2*, *VPS35*, and *SNCA* are associated with autosomal dominant PD, whereas mutations in *PRKN*, *DJ1*, and *PINK1* lead to early-onset autosomal recessive form of the disease (Lange et al. 2022; Bandres-Ciga et al. 2020). Variants in *GBA1*, a gene encoding the lysosomal enzyme glucocerebrosidase, represent the most prevalent genetic risk factor, predisposing individuals to early-onset and more severe forms of PD (Ryan et al. 2019; Blauwendraat et al. 2020).

Advances in genome-wide association studies (GWAS) have identified 90 independent genetic variants across 78 loci associated with increased PD susceptibility, underscoring the polygenetic nature of the disorder (Kim et al. 2024; Blauwendraat et al. 2020). However, genetic heritability accounts for only an estimated 16-36 % of disease risk in sporadic PD, highlighting the importance of other non-genetic disease risk factors (Nalls et al. 2019).

1.2.2 Environmental factors

Environmental factors are likely to contribute to PD pathogenesis. The possibility that toxic agents may play a role in the development of nigrostriatal degeneration is strongly supported by the effects of 1-methyl-1,2,3,4-tetrahydropyridine (MPTP), a well-known neurotoxin capable of inducing Parkinsonian syndrome in humans (Langston 2017; Nonnekes et al. 2018). Exposure to other toxic agents, in particular pesticides such as paraquat and rotenone, has long been suspected to increase PD risk based on both epidemiological and experimental evidence (Sherer et al. 2003; Li et al. 2005; Dhillon et al. 2008; Costello et al. 2009; Tanner et al. 2011). Chronic exposure to air pollutants and certain industrial by-products, such as solvents, may further increase disease risk (Murata et al. 2022; Goldman et al. 2024). Additionally, traumatic brain injury, anxiety, depression, and beta-blocker usage have also been proposed as PD risk factors, although further investigations are needed to strengthen these associations (Ascherio and Schwarzschild 2016; Bellou et al. 2016; Grotewold and Albin 2024). Finally, it is noteworthy that environmental variables may not only contribute to PD by promoting its pathology and enhancing disease risk but could also act as protective factors. Perhaps the clearest example of this protective effect is the consistently observed negative association between smoking and PD risk, as demonstrated in epidemiological and experimental studies (Shahi et al. 1991; Ritz et al. 2007; Li et al. 2015). Other suggested protective factors that may reduce PD risk, based on both epidemiological and experimental evidence, include caffeine consumption, anti-inflammatory drug use, uric acid levels, and physical activity (Ascherio and Schwarzschild 2016; Bellou et al. 2016; Grotewold and Albin 2024).

1.2.3 Epigenetic factors

The role of epigenetic changes in PD pathogenesis represents a relatively new and highly relevant area of investigation (Pavlou and Outeiro 2017; Song et al. 2023). Epigenetic mechanisms, including DNA methylation, histone modifications, and microRNA regulation, modulate gene expression by altering chromatin structure and accessibility of the transcriptional machinery without changing the underlying DNA sequence; they could thereby link, for example, environmental factors to genetic predisposition (Li 2021). The importance of epigenetic factors in PD is highlighted by the observation that most of the GWAS-identified risk variants are located in non-coding, regulatory genomic regions (Maurano et al. 2012). Furthermore, the relatively low concordance rate for PD among monozygotic twins (approximately 17 %) suggests an important role for epigenetic variations in disease susceptibility and progression (Goldman et al. 2019). Environmental factors, including diet, stress, and physical activity, can induce lasting epigenetic modifications and, through these effects, contribute to disease pathogenesis. In summary, increasing evidence points to a complex interplay between genetic, epigenetic, and environmental factors that affects disease susceptibility and initiates pathological processes underlying the onset and progression of PD (Cavalli and Heard 2019; Schaffner and Kobor 2022; Klokkaris and Migdalska-Richards 2024).

1.3 Pathophysiology of PD

PD is characterized by two defining neuropathological features: the progressive degeneration of dopaminergic neurons in the SNpc and the increasingly widespread accumulation of LB pathology throughout the brain. Although neither feature is exclusive to PD, their co-occurrence provides a definite diagnosis of idiopathic PD (Dickson et al. 2009; Halliday et al. 2011).

1.3.1 Neuronal vulnerability of dopaminergic neurons

Motor symptoms of PD typically emerge after a critical threshold of pathological and neurochemical changes are reached: a loss of approximately 50 % of dopaminergic neurons in the SNpc and a depletion of 70-80 % of striatal dopamine (Whone et al. 2003). Dopaminergic neurons in the SNpc exhibit a unique susceptibility to PD neurodegenerative processes (Halliday et al. 2005; Mosharov et al. 2009). This unique

vulnerability may not only be explained by the observation that nigral dopaminergic neurons are sites of Lewy inclusion accumulation; in fact, these inclusions are widespread throughout the Parkinsonian brain and also affect neuronal populations relatively resistant to neurodegenerative processes (Wakabayashi and Takahashi 1997; Sulzer and Surmeier 2013). Several intrinsic factors are thought to predispose nigral neurons to PD-induced demise. First, neurons in the SNpc have highly branched axons with numerous synaptic terminals, imposing high bioenergetic demands and causing higher susceptibility to metabolic stress (Pissadaki and Bolam 2013). Second, they exhibit autonomous pacemaking activity, which results in sustained cytosolic calcium influx, exacerbating mitochondrial stress and promoting excitotoxicity (Surmeier et al. 2011). Third, dopamine metabolism within nigral neurons generates reactive oxygen species (ROS) and toxic quinones capable of inducing oxidative damage (Burbulla et al. 2017). Finally, mitochondrial dysfunction and increased oxidative stress can deplete lysosomes and impair lysosomal autophagic activity, thus compromising the clearance of misfolded proteins and damaged organelles (Xilouri et al. 2016).

1.3.2 Lewy body pathology

Lewy bodies (LB), first described by Friedrich Lewy (1912) and later linked to PD nigral pathology by Tretiakoff (1919), are cytoplasmic inclusions characteristic of PD and other neurodegenerative diseases, such as dementia with Lewy bodies (DLB) and multiple system atrophy (MSA). These structures primarily consist of misfolded and aggregated αSyn (Spillantini et al. 1997). Beyond αSyn, LBs comprise a heterogeneous mixture of lipids, membrane fragments, and other neuronal proteins, including ubiquitin, neurofilament proteins, tau, and proteins related to mitochondrial and autophagic processes (Forno and Norville 1976; Shahmoradian et al. 2019). LB pathology exhibits a predictable spatial and temporal progression, initially affecting specific brainstem and olfactory regions before advancing to other brain areas (Braak et al. 2003). This propagation is thought to occur through intraneuronal αSyn transfer, and for this reason, the spreading of LB pathology progressively affects anatomically interconnected brain regions. LB formation is prominent within the dopaminergic neurons of the SNpc; it also involves, however, other populations of neurons using various neurotransmitter transmissions, including serotonergic, glutamatergic, and cholinergic cells, possibly

explaining the broad spectrum of non-motor symptoms observed in PD (Qamhawi et al. 2015; Liu et al. 2019; Braak et al. 2005).

1.4 The Alpha-Synuclein protein

The central role of αSyn in PD pathogenesis became evident following the discovery of single-point mutations and multiplications that cause familial forms of PD (Polymeropoulos et al. 1997; Krüger et al. 1998; Singleton et al. 2003; Chartier-Harlin et al. 2004; Zarranz et al. 2004; Lesage et al. 2013; Pasanen et al. 2014). Another key discovery that αSyn is a major component of LBs (Spillantini et al. 1997) underscored the fact that changes in αSyn are not only causative factors in genetic forms of Parkinsonism but are also critically involved in pathological processes underlying the onset and progression of sporadic (i.e., non-genetic) PD.

1.4.1 Structure of αSyn

αSyn, a 15 kDa protein encoded by the *SNCA* gene, belongs to the Synuclein family of proteins, which also includes β- and γ-Synucleins. Despite the structural similarities between α-, β-, and γ-Synucleins, only αSyn is strongly associated with neurodegenerative diseases (Maroteaux and Scheller 1991). In its native state, αSyn is intrinsically disordered but adopts an α-helical conformation upon binding to lipid membranes (Davidson et al. 1998; Weinreb et al. 1996; Eliezer et al. 2001). The protein features α-helices and a highly unstructured, acidic C-terminal tail. The N-terminal domain, which is positively charged due to the KTKEGV motif, facilitates lipid binding and the formation of α-helical structures (Davidson et al. 1998; Eliezer et al. 2001). Another α-helix contains the non-amyloid component (NAC), a hydrophobic region critical for αSyn aggregation and LB formation (Giasson et al. 2001). The C-terminus of αSyn, largely unstructured and highly acidic (Davidson et al. 1998; Ulmer et al. 2005), is susceptible to post-translational modifications (Oueslati et al. 2010). This region plays an important role in interactions with proteins, metal ions, and other ligands (Nielsen et al. 2001; Brown 2007; Liu et al. 2021), stabilizes membrane associations (Sevcsik et al. 2011), and may modulate αSyn aggregation (Hoyer et al. 2004).

1.4.2 Aggregation of αSyn

Under physiological conditions, αSyn is a soluble, intrinsically disordered protein. However, αSyn is also characterized by its tendency to acquire β-sheet-rich conformations that promote aggregation and could ultimately generate insoluble amyloid-like aggregates. The process of αSyn aggregation bears relevant pathophysiological implications since it may compromise cellular function and play a role in neuronal demise (Tuttle et al. 2016). The amyloidogenic aggregation of αSyn follows a nucleation-dependent process that can be represented by a sigmoidal curve comprising three distinct phases: lag, elongation, and plateau (Gillam and MacPhee 2013). During the lag phase, αSyn monomers interact to form oligomers and protofibrils - intermediate species that exhibit significant cytotoxicity and prion-like intercellular transmissibility (Winner et al. 2011). These structures act as nucleation sites for further aggregation. The elongation phase is characterized by rapid, exponential growth of fibrils as monomers attach to these nuclei. This phase may also involve secondary processes such as fibril fragmentation and seeding, which can amplify the aggregation process by creating additional nucleation sites (Villar-Piqué, Lopes da Fonseca and Outeiro 2016).

Large aggregates and fibrils have been considered the primary drivers of neurodegenerative processes. However, abundant and increasing experimental evidence underscores the toxic potential of smaller αSyn oligomers, which appear particularly harmful to cellular homeostasis (Alam et al. 2019; Ingelsson 2016). For instance, overexpression of oligomer-inducing αSyn mutants has been shown to be more toxic than overexpression of αSyn variants that promote fibril formation (Winner et al. 2011). Furthermore, antibodies specifically targeting oligomers have demonstrated protective effects against αSyn-induced toxicity (Lindström et al. 2014). αSyn oligomers have been implicated in various pathogenic effects, including disruption of cytoskeletal structures, permeabilization of membranes (plasma membrane, mitochondrial membranes, endoplasmic reticulum (ER), and vesicle membranes), increased Ca^{2+} influx, enhanced ROS production, and synaptotoxicity characterized by reduced neuronal excitability and diminished synaptic firing (Danzer et al. 2007; Parihar et al. 2009; Colla et al. 2012; Choi et al. 2013; Volles and Lansbury 2002). Additionally, these oligomers could impair the two major cellular protein degradation pathways: the autophagy-lysosomal system and the ubiquitin-proteasomal system (Lindersson et al. 2004; Tanik et al. 2013).

1.4.3 Cell-to-cell propagation of αSyn

Although the precise mechanisms underlying αSyn-associated pathology are not fully understood, cell-to-cell transmission of αSyn may play a role in the propagation of pathology from neuron to neuron and from one brain region to another.

Cells can secrete misfolded and aggregated αSyn via exocytosis, occasionally involving exosomes or other extracellular vesicles; they may also directly release αSyn into the surrounding environment upon cell death (Lee et al. 2005; Jang et al. 2010; Emmanouilidou et al. 2010; Alvarez-Erviti et al. 2011). As supported by the Braak staging of Lewy pathology (Braak et al. 2003; Braak et al. 2005), spreading of this pathology over long distances might be facilitated by axonal transport. Braak and colleagues were among the first to propose that αSyn could be taken up and released at the level of axonal terminals, suggesting a mechanism of transsynaptic cell-to-cell transfer followed by both antero- and retrograde transport of αSyn along axons (Jensen et al. 1999; Braak et al. 2003; Utton et al. 2005; Danzer et al. 2011). Neighboring cells may internalize extracellular αSyn through specific receptor-mediated or bulk endocytosis (Sung et al. 2001; Lee et al. 2008; Grozdanov and Danzer 2018). Misfolded or aggregated αSyn could also enter neurons directly by disrupting their plasma membrane (Lee et al. 2008; Ahn et al. 2006). Finally, experimental evidence supports tunneling nanotubes as structures that could facilitate the transfer of various αSyn species (including aggregated species) between two cells (Abounit et al. 2016; Dieriks et al. 2017; Scheiblich et al. 2024).

Interneuronal αSyn transfer has been hypothesized as the mechanism underlying the development of Lewy-like inclusions in PD patients who received embryonic nigral graft transplantation (Li et al. 2008; Kordower et al. 2008). Similar inclusion formation observed in experimental animals suggests direct host-to-graft αSyn transmission, potentially replicating findings in transplanted PD patients (Desplats et al. 2009). Various *in-vivo* models have been developed to investigate αSyn interneuronal transfer and brain spreading. For example, brain propagation of αSyn pathology has been successfully reproduced in rodents through injections of brain homogenate-derived or recombinant pre-formed αSyn fibrils (PFFs) into specific brain regions (e.g., striatum or SNpc) or peripheral tissues (Luk et al. 2012; Recasens et al. 2014; Peelaerts et al. 2015; Abdelmotilib et al. 2017; Karampetsou et al. 2017; Duffy et al. 2018). The primary

pathological effects observed from these PFF injections include a progressive accumulation of intraneuronal αSyn inclusions throughout the brain, a pathology attributed to a prion-like mechanism of protein seeding and propagation (Peelaerts et al. 2015; Chung et al. 2019).

1.4.4 Other in-vivo models of αSyn pathology

Several models have been developed, characterized, and used to study αSyn aggregation, transmission, and toxicity (Lama et al. 2021). Two models particularly relevant to this project are described in detail below.

1.4.4.1 AAV-mediated αSyn overexpression model

The first model employs adeno-associated viruses (AAVs) to induce overexpression of wild-type or mutant αSyn (Lo Bianco et al. 2002; Kirik, Rosenblad, et al. 2002). AAVs enable targeted protein expression in specific brain regions, including the SNpc or striatum, and facilitate transgene induction in adult animals, thereby avoiding developmental compensation (Van der Perren et al. 2015). Recombinant AAV vectors exhibit high tropism for nigral dopaminergic neurons, achieving over 90 % transduction efficiency in tyrosine hydroxylase (TH)-positive neurons (Kirik, Rosenblad, et al. 2002; Maingay et al. 2006; Ulusoy et al. 2010). AAV-mediated αSyn overexpression in the SNpc results in progressive dopaminergic neurodegeneration and reduced striatal dopaminergic projections within several weeks. This neuronal loss occurs more gradually compared to conventional toxin models, with the extent varying based on virus titer, serotype, age, sex, strain, and animal species (Klein et al. 2002; Van der Perren et al. 2011; M Decressac et al. 2012; McFarland et al. 2009; Ulusoy et al. 2010). AAV overexpression models have also been instrumental in studying αSyn long-distance transmission from the medulla oblongata to more rostral brain regions (e.g., pons, mid-, and forebrain). Such transfer and spreading can be triggered by targeted overexpression in the medullary vagal system (Ulusoy et al. 2013; Helwig et al. 2016).

The expression of AAV-delivered genes can be fine-tuned using inducible synthetic promoters that permit switching gene expression on or off (Domenger and Grimm 2019). The tetracycline (Tet)-dependent system is the most commonly used inducer/repressor method, allowing precise control over gene expression both *in-vitro* and *in-vivo* (Das et al.

2016; Gossen and Bujard 1992). In the TetOn system, gene expression remains inactive until activated by doxycycline, while the TetOff system operates oppositely, being active by default and suppressed upon doxycycline addition. Both systems have been successfully implemented in animal models using AAVs (de Solis et al. 2016; Le Guiner et al. 2014; Pichard et al. 2012; Sohn et al. 2017; Ali Hosseini Rad et al. 2020).

1.4.4.2 Toxin-based models

The second approach utilizes neurotoxins such as 6-hydroxydopamine (6-OHDA), MPTP, paraquat, and rotenone to replicate PD pathology. These compounds preferentially accumulate in the dopaminergic neurons of the SNpc, inducing mitochondrial dysfunction, oxidative stress, and, ultimately, neuronal death (Ungerstedt et al. 1974; Heikkila et al. 1984; Betarbet et al. 2000; Corasaniti et al. 1992). However, a limitation of these models is the acute neurotoxicity they produce, which contrasts markedly with the progressive neurodegenerative course observed in human PD (Khan et al. 2023). The unilateral 6-OHDA model has been extensively used as a preclinical tool for evaluating pharmacological interventions (Jiang et al. 1993; Kirik, Georgievska, et al. 2002; Ilijic et al. 2011). MPTP-based models have provided insights into environmental toxicity contributions to sporadic PD and mitochondrial dysfunctions implicated in disease pathogenesis (Fox and Brotchie 2010). Paraquat exposure represents a particularly relevant model for our investigations, as it has been demonstrated to elevate endogenous αSyn levels in both the cytosolic and nuclear neuronal compartments while simultaneously promoting αSyn aggregation (Manning-Bog et al. 2002; Goers et al. 2003; Uversky et al. 2001).

1.4.5 Localization and function of αSyn

αSyn is highly expressed throughout the brain and primarily localized at the level of presynaptic terminals (Iwai et al. 1995; Shibayama-Imazu et al. 1993). Our understanding of the physiological roles of αSyn within neurons is still incomplete. However, presynaptic αSyn is central to synaptic vesicle trafficking and neurotransmitter release; it facilitates the assembly of neuronal N-ethylmaleimide-sensitive factor attachment protein receptor (SNARE) complex, thereby aiding in the maintenance of synaptic plasticity (Burré et al. 2010). Additionally, αSyn enhances endocytosis (Varkey et al. 2010; Ben Gedalya et al.

2009) and may act as a neuroprotective chaperone, preserving the function of the SNARE complex (Chandra et al. 2003).

Its primary localization at presynaptic terminals does not exclude the possibility that αSyn may be present in other cellular compartments where it may also play important pathophysiological roles. These additional localizations may include mitochondria (Devi et al. 2008; Chinta et al. 2010), ER (Oaks et al. 2013; Colla et al. 2012), Golgi apparatus/lysosomes (Volpicelli-Daley et al. 2014; Mazzulli et al. 2016), and the nucleus (Maroteaux and Scheller 1991; Specht et al. 2005; Koss et al. 2022).

Together, these findings suggest that our understanding of αSyn localization and function is still evolving; indeed, αSyn appears to play a more dynamic role in regulating intracellular processes than previously recognized. Particularly relevant is its potential localization within the nucleus, which hints at the possible involvement of nuclear αSyn in gene expression and/or epigenetic regulation.

1.5 αSyn in the nucleus

When αSyn was first discovered by Maroteaux et al. (1988) in the electric organ of *Torpedo California*, the focus was primarily on identifying proteins involved in presynaptic function. Surprisingly, the researchers also noted αSyn immunoreactivity localized to a portion of the nuclear envelope, leading them to propose a dual role for αSyn in both presynapses and nuclei - a hypothesis reflected in the protein's blended name "synuclein". Despite this initial observation, convincing confirmation of αSyn nuclear localization did not emerge for several years (George et al. 1995; Iwai et al. 1995; Jakes et al. 1994). Results of initial reports showing αSyn nuclear localization were questioned due to lack of antibody specificity and/or cross-reactivity of αSyn antibodies with non-αSyn nuclear antigens. For example, the 3D5 αSyn antibody clone produced strong immunohistochemical signals in the nuclei of rat and mouse tissue, which were later shown to be non-specific in αSyn knock-out mice (Iwai et al. 1995; Yu et al. 2007; Zhang et al. 2008; Huang et al. 2011; Vivacqua et al. 2011).

In recent years, a growing body of evidence from αSyn pathology models has consistently demonstrated nuclear localization of the protein. Several *in-vitro* studies using various cell models transiently transfected with αSyn or overexpressing αSyn reported its presence in the nucleus (McLean et al. 2000; Kontopoulos et al. 2006; Schneider et al.

2007; Gonçalves and Outeiro 2013; Fares et al. 2014). Findings in organotypic rat hippocampal slice cultures expressing αSyn-eGFP fusion protein further supported αSyn nuclear presence, emphasizing the critical role of the C-terminal domain of αSyn in facilitating its nuclear localization (Specht et al. 2005). *In-vivo*, transgenic mice overexpressing human αSyn revealed nuclear αSyn accumulation through electron microscopy (Masliah et al. 2000). Various stressors, including 6-OHDA and iron, have also been shown to promote αSyn nuclear translocation of αSyn (Sangchot et al. 2002; Monti et al. 2007); similarly, neurotoxins, such as paraquat, rotenone, and MPTP, induce nuclear accumulation of αSyn within rodent nigral neurons (Goers et al. 2003; Monti et al. 2010; Vila et al. 2000).

Nuclear αSyn accumulation is increasingly recognized as a feature of neurodegenerative diseases characterized by αSyn pathology, underscoring its potential pathogenic relevance. In patients with MSA, αSyn-positive inclusions composed of tightly packed straight filaments were identified within neuronal and oligodendroglial nuclei (Lin et al. 2004; Nishie et al. 2004). In human post-stroke brains, nuclear translocation of αSyn was observed following transient focal ischemia (Kim et al. 2016). More recently, Koss et al. (2022) described the presence of nuclear αSyn in post-mortem brains of DLB patients. Their results revealed oligomerization and post-translational modifications of nuclear αSyn; in particular, phosphorylated αSyn levels were 14-fold higher in the nuclear fraction of brain homogenates from DLB patients compared to age-matched controls (Koss et al. 2022).

1.5.1 Translocation of αSyn to the nucleus

The precise mechanisms by which αSyn translocates into the nucleus remain elusive. Given its small size, αSyn is capable of passing through nuclear pores without the need for transport carriers (Timney et al. 2016). Alternatively, several active mechanisms have been proposed to regulate αSyn nuclear translocation, including its interaction with TRIM28 or RAS-related nuclear protein (Rousseaux et al. 2016; Chen et al. 2020). Additionally, it has been shown that αSyn can bind to retinoid acid and subsequently be translocated into the nucleus through a calreticulin-dependent mechanism (Davidi et al. 2020). Although αSyn does not have a canonical nuclear localization signal (NLS), importin α has been suggested to aid αSyn nuclear import (Ma, Song, Yuan, Zhang, Han,

et al. 2014). Post-translational modifications of αSyn, such as phosphorylation and SUMOylation, have been proposed to influence its nuclear translocation (Schaser et al. 2019; Pinho et al. 2019; Schell et al. 2009; Ryu et al. 2019). Finally, it is noteworthy that αSyn nuclear localization may have particular functional relevance during embryonic development. This conclusion is supported by the observation that αSyn is equally distributed between nucleus and cytoplasm at embryonic stages before its translocation to neuronal terminals during neuronal differentiation (Zhong et al. 2010; Pinho et al. 2019; Pieger et al. 2022).

1.5.2 Toxic effects of nuclear αSyn localization

Nuclear translocation of αSyn during or following pathological processes may play a role in cellular dysfunction and demise. Nuclear αSyn has been reported to exert toxic effects by interfering with cell cycle regulation (Lee et al. 2003; Liu et al. 2011; Ma, Song, Yuan, Zhang, Han, et al. 2014), modulating RNA metabolism (Chung et al. 2017; Popova et al. 2021), disrupting nucleocytoplasmic transport (Chen et al. 2020), and impairing nuclear envelope integrity (Tagliafierro et al. 2019; Jiang et al. 2016; Pinho et al. 2019; Chen et al. 2020). Early *in-vitro* studies have shown that αSyn binds to DNA and disrupts its integrity (Hegde and Rao 2007; Padmaraju et al. 2011; Cherny et al. 2004; Dent et al. 2022). Consistent with these findings, nuclear αSyn has also been shown to bind chromatin and induce oxidative DNA breaks *in-vitro* (Vasquez et al. 2017). The *in-vivo* relevance of these findings is underscored by a study in which DNA damage and activation of the DNA damage response were observed in dopaminergic neurons in rodent models of αSyn pathology (Milanese et al. 2018).

While the majority of studies support the toxic potential of nuclear αSyn, a few investigations suggest that nuclear translocation of αSyn may also result in protective effects; for example, it may contribute to the repair of double-stranded DNA breaks (Schaser et al. 2019; Pinho et al. 2019).

1.5.3 Transcriptional dysregulation caused by nuclear αSyn

An important mechanism by which nuclear αSyn may affect cellular pathophysiology is through the regulation of gene expression. Various studies have demonstrated significant changes in gene expression in PD patients (Grünblatt et al. 2004; Pinho et al. 2016) and

experimental models of αSyn pathology, including cellular systems (Ding et al. 2013; Pinho et al. 2019; Paiva et al. 2017) and transgenic animals (Soreq et al. 2012; Miller et al. 2007; Yacoubian et al. 2008; Paiva et al. 2018; Du et al. 2024). These effects may result from a variety of mechanisms, some of which could be triggered by αSyn nuclear translocation and subsequent transcriptional dysregulation. αSyn-induced transcriptional dysregulation may arise from direct interactions with DNA, engagement of nuclear receptors, modulation of immediate gene pathways, and/or epigenetic mechanisms (see below).

αSyn has been shown to bind directly to DNA, with a preference for GC-box-like sequences, thereby altering its conformation and contributing to transcriptional dysregulation (Vasudevaraju et al. 2012; Ma, Song, Yuan, Zhang, Yang, et al. 2014; Pinho et al. 2019). Notably, αSyn nuclear translocation was found to be paralleled by enhanced chromatin binding in both experimental models of oxidative stress and PD brain tissue (Siddiqui et al. 2012). αSyn has also been shown to bind to the promoter region of PGC-1α, a key modulator of mitochondrial homeostasis that is typically dysregulated in PD (Eschbach et al. 2015; Siddiqui et al. 2012), as well as in proximity to the *NOTCH1* promoter, which is critical for neuronal development and differentiation (Desplats et al. 2012).

αSyn is also implicated in regulating gene transcription by interacting with nuclear proteins, including retinoid acid receptors, peroxisome proliferator-activated receptor-γ, Nurr1, and *BRCA1*-associated protein 1. Interestingly, these interactions modulate the expression of genes associated with PD (Yakunin et al. 2014; Davidi et al. 2020; Lin et al. 2012; Mickael Decressac et al. 2012; Sharma et al. 2024). Furthermore, multiple studies indicate that αSyn may be involved in at least two signaling pathways that regulate the expression of early genes: MAPK/ERK and Ca^{2+}/CAMKII-mediated transcriptional control (Hashimoto et al. 2003; Shi et al. 2018; Martinez et al. 2003; Iwata et al. 2001; Chung et al. 2019; Somayaji et al. 2021).

Epigenetic regulation involves RNA-mediated mechanisms, such as non-coding RNAs, DNA methylation, and specific modifications of histones. In PD models and patients, downregulation of several microRNAs targeting *SNCA* has been observed, resulting in the accumulation and aggregation of αSyn (Junn et al. 2009; Doxakis 2010; Zhang and Cheng 2014; Kabaria et al. 2015; Li et al. 2020; Lang et al. 2022). DNA

methylation is another mechanism by which αSyn may participate in epigenetic regulation (Song et al. 2023). The expression of human *SNCA* is dependent on the methylation of intron 1. A significant reduction in this methylation, particularly within CpG-rich promoter regions, has been observed in the SNpc of PD patients, potentially leading to increased expression of αSyn (Jowaed et al. 2010; Matsumoto et al. 2010; Miranda-Morales et al. 2017; Bakhit et al. 2022). This altered methylation pattern may result from the ability of αSyn to sequester DNA methyltransferase 1 (DNMT1) from the nucleus to the cytosol, thereby inhibiting normal DNA methylation (Desplats et al. 2011).

1.5.3.1 Interaction of αSyn with histones

Histones are proteins critically involved in the packaging and organization of nuclear DNA. They serve as spools around which DNA winds, forming structures called nucleosomes that facilitate the arrangement of DNA within the nucleus while also playing a role in gene regulation. A nucleosome comprises two copies of core histones, namely H2A, H2B, H3, and H4, while H1 aids in linking nucleosomes into higher-order structures (Luger et al. 2012; Park et al. 2022).

The association between αSyn and histones was first reported when αSyn was found to accumulate in the nuclei and co-localize with histone H3 within SNpc neurons in the brains of paraquat-treated mice (Goers et al. 2003). *In-vitro*, αSyn was shown to form stable complexes with histones, suggesting a potential mechanism by which αSyn may diminish the availability of histones for DNA binding, thereby altering gene transcription (Goers et al. 2003). Another important finding arising from *in-vitro* experiments was that the binding of αSyn to histones not only affected histone complexes but also accelerated αSyn fibrillation (Goers et al. 2003). The pathophysiological relevance of this observation remains to be further explored since, for example, nuclear aggregation of αSyn has yet to be investigated in the *in-vivo* setting. Subsequent research has confirmed the interaction of nuclear αSyn with histone H3 both *in-vitro* and in *Drosophila* (Kontopoulos et al. 2006). More recently, it has been demonstrated that αSyn binds to the N-terminal flexible tails of H3, H4, and H1 (Jos et al. 2021). Other investigations have also suggested that histones may act as nuclear pro-aggregant factors for αSyn in neurons with compromised nuclear membrane integrity, leading to the rapid formation of αSyn aggregates (Jiang et al. 2017; Jiang et al. 2021).

Chromatin accessibility is influenced by various post-translational modifications of histone tails, including acetylation, dopaminylation, methylation, phosphorylation, serotonylation, SUMOylation, and ubiquitination (Farrelly et al. 2019; Lepack et al. 2020; Nitsch et al. 2021). These modifications alter the surface charge of histones, thereby modulating chromatin conformation and DNA accessibility for transcription factors and other transcription-related proteins (Park et al. 2022). Histone acetylation is typically associated with gene activation, whereas removal of the acetyl mark leads to a more closed chromatin structure. Notably, the tightly regulated balance between the activities of lysine acetyltransferases (KAT) and histone deacetyltransferases (HDAC) can be disrupted in PD and PD models (Jin et al. 2011; Mazzocchi et al. 2019; Lee et al. 2021). Several studies have investigated αSyn-induced changes in histone acetylation, yielding somewhat inconsistent results, with some reporting αSyn-induced reductions while others show αSyn-associated increases in histone acetylation (Kontopoulos et al. 2006; Liu et al. 2011; Paiva et al. 2017). Most likely, these conflicting findings reflect the complex nature of αSyn's role in epigenetic regulation; this role could vary, for example, under different pathophysiological conditions and may be affected by αSyn levels and genetic variations. Histone methylation can be linked to transcriptional repression and activation, depending on the specific residues that methylation affects (Di Nisio et al. 2021). Distinctly altered histone marks, including the methylation of H3K36 and H3K9, have been identified in models of αSyn overexpression, both *in-vitro* and in *Drosophila*. In these studies, the transcriptional dysregulation resulting from this altered histone methylation was linked to disrupted SNARE complex assembly and synaptic vesicle fusion (Sugeno et al. 2016; Chen et al. 2018).

1.5.4 Open questions around nuclear αSyn

A careful review of our current understanding of αSyn nuclear localization highlights the pathophysiological relevance of this translocation and reveals important gaps in knowledge that warrant further investigation. A critical issue in studies of αSyn nuclear localization is the need for new methodological approaches that allow for the detection of nuclear αSyn and facilitate investigations into αSyn-histone interactions. As previously mentioned, this need partly arises from the questionable specificity and sensitivity of αSyn antibodies, which may, for instance, cross-react with non-specific nuclear antigens.

Among currently open questions concerning nuclear αSyn localization, a fundamental one relates to the conditions and mechanisms underlying αSyn translocation. In particular, whether a direct relationship exists between increases in cytosolic levels and the transfer of αSyn into the nuclear compartment remains unclear, especially in the *in-vivo* setting. Answers to these questions bear important pathophysiological implications since elevations in cytosolic αSyn levels are associated with conditions (e.g., toxicant exposure) that may promote or predispose individuals to PD pathogenesis.

Once αSyn is accumulated in the nuclear compartment, direct evidence of αSyn-histone interactions and αSyn-induced histone modifications is lacking in *in-vivo* models of PD-like pathology. Furthermore, it remains unclear whether accumulation and "crowding" of αSyn within neuronal nuclei lead to protein aggregation that may contribute to the long-term toxic effects of αSyn nuclear translocation. For instance, due to its aggregation, αSyn may become "trapped" in the nucleus, potentially causing sustained histone alterations. Another unexplored issue regarding nuclear αSyn localization concerns again the relationship between cytosolic and nuclear αSyn levels. If αSyn gains access to the nucleus as a consequence of increased cytosolic levels, what happens if and when cytosolic αSyn returns to basal, low levels? Does nuclear αSyn reverse at a similar rate and over a comparable time frame? Or does it persist longer in the nucleus, possibly due to changes resulting from interactions with histones and/or protein aggregation? An important corollary to these questions relates to the mechanisms involved in αSyn clearance. Very little is understood about these mechanisms in the context of neuronal nuclear αSyn accumulation and their role during protein translocation into and out of the nuclear compartment. It can be hypothesized, for example, that specific clearance mechanisms may be responsible for or contribute to the reversibility of nuclear localization after changes in cytosolic αSyn levels.

1.6 Aims

This project addresses these aforementioned important questions and gaps in current knowledge regarding αSyn nuclear localization. Investigating nuclear αSyn is likely to have relevant implications for our overall understanding of the pathogenic processes underlying the development of PD. As discussed above, αSyn plays a central role in PD development, and changes in αSyn pathophysiology are thought to trigger, contribute to, or predispose individuals to PD-related pathological processes. These processes may be promoted by well-recognized changes in αSyn molecular properties, such as enhanced aggregation propensity and increased interneuronal mobility. They could also arise, however, from less-studied cellular events including nuclear translocation.

This project encompasses the following five principal aims:

(i) To investigate the relationship between αSyn accumulation and nuclear translocation using both AAV-mediated and paraquat-induced αSyn overexpression models.

(ii) To examine the interaction between αSyn and histones *in-vivo* through the development and optimization of a novel proximity ligation assay (PLA).

(iii) To evaluate potential epigenetic alterations resulting from nuclear αSyn-histone interactions, with a specific focus on histone modifications.

(iv) To explore αSyn aggregation within the neuronal nucleus *in-vivo*.

(v) To determine the stability or reversibility of nuclear αSyn accumulation and αSyn-histone interactions following cytosolic αSyn clearance, utilizing a doxycycline-inducible AAV-mediated TetOn system.

2. Material and Methods

2.1 Viral vectors

All recombinant AAVs used in this study were generated using a backbone plasmid derived from an AAV2 genome encapsulated in an AAV6 capsid. Transgene expression of human wild-type αSyn (αSyn-AAV), enhanced green fluorescent protein (GFP-AAV), tetracycline transactivator (TetOn-AAV), and the control empty AAV (Null-AAV) is regulated by the human Synapsin1 promoter. Meanwhile, the tetracycline-inducible transgene expressions of αS^{TRE}-AAV and GFP^{TRE}-AAV are controlled by the tetracycline-responsive element (TRE). Gene expression was enhanced using a woodchuck hepatitis virus posttranscriptional regulatory element (WPRE) along with a polyadenylation signal sequence (pA) downstream of the promoter and transgene sequences. Production and titration of the AAVs were conducted by Vector Biolabs (αS^{TRE}-, and TetOn-AAVs) and Sirion Biotech (αSyn-, GFP-, Null-AAVs). Quantitative PCR targeting WPRE was used to determine the stock titer, and high-titer stock AAV preparations were diluted with phosphate-buffered saline (PBS; pH 7.4; 140 mM NaCl, 7.5 mM NaH_2PO_4, 2.5 mM Na_2HPO_4; 3 mM KCl; Merck) (Tab. 1).

Tab. 1: List of AAVs and injected AAV titers

Viral vector	Final titers
αSyn-AAV	1e12 gc/ml 5e11 gc/ml 2.5e11 gc/ml
GFP-AAV	5e11 gc/ml
Null-AAV	5e11 gc/ml
αS^{TRE}-AAV	1.125e13 gc/ml
TetOn-AAV	3.75e12 gc/ml

2.2 Animals

Animal experiments received approval from the State Agency for Nature, Environment, and Consumer Protection in North Rhine-Westphalia, Germany. Experiments were

conducted on female Sprague Dawley rats aged 9 and 11 weeks, as well as wild-type C57BL/6J mice aged 18 to 21 weeks (Janvier). Animals were housed in individually ventilated cages within a specific pathogen-free facility. They were maintained on a 12-h light/dark cycle with ad libitum access to food and water.

2.3 Surgical procedure

During stereotaxic surgeries, rats were anesthetized with 2 % isoflurane (Vetflurane, Virbac) mixed with O_2 and N_2O, and received a subcutaneous injection of the analgesic buprenorphine (0.05 mg/kg; Bupresol, CP-Pharma) diluted in 0.9 % saline (B. Braun). To induce transgene expression in the SNpc, a solution containing either a single AAV preparation or multiple AAVs (1 µl) was injected intraparenchymally into the right ventral mesencephalon, immediately dorsal to the SNpc. The following coordinates were used on a standard U-frame stereotactic instrument (Harvard Apparatus) with a tooth bar setting of −2.5: 5.0 mm posterior, 2.0 mm lateral to bregma, and 7.2 mm ventral to the dura mater. Injections were performed at a rate of 0.2 µl/min using a Microliter syringe (5 µl, removable needle; Hamilton) fitted with a glass capillary. The capillary was left in place for 5 min to prevent backflow before being withdrawn. Post-surgery treatment included administering tramadol hydrochloride in drinking water (0.5 mg/kg; Aliud Pharma) for 3 days following surgery.

2.4 Drug treatment

To initiate transgene expression of αSyn or GFP, animals were treated with various concentrations of doxycycline hydrochloride (doxycycline; Santa Cruz Biotechnology) in their drinking water. Doxycycline-containing water was freshly prepared and replaced every 3 to 4 days. In pilot experiments, animals received different doses of doxycycline (0.5 mg/ml, 1 mg/ml, and 1.5 mg/ml). Subsequently, the 0.5 mg/ml concentration was maintained for the remainder of the experiments. During treatment, animals were regularly monitored for drinking volume, body weight, and general welfare.

Paraquat dichloride hydrate (Paraquat; Sigma-Aldrich) was dissolved in 0.9 % saline and administered intraperitoneally in two doses of 20 mg/kg, with a one-week‘s interval between the doses. Animals injected with 0.9 % saline served as controls. Mice were regularly monitored for body weight and general welfare.

2.5 Tissue preparation

Animals were sacrificed via an intraperitoneal injection of sodium pentobarbital (600mg/kg; Release, WDT). For histological analyses, rats were perfused through the ascending aorta with saline, followed by ice-cold 4 % (w/v) paraformaldehyde (PFA; Roth) in 0.2 M phosphate buffer (pH 7.4; 78 mM NaH_2PO_4, 122 mM Na_2HPO_4; Roth). Brains were removed, immersion-fixed in 4 % PFA for 24 h, and cryopreserved in 25 % (w/v) sucrose (Roth) dissolved in 0.2 M phosphate buffer (pH 7.4). Subsequent analyses were carried out on 40 µm coronal sections of the brain obtained using a freezing microtome. Sections were stored at -20 °C in 0.2 M phosphate buffer (pH 7.4) containing 30 % glycerol (Roth) and 30 % ethylene glycol (Roth). For analyses requiring nonfixed tissue, such as co-immunoprecipitation (Co-IP) and proteasome activity assays, brains were dissected, snap-frozen on dry ice, and stored at –80 °C until use.

2.6 Immunohistochemical and immunofluorescent staining procedure

A summary of primary antibodies, their sources, and working dilutions is presented in Table 2. All immunohistochemical and immunofluorescent stainings were performed on free-floating sections in glass vials. Brain sections were rinsed with Tris-buffered saline (TBS; pH 7.6; 20 mM Tris, 150 mM NaCl; Roth).

2.6.1 Immunohistochemical staining

For immunohistochemical staining, endogenous peroxidase activity was quenched by incubating the sections in a mixture of 3 % H_2O_2 (Sigma-Aldrich) and 10 % methanol (Roth) in TBS. Non-specific binding sites were blocked by incubation in TBS with 0.25 % Triton-X-100 (TBS-T; Roth) containing 5% normal serum (Jackson ImmunoResearch). Samples were then incubated overnight at room temperature in a primary antibody solution containing 1 % bovine serum albumin (BSA; Sigma-Aldrich) in TBS-T. After rinsing, samples were incubated in an appropriate biotinylated secondary antibody solution (1:200; Vector Laboratories) for 1 h at room temperature, followed by treatment with avidin-biotin-peroxidase complex (ABC Elite kit, Vector Laboratories). The color reaction was developed using the 3,3′-diaminobenzidine kit (Vector Laboratories).

Sections were mounted on coated slides, dried, optionally stained with cresyl violet (FD Neurotechnologies), and coverslipped with Depex (Merck).

2.6.2 Immunofluorescent staining

Tissue samples underwent antigen retrieval in 10 mM sodium citrate buffer (pH 6.0; 8.3 mM $C_6H_5Na_3O_7$, 1.7 mM $C_6H_8O_7$; Sigma-Aldrich) containing 0.05 % Tween 20 (Roth) at 95 °C for 10 min. Following retrieval, samples were subjected to the blocking procedure described previously. For single-antibody detection, tissue sections were incubated with primary antibodies overnight at 4 °C (Tab. 2). Subsequently, sections were incubated with goat anti-mouse secondary antibodies conjugated with Alexa Fluor 488 (1:300; Jackson Immunoresearch) for 2 h at room temperature. Nuclei were visualized by counterstaining with DAPI (1:10,000; Biotium).

For double immunolabeling with TH, midbrain sections were incubated simultaneously with directly conjugated αSyn and TH primary antibodies overnight at 4 °C (Tab. 2). For striatal sections, a sequential staining approach was employed, beginning with overnight incubation with TH primary antibody followed by detection using goat anti-rabbit Alexa Fluor 647-conjugated secondary antibodies (1:300; Jackson Immunoresearch). To minimize cross-reactivity between multiple rabbit-derived antibodies, sections were treated with normal rabbit serum (NRS) for 1 h at room temperature before undergoing an additional overnight incubation with directly labeled αSyn primary antibody.

For quadruple immunofluorescence labeling, samples were processed using a sequential labeling approach. First, for detection of H3K27 acetylation or trimethylation, sections were incubated with respective primary antibodies (Tab. 2), followed by donkey anti-rabbit Fab fragment (1:200, Jackson Immunoresearch), and goat anti-donkey Alexa Fluor 594 (1:300; Jackson Immunoresearch). Second, TH and total H3 were labeled with respective primary antibodies (Tab. 2) and visualized using goat anti-mouse Alexa Fluor 647- and goat anti-rabbit Alexa Flour 405-conjugated secondary antibodies (1:300; Jackson Immunoresearch). Third, human αSyn was detected through overnight incubation with directly labeled αSyn primary antibody (Tab. 2).

Following all immunolabeling procedures, samples were mounted onto coated slides and coverslipped with Vectaschield Hardset medium (Vector Laboratories).

Tab. 2: List of primary antibodies
This table presents all primary antibodies and their respective dilutions used in immunohistochemistry (IHC), immunofluorescence (IF), proximity ligation assay (PLA), and co-immunoprecipitation (Co-IP). For immunofluorescence applications, antibody dilutions were specifically adjusted based on the experimental context, including quadruple staining protocols (quad) or the specific brain region analyzed, such as midbrain sections containing the substantia nigra (SN) or striatal sections (striatum).

Target	Antibody	Host	Supplier/ Catalog	Applica-tion	Concen-tration
α-Synuclein (human-specific)	monoclonal MJFR1	rabbit	abcam ab138501	IHC IF	1:30,000 1:1,000
α-Synuclein (human-specific)	monoclonal MJFR1 - conjugated to Alexa Fluor 488	rabbit	abcam ab195025	IF-SN IF-striatum IF-quad	1:2,000 1:500 1:400
α-Synuclein (human-specific)	monoclonal Syn211	mouse	Merck 36-008	IF PLA	1:1,000 1:20,000
α-Synuclein (total)	monoclonal Syn-1 42/α-synuclein	mouse	BD Biosciences 610787	IHC IF	1:10,000 1:1,000
aggregated α-Synuclein	monoclonal SynO2	mouse	Creative Biolabs TAB-0748CLV	IHC IF PLA	1:20,000 1:10,000 1:10,000
aggregated α-Synuclein	monoclonal 5G4	mouse	Merck MABN389	IHC IF PLA	1:20,000 1:10,000 1:10,000
H3K27 acetylation	polyclonal	rabbit	abcam ab4729	IF-quad	1:1,000
H3K27 trimethylation	polyclonal	rabbit	Merck 07-449	IF-quad	1:100
histone H3	monoclonal EPR16987	rabbit	abcam ab176842	PLA	1:10,000
histone H3	polyclonal	rabbit	abcam Ab21054	IF-quad	1:500
tyrosine hydroxylase	polyclonal	rabbit	Merck Ab152	IHC IF-striatum	1:2,000 1:200

tyrosine hydroxylase	monoclonal LNC1	mouse	Merck MAB318	IF-quad	1:300
tyrosine hydroxylase	monoclonal LNC1-conjugated to Alexa Fluor 555	mouse	Merck MAB318-Ab555	IF	1:1,000

2.7 Stereology

The total number of TH-positive neurons was estimated using an unbiased stereological quantification method based on the optical fractionator principle (Stereo Investigator, version 9, MBF Bioscience) as described by Ulusoy et al. (2010). The SNpc was delineated at low magnification in every 6th section throughout the region. Neuronal counting was performed using a 63 x Plan-Apochromat oil objective on an Olympus IX2 UCB microscope equipped with an MBF Mac6000 System stage (Microbrightfield) and a high-precision encoder. The coefficient of error was calculated according to Gundersen and Jensen (1987), and values were < 0.10.

2.8 *In-situ* proximity ligation assay

Free-floating sections containing the SNpc were processed using Duolink *In-Situ* Proximity Ligation Assay (PLA; Merck) following the manufacturer's protocols. Aggregated αSyn and interaction between H3 and endogenous αSyn were detected using a previously described "direct" PLA method (Roberts et al. 2015). This method involved overnight incubation of sections in solutions (supplied in kit) containing PLA probes directly conjugated to a human-specific αSyn antibody (1:120, clone Syn211, Merck).

For "indirect" PLAs, sections were incubated overnight in a solution containing two primary antibodies and subsequently with secondary antibodies conjugated with oligonucleotide probes (anti-rabbit PLUS and anti-mouse MINUS, provided in kit). After ligation and amplification, specific PLA signals were visualized using a bright-field or fluorescence detection kit (Duolink, Merck). Sections were mounted on coated slides. For brightfield imaging, samples were optionally stained with hematoxylin and coverslipped with Histomount (ThermoFisher). For fluorescent microscopy, sections were co-stained with DAPI if necessary and coverslipped with Prolong Gold Antifade (ThermoFisher).

Negative controls were included and underwent the same procedures, except that one of the primary or secondary antibodies was omitted to validate specificity.

2.9 Cytoplasmic and nuclear fractionation

The SNpc-containing ventral midbrain was dissected from αSyn-AAV-injected rats using a brain matrix (Stoelting) approximately 4 to 7 mm posterior to bregma. Protein content in the nuclear and cytoplasmic fractions was quantified using a bicinchoninic acid (BCA) assay (Pierce Biotechnology).

2.9.1 Fractionation for Co-Immunoprecipitation

Nuclear extracts for Co-Immunoprecipitation (Co-IP) were prepared using a specialized Nuclear Complex Co-IP kit (Active Motif) to enhance the recovery of intact nuclear protein complexes. Tissue samples were homogenized with a Dounce homogenizer (Wheaton) in a hypotonic lysis buffer (provided in the kit) supplemented with phosphatase inhibitors, 1 mM dithiothreitol (DTT; ThermoFisher), and detergent (supplied in the kit). After a 15-min incubation on ice to ensure complete homogenization, samples were centrifuged to pellet cells (850 x g, 10 min, 4 °C). The supernatant was discarded, and the cellular pellets were resuspended in a hypotonic lysis buffer and incubated on ice for an additional 15 min. Cell lysis was completed by adding detergent (provided in the kit) and rigorous vortexing. Lysates were centrifuged (14,000 x g, 5 min, 4 °C) to pellet nuclei. The supernatant containing the cytoplasmic fraction was separated and used as a control. The nuclear pellet was resuspended in a digestion buffer with protease inhibitors (provided in the kit). Samples were then incubated with an enzymatic cocktail (kit component) to shear DNA (10 min, 37 °C). The suspension was centrifuged (14,000 x g, 10 min, 4 °C), and the supernatant containing the nuclear proteins was collected for further processing.

2.9.2 Fractionation for proteasome activity assay

For the proteasome activity assay, dissected samples were washed in ice-cold PBS. Cell lysis and extraction of cytosolic and nuclear protein fractions were performed using the NE-PER kit (ThermoFisher). Briefly, samples were mechanically homogenized using a Dounce homogenizer. A hypotonic lysis buffer containing detergent (kit component) was added to disrupt cellular membranes and release cytoplasmic contents. The supernatant,

representing the cytoplasmic fraction, was collected following centrifugation (16,000 x g, 5 min, 4 °C). Nuclear proteins were extracted from the remaining cell pellet by incubating it with a nuclear extraction reagent (supplied in the kit), followed by vigorous vortexing and a second centrifugation (16,000 x g, 10 min, 4 °C).

2.10 Co-Immunoprecipitation

Co-IP was conducted using the Nuclear Complex Co-IP kit (Active Motif) following the manufacturer's instructions. Briefly, 100 µg nuclear extracts were diluted in IP buffer (provided in the kit) to 100 µl, precleared with 10 µl pre-blocked ChIP-IT G Magnetic Beads (Active Motif, blocked with 1 % BSA in TBS) (1 h, 4 °C, rotation), and then incubated with αSyn antibody (Syn211; 1:200; Abcam) or H3 antibody (ERP16987; 1:200; Abcam) in incubation buffer (overnight, 4 °C, rotation). Following primary antibody incubation, lysates were incubated with pre-blocked ChIP-IT Protein G Magnetic Beads (1 h, 4 °C, rotation). With the help of a magnetic rack, immune complexes bound to the magnetic beads were washed 4 times with ice-cold IP wash buffer supplemented with 1 mg/ml BSA to remove non-specifically bound proteins. For the final wash, no BSA was added to the IP wash, and IP buffer was supplemented with 0.2 M NaCl to increase wash stringency. After removing the last washing buffer, the bead pellet was eluted by boiling the beads in 50 µl of 2x reducing loading buffer (130 mM Tris-HCl pH 6.8, 4 % SDS, 0.02 % bromophenol blue, 20 % glycerol, 100 mM DTT) at 95 °C for 5 min.

2.11 Western blot

For western blot analysis, boiled samples were loaded onto a pre-cast 4-12 % Bis-Tris polyacrylamide gel (12 wells, ThermoFisher) and subjected to electrophoresis in MES-SDS running buffer (pH 7.3; 50 mM MES, 50 mM Tris, 1 mM EDTA, 0.1 % SDS; Roth) using a XCell SureLock Mini-Cell system (1.5 h, 100 V, ThermoFisher). Following electrophoresis, proteins were transferred onto a methanol-activated polyvinylidene difluoride membrane (0.45 µm, Merck) in Towbin transfer buffer (pH 8.6; 25 mM Tris, 192 mM glycine) using a Mini-Protean Tetra system (400 mA; 90 min; Bio-Rad). Post-transfer, membranes were treated with 0.4 % PFA (30 min) and blocked with 3 % BSA dissolved in TBS-T for 1 h. Membranes were incubated overnight with antibodies against αSyn (Syn211, 1:5000, Abcam) or H3 (ERP16987, 1:5000, Abcam) in a 1 % BSA in TBS-T. After rinsing with TBS-T, samples were incubated with horse radish peroxidase-conjugated goat

anti-mouse (1: 2,500; Bio-Rad) or goat anti-rabbit secondary antibodies, respectively (1:2,500; Bio-Rad). The immunoreactive signal was visualized using an enhanced chemiluminescent substrate (Cytiva) and detected with a ChemiDoc MP imaging system (Bio-Rad).

2.12 Proteasome activity assay

Proteasome activity within the cytosolic and nuclear fractions was assessed using a fluorogenic assay kit (Abcam) according to the manufacturer's instructions. This assay exploits the chymotrypsin-like activity of the proteasome, employing a 7-amino-4-methylcoumarin (AMC)-tagged peptide substrate (provided in kit) that releases highly fluorescent AMC upon cleavage. Nuclear fractions were diluted 20-fold with sample buffer (kit component) and loaded into a 96-well microplate (ThermoFisher) in duplicates. Each sample was tested in the presence and absence of the proteasome inhibitor MG-132 (also known as N-benzyloxycarbonyl-L-leucyl-L-leucyl-L-leucinal). Fluorescent emission (Excitation/Emission = 350/440 nm; gain 1000) was measured at two time points, separated by a 30-min window, at 37 °C using a Fluostar Omega microplate reader (BMG Labtech). Fluorescence readings were corrected for background fluorescence by subtracting the mean absorbance value of the blank wells. Specific proteasome activity was determined by subtracting the fluorescence signal of the MG-132 inhibited samples from the total signal, thereby accounting for non-proteasomal proteolytic activity. The change in fluorescence between the two time points was calculated and applied to the AMC standard curve. The data were then adjusted for dilution, time between measurements, and volume. Final activity measurements were normalized to the protein concentrations of the respective fractions.

2.13 Image acquisition and analysis

Axioscan Z1 Microscope Slide Scanner (Zeiss) with a 20 x Plan-Apochromat objective (Zeiss) was used to take brightfield and fluorescent images of entire sections. Confocal fluorescence images were collected on LSM800 and LSM880 microscopes (Zeiss) equipped with a 40 x or 63 x Plan-Apochromat objective (Zeiss) using the Zen software (Zeiss). Image analysis was conducted with Fiji software (ImageJ; version 2.14; https://imagej.net/software/fiji/).

2.13.1 Quantification of nuclear and cytosolic fluorescence intensities

Confocal fluorescence images were acquired using LSM800 or LSM 880 microscopes equipped with a 40 x Plan-Apochromat objective, operated via Zen Blue software (Zeiss). Full Z-stack images were captured from the dorsal, medial, and ventral regions of the SNpc in 3 consecutive midbrain sections. All imaging parameters, including laser power, exposure time, gain, offset, z-stack interval, and scanning speed, were maintained at constant levels throughout the study. Nuclear and cytosolic compartments were delineated via the freehand tool in Fiji. Neurons within the 5 µm border regions at the top and bottom of the tissue section were excluded from analysis to mitigate potential artifacts from uneven antibody penetration in thick tissue sections. Fluorescence intensity was then quantified for all remaining αSyn- and TH-positive neurons on the injected and TH-positive neurons on the intact hemisphere, with measurements focused on a single focal plane where the nucleus was clearly visible. Background fluorescence was measured in adjacent cell-free areas at the same focal depth for each neuron. Corrected total cell fluorescence (CTCF) was calculated using the following formula: Integrated density – (selected area * mean fluorescence of background readings).

2.13.2 Quantification of striatal fluorescent signal

Epifluorescent images were acquired on Axioscan Z1 Microscope Slide Scanner utilizing a 20 x Plan-Apochromat objective and controlled through Zen Blue software. Z-stack projections of 3 striatum sections per animal were analyzed, with the striatal region delineated in Adobe Photoshop software. Automated quantification was conducted by applying consistent background subtraction across all samples in Fiji. A standardized intensity threshold was then applied to quantify the density of the fluorescent signal within the striatal region. Accumulations of αSyn-positive signal were detected and quantified using Fiji's "Analyze Particles" function. All imaging parameters, including background subtraction, intensity threshold, threshold mode, and brightness, were standardized throughout the study. The area fraction of immuno-positive signal and the number of particles were calculated and averaged per animal.

2.13.3 Histological quantification of PLA signal

Brightfield images for quantifying PLA signal were acquired using Axioscan Z1 Microscope Slide Scanner equipped with a 20 x Plan-Apochromat objective and operated via Zen Blue software. Z-stack projections of 3 consecutive midbrain sections were analyzed, with the SNpc region delineated and selected using Adobe Photoshop software. Automated quantification was performed using consistent background subtraction and color deconvolution for hematoxylin and DAB stains. A constant intensity threshold was employed on the DAB-stained images to detect and quantify PLA-positive structures using the “Analyze Particles” function. All imaging parameters, including background subtraction, intensity threshold, threshold mode, and brightness, were standardized throughout the study. The area fraction of PLA-positive signals was calculated and averaged for each animal.

2.14 Statistical analysis

Statistical analyses were conducted using Prism 10 (GraphPad). A two-way analysis of variances (ANOVA) was employed for datasets involving comparisons across multiple groups, followed by Tukey’s post-hoc test to adjust for multiple comparisons. The non-parametric Mann-Whitney *U* test was applied for pairwise comparisons between two groups. All data is represented with the standard error of the mean (SEM) as error bars. Box and whisker plots show median, upper and lower quartiles and maximum and minimum as whiskers. Statistical significance is set at a threshold of $p < 0.05$ and denoted as $*p < 0.05$, $**p < 0.01$, $***p < 0.001$, and $****p < 0.0001$. The number of biological samples is indicated as n.

3. Results

3.1 Nigral pathology caused by AAV-mediated αSyn overexpression

To develop a model for studying αSyn's nuclear entry, human αSyn-carrying AAVs (αSyn-AAVs) were injected unilaterally into the rat ventral mesencephalon, immediately dorsal to the SNpc. Three experimental groups received AAV titers of 1e12 gc/ml (high titer), 5e11 gc/ml (medium titer), and 2.5e11 gc/ml (low titer) and were sacrificed for analysis at 4 weeks post-injection (Fig. 1A). Nigral αSyn-AAV injection induced robust human αSyn immunoreactivity in the midbrain and in regions anatomically connected to the transduced area, especially the striatum (Figs. 1B and 1C) (Kirik, Rosenblad, et al. 2002; Ulusoy et al. 2017). To determine the optimal AAV titer for subsequent experiments, αSyn expression levels in SNpc neurons and striatal fibers were compared across groups. Immunofluorescent analysis revealed no significant difference in αSyn intensity between low and high titer groups within SNpc neurons (Fig. 1D). Similarly, the area fraction of the αSyn fluorescent signal did not differ between these groups. However, quantitative analysis of striatal sections demonstrated a titer-dependent increase in αSyn-positive fibers in the injected hemisphere (Fig. 1E).

Next, potential pathological effects of αSyn overexpression were investigated. TH-positive neurons were counted in the injected SNpc, revealing a significant titer-dependent loss of 39.16 % and 19.53 % in the high and medium titer groups, respectively. In contrast, only a minor, non-significant decrease in TH-positive cells was observed in the SNpc from rats in the low-titer group (Fig. 1F). αSyn accumulation within presynaptic terminals, a known marker of synaptic dysfunction (Phan et al. 2017; Garcia-Reitböck et al. 2010), was assessed by quantifying fluorescently labeled striatal sections. Accumulation was significantly increased on the injected compared to the contralateral hemisphere in animals treated with medium and high AAV titers, whereas treatment with the low AAV titer did not result in significant differences (Fig. 1G).

Taken together, αSyn overexpression driven by an AAV injection leads to increased αSyn levels within nigrostriatal dopaminergic neurons. While total αSyn levels remained similar across titer groups in the SNpc (where the neuronal cell bodies are localized), higher AAV titers were associated with increased accumulation of αSyn in striatal fibers and terminals. This latter effect was paralleled by more pronounced titer-dependent

pathological changes, including a significant loss of nigrostriatal dopaminergic neurons. Significant, albeit not excessive overexpression and pathology were achieved in rats injected with the medium AAV titer. For this reason, this medium titer was selected and used for most of the experiments carried out as part of this project. On the other hand, when specific experimental questions required a quantitative comparison among different AAV titers, this comparison was made between groups of animals injected with the low versus the high titers.

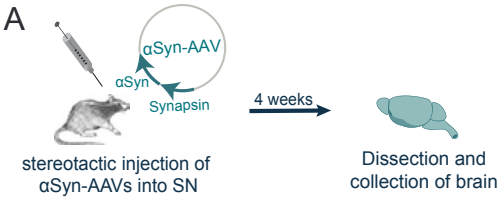
A
αSyn-AAV
αSyn
Synapsin
4 weeks
stereotactic injection of
αSyn-AAVs into SN
Dissection and
collection of brain

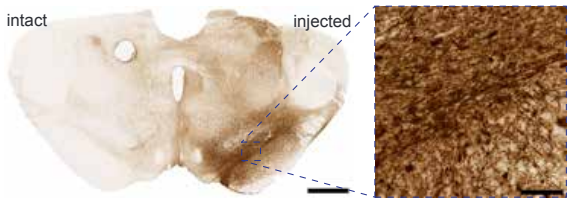
B
intact
injected

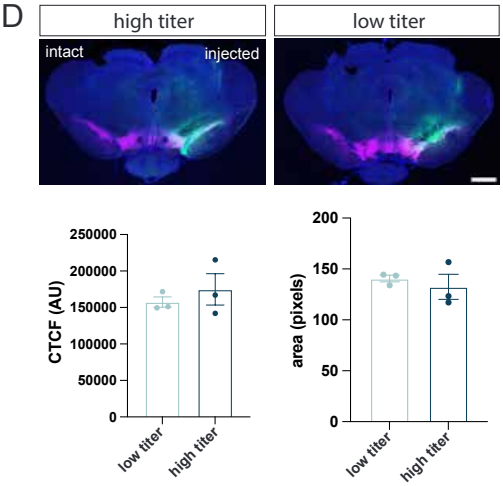
D
high titer
low titer
intact
injected
CTCF (AU)
area (pixels)
low titer
high titer


C
intact
injected

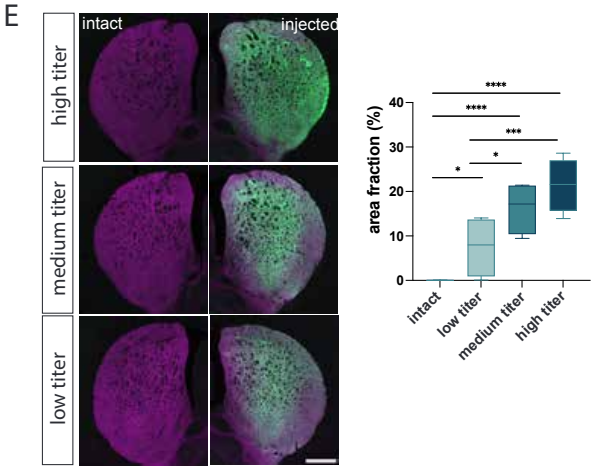
E
high titer
medium titer
low titer
intact
injected
area fraction (%)
intact
low titer
medium titer
high titer

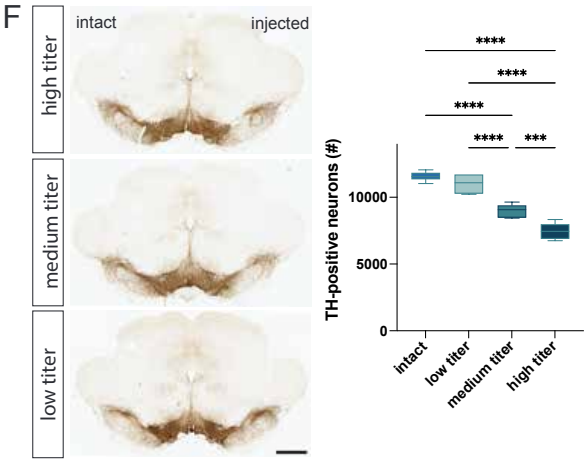
F
high titer
medium titer
low titer
intact
injected
TH-positive neurons (#)
intact
low titer
medium titer
high titer

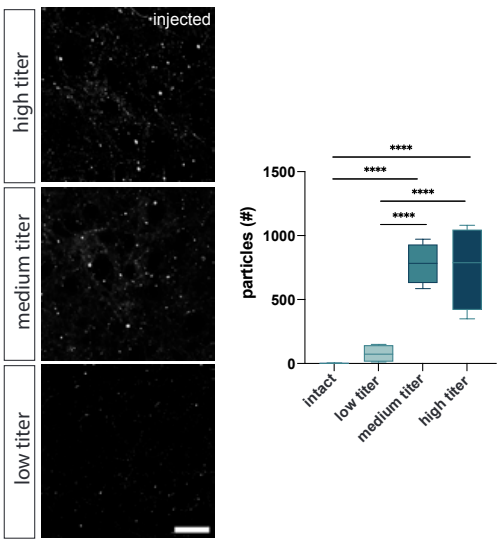
G
high titer
medium titer
low titer
injected
particles (#)
intact
low titer
medium titer
high titer

Fig. 1: Neuronal pathology induced by AAV-mediated αSyn overexpression. (**A**) Rats received a unilateral injection of 1e12 gc/ml (high titer), 5e11 gc/ml (medium titer), or 2.5e11 gc/ml (low titer) of αSyn-AAVs into the right ventral midbrain, immediately dorsal to the SNpc and were sacrificed 4 weeks later (n = 10 rats/titer group). (**B** and **C**) Representative bright-field images show human αSyn-positive transduction signal in SNpc neurons (B) and striatal terminals (C) of the injected hemisphere. Scale bars, 1000 and 100 μm in low- and high-magnification images, respectively. (**D**) Rats treated with high titer (n = 3, dark blue) or low titer (n = 3, light blue) of αSyn-AAV were analyzed for intensity of human αSyn expression within nigral neurons. Representative images of midbrain sections show DAPI (blue), TH-positive neurons (violet), and human a-Syn (green) in both titer groups. Scale bar, 1000 μm. Corrected total cell fluorescence (CTCF) and area of fluorescent human αSyn signal were measured within human αSyn-positive neurons (approximately 70 neurons per animal). For each animal, CTCF and area values were averaged. (**E**) Samples from rats treated with low, medium, or high AAV titer (n = 4/titer groups) were analyzed for striatal αSyn expression. Representative images of tissue sections containing the striatum show TH-positive (violet) and human αSyn (green) signals. Scale bar, 1000 μm. The area of human αSyn fluorescent signal was measured in samples from the intact and injected hemispheres (n = 3/per rat). For each animal, values were averaged. (**F**) Representative bright-field images of midbrain sections show TH-positive neurons. Scale bar, 1000 μm. The number of TH-positive neurons was counted in the intact and injected SNpc (n = 5/titer group; values from the intact side were averaged). (**G**) Tissue sections from AAV-treated rats (n = 4/titer groups) were analyzed for αSyn accumulations within striatal axons. Representative images show human αSyn immunoreactivity (white) in all sections analyzed, regardless of the titer of the AAV treatment. Scale bar, 100 μm. The number of αSyn particles was measured on both intact and injected hemispheres (n = 4 rats/titer group; 3 sections/rat; values from the intact side were averaged). For each animal, values were averaged. Error bars indicate SEM. Box and whisker plots show median, upper and lower quartiles, and maximum and minimum as whiskers. Statistical significance is denoted as $*p < 0.05$, $**p < 0.01$, $***p < 0.001$, and ****p < 0.0001.

3.2 Syn enters the nucleus and binds to histones

To investigate the relationship between αSyn expression and its accumulation within neuronal nuclei, midbrain tissue sections from AAV-injected rats were processed for immunohistochemical staining combined with confocal microscopy. Specific antibodies recognizing either human αSyn (MJFR1, Syn211) or total αSyn (Syn1) revealed robust nuclear αSyn signal co-localizing with DAPI-stained nuclei (Fig. 2A). Quantitative comparison of nuclear αSyn expression between the high and low AAV titer groups showed no statistically significant differences in αSyn intensity within neuronal nuclei (Fig. 2B). Similarly, the area fraction of nuclear αSyn-positive signal was comparable between the two groups. Interestingly, this lack of titer-dependent effect of protein overexpression on nuclear αSyn accumulation parallels the lack of changes in intraneuronal αSyn levels between rats injected with the low as compared to the high AAV titer (see Fig. 1D). These findings suggest, therefore, a relationship between nuclear and cytosolic αSyn levels.

Previous *in-vitro* studies have indicated potential interactions between αSyn and histones (Kontopoulos et al. 2006; Goers et al. 2003). Having demonstrated nuclear αSyn accumulation under our paradigm of AAV-induced αSyn overexpression, the next set of experiments aimed at investigating the occurrence of αSyn-histone interactions *in-vivo*. To achieve this goal, a proximity ligation assay (PLA), which detects close protein-protein interactions, was employed. Brain sections were incubated with human αSyn- and histone H3-specific antibodies, followed by secondary antibodies conjugated to oligonucleotide probes. After amplification, chromogenic dots indicative of αSyn-histone proximity and interaction were detected within neuronal nuclei on the injected hemispheres (Fig. 2C). Importantly, no PLA signal was observed in the contralateral (non-injected) hemisphere, nor in brain sections from naïve or GFP-AAV-injected animals (Fig. 2D). To further ensure assay specificity, technical controls omitting one or both primary antibodies were prepared and shown to produce no detectable signal (Fig. 2E). To assess whether AAV titers influenced the extent of αSyn-histone interactions, PLA signals were quantified across the experimental groups treated with different AAV titers. Automated image analysis revealed no significant differences in PLA-positive area fraction between the high, medium, and low titer groups (Fig. 2F). Manual counting of PLA-positive nuclei corroborated these findings (Fig. 2F).

To validate the PLA results and confirm interactions between αSyn and histones at the biochemical level, co-immunoprecipitation (Co-IP) was performed. Nuclear and cytosolic fractions were immunoprecipitated using antibodies against αSyn or histone H3, followed by immunoblotting to detect the reciprocal protein. Pull-down of histone H3 detected αSyn in the nuclear fraction, and conversely, αSyn pull-down yielded a clear H3 signal (Fig. 2G).

These findings collectively highlight the effectiveness of PLA in detecting nuclear αSyn, providing robust evidence of αSyn accumulation within neuronal nuclei. Moreover, data provide compelling *in-vivo* confirmation of the interaction between αSyn and histone H3, underscoring the potential significance of nuclear αSyn accumulation as a mechanism for translational dysregulation.

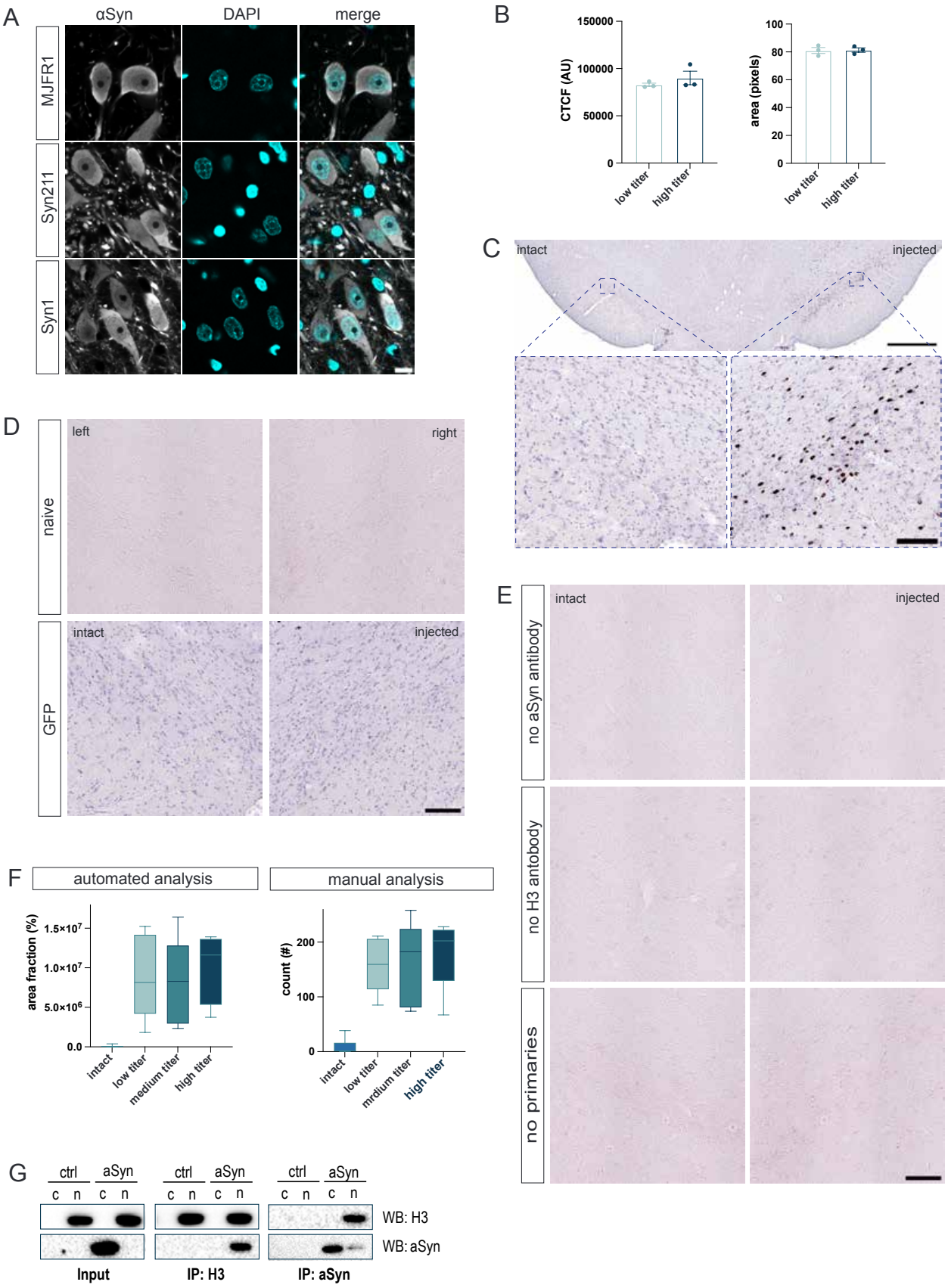
A
αSyn
DAPI
merge
MJFR1
Syn211
Syn1
B
CTCF (AU)
150000
100000
50000
0
low titer
high titer
area (pixels)
100
80
60
40
20
0
low titer
high titer
C
intact
injected
D
naive
left
right
GFP
intact
injected
E
no aSyn antibody
no H3 antobody
no primaries
intact
injected
F
automated analysis
manual analysis
area fraction (%)
1.5×10^7
1.0×10^7
5.0×10^6
0.0
intact
low titer
medium titer
high titer
count (#)
200
100
0
intact
low titer
mrdium titer
high titer
G
ctrl
aSyn
c n c n
ctrl
aSyn
c n c n
ctrl
aSyn
c n c n
WB: H3
WB: aSyn
Input
IP: H3
IP: aSyn

Fig. 2: Nuclear accumulation of αSyn and αSyn-histone interactions in-vivo. (**A** and **B**) Rats received a unilateral injection of αSyn-AAV at titers of 1e12 gc/ml (high titer), 5e11 gc/ml (medium titer), or 2.5e11 gc/ml (low titer) into the right ventral midbrain, immediately dorsal to SNpc. Animals were sacrificed at 4 weeks post-injection for analysis. Nuclear accumulation of αSyn was evaluated immunohistochemically using three different anti-αSyn antibodies, namely MJFR1, Syn211, or Syn1 (n = 5 rats, titer: 5e11 gc/ml). Representative images show αSyn-immunoreactivity (white) co-localizing with DAPI (blue) within the nuclei of nigral neurons. Scale bar, 10 μm (A). Quantitative analysis of nuclear αSyn accumulation was carried out on MJFR1-stained sections from rats injected with high (n = 3, dark blue) or low (n = 3, light blue) AAV titer. Corrected total cell fluorescence (CTCF) and the area of αSyn-positive fluorescence within the nuclei of approximately 70 αSyn-positive neurons per animal were measured. For each animal, CTCF and area values were averaged (B). **(C** to **G)** Interactions between histone H3 and αSyn were evaluated using PLA on midbrain sections from naïve rats (n = 3 rats) and AAV-injected rats (n = 6 rats/AAV group). Representative images show chromogenic PLA puncta specifically localized within nuclei of nigral neurons in the injected hemisphere of αSyn-AAV-treated rats (titer: 5e11 gc/ml). Scale bars, 1000 and 100 μm in low- and high-magnification images, respectively (C). In contrast, no specific PLA labeling was detected in samples from naïve rats or rats injected with GFP-AAV (5e11 gc/ml; please note that sections from this latter group of animals were also stained with hematoxylin). Scale bar, 100 μm (D). Technical controls to verify probe specificity were conducted by omitting one or both primary antibodies (representative images were obtained from tissue sections from a rat injected with 5e11 gc/ml αSyn-AAV). Scale bar, 100 μm (E). Quantitative analysis compared PLA signals in samples from rats treated with 1e12 gc/ml, 5e11 gc/ml, or 2.5 gc/ml (n = 5/titer group). Automated analysis measured the area fraction of PLA-positive signal, while manual analysis quantified the number of nuclei displaying αSyn-H3 signal. For each rat, three sections were analyzed, and the results were averaged. For each titer group, values of individual rats were also averaged (F). Co-immunoprecipitation (IP) of H3 and αSyn was conducted in nuclear (n) and cytosolic (c) fractions of αSyn-AAV- and GFP-AAV-injected (ctrl) rats. Immunoblots (WB) for reciprocal proteins are shown (G). Error bars represent SEM. Box and whisker plots display median, upper, and lower quartiles, with whiskers indicating maximum and minimum. Statistical significance is denoted as *$p < 0.05$, **$p < 0.01$, ***$p < 0.001$, and ****$p < 0.0001$.

3.3 Endogenous αSyn interacts with histones upon paraquat exposure

The results described above support a relationship between the expression of exogenous human αSyn, its translocation into the nucleus, and its interaction with histones following AAV-mediated human αSyn transduction. Subsequent experiments were designed to demonstrate a similar relationship using an alternative *in-vivo* model that involved exposure of mice to paraquat. Paraquat is a bipyridyl herbicide that generates substantial reactive oxygen species (ROS) via redox cycling with molecular oxygen. It has previously been shown to elevate endogenous αSyn levels in the cytosolic and nuclear neuronal compartments (Manning-Bog et al. 2002; Goers et al. 2003). In the present study, mice were administered 2 intraperitoneal injections of either vehicle (saline) or paraquat (20 mg/kg), separated by a 1-week interval, and sacrificed 2 days after the second injection (Fig. 3A). Consistent with earlier findings, paraquat treatment led to a robust increase in endogenous αSyn levels in both the cytosol and nucleus of dopaminergic neurons in the SNpc (Fig. 3B).

To further investigate whether increased endogenous αSyn, induced by paraquat exposure, was also capable of interacting with histones, a new PLA was established. Primary antibodies against endogenous αSyn and histone H3 were conjugated directly with oligonucleotide probes, allowing for probe hybridization, signal amplification, and bright-field microscopic visualization. Preliminary results indicated a markedly increased PLA positive-signal in paraquat-treated mice as compared to control (saline-injected) animals (Fig. 3C), providing compelling evidence that αSyn-histone interactions represent a consistent consequence of enhanced αSyn expression, likely of pathophysiological relevance.

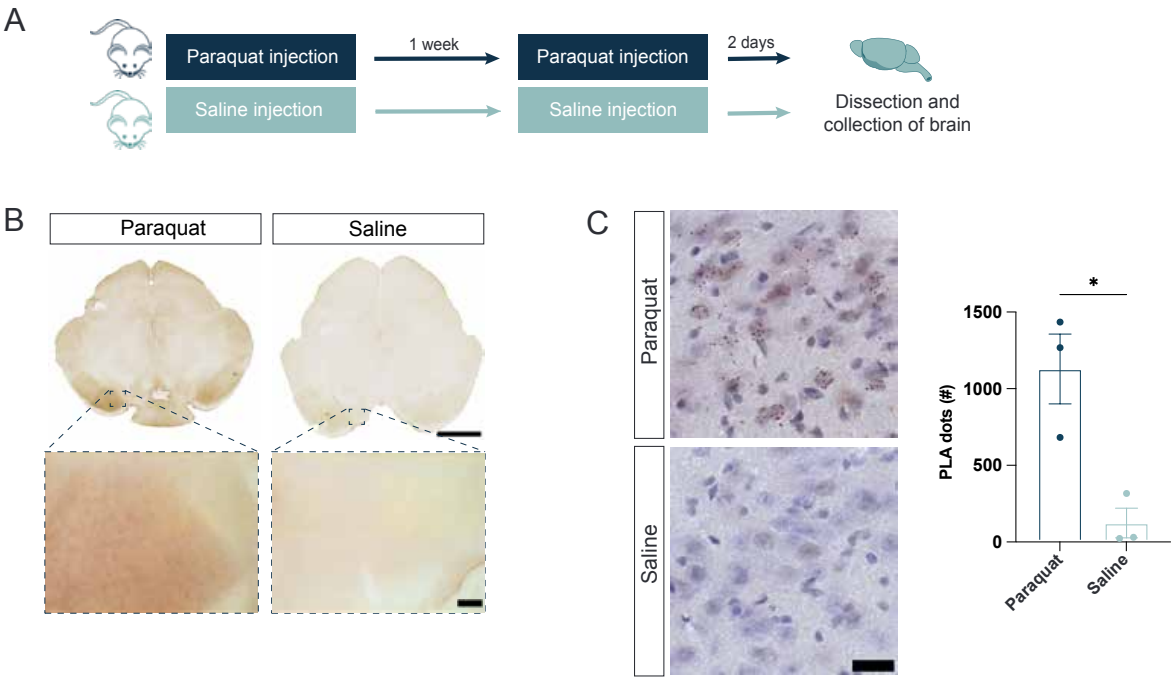

Fig. 3: Interaction of endogenous αSyn with histones following Paraquat exposure. (**A**) Mice were treated with 2 intraperitoneal injections of either vehicle (saline) or paraquat (20 mg/kg), administered one week apart. Animals were sacrificed 2 days after the second paraquat injection (n = 5 mice/treatment group). (**B**) Representative immunohistochemical images illustrate endogenous αSyn expression in paraquat- and saline-treated animals. Scale bars, 1000 µm and 100 µm in low- and high-magnification images, respectively. (**C**) Midbrain sections were subjected to PLA to assess interactions between endogenous αSyn and histone H3. Representative images reveal a marked increase in specific chromogenic PLA puncta in paraquat-injected mice. Scale bar, 20 µm. Quantification of PLA puncta was conducted on a single section from 3 animals in each treatment group. Error bars represent SEM. Statistical significance is indicated as *$p < 0.05$, **$p < 0.01$, ***$p < 0.001$, and ****p < 0.0001.

3.4 αSyn aggregates within the nucleus that bind to histones

A series of experiments was conducted to determine whether, once it gains access to the nucleus, αSyn forms intranuclear aggregate species. The rationale for this work stems from at least two considerations. First, protein crowding within the nuclear compartment would likely promote αSyn assembly. Secondly, earlier *in-vitro* studies showed that histones are capable of facilitating αSyn aggregation (Goers et al. 2003; Jiang et al. 2017).

For these analyses, we used tissue from rats injected intraparenchymally with AAV delivering human αSyn DNA (see above). Midbrain sections were initially stained with two conformation-specific antibodies, SynO2 and 5G4, which preferentially detect aggregated forms of αSyn. Immunohistochemical analysis revealed a strong positive signal for aggregated αSyn within nigral neurons in the injected hemisphere, even at low antibody concentrations (Fig. 4A). Aggregates identified by SynO2 or 5G4 antibodies were localized not only to the perikarya but also within nuclei, as indicated by nuclear co-localization with DAPI using fluorescent confocal imaging (Fig. 4B).

To further validate the presence of nuclear αSyn aggregates, a specific PLA (Syn-Syn PLA) was employed. This assay has been shown to detect αSyn aggregates, in particular oligomeric αSyn forms, with high sensitivity and specificity (Roberts et al. 2015; Helwig et al. 2016; Behere et al. 2021). PLA analysis demonstrated the formation of human αSyn oligomers within nigral neurons in the AAV-injected brain hemisphere (Fig. 4C). αSyn aggregates were clearly present within the nucleus, as indicated by the co-localization of fluorescent Syn-Syn PLA signal with DAPI (Fig. 4D).

A separate set of analyses investigated the potential interactions of aggregated αSyn with histones. Two distinct PLAs were developed using SynO2 or 5G4 antibodies in combination with histone H3. The SynO2-H3 PLA generated a strong nuclear signal within nigral dopaminergic neurons in the injected hemisphere, whereas the PLA signal from the 5G4-H3 PLA, although present, was less intense (Fig. 4E).

To corroborate these PLA findings and further demonstrate interactions between nuclear αSyn aggregates and histones, biochemical analyses using Co-IP were conducted. Fresh ventral mesencephalic homogenates from αSyn-AAV-injected and control (GFP-AAV injected) rats were immunoprecipitated with SynO2, followed by immunoblotting to detect histone H3. Results of these analyses showed that pull-down with SynO2 yielded a signal for histone H3 in samples from injected rats but not in tissue

from control animals. Co-IP was also carried out using anti-histone H3 as pull-down antibody. In this instance, however, no SynO2 signal was detected, most likely due to the loss of the aggregated αSyn conformation during Western blotting. Consistent with this interpretation, following pull-down with anti-histone H3, a clear signal for total αSyn could still be detected in the samples from injected rats devoid of SynO2 immunoreactivity (Fig. 4F).

Collectively, these results, obtained using conformation-specific antibodies, targeted PLAs, and Co-IP, provide strong evidence that, once accumulated within neuronal nuclei, αSyn forms aggregates, in particular oligomeric αSyn species. Data also reveal that these nuclear aggregates are closely associated with and interact with histones.

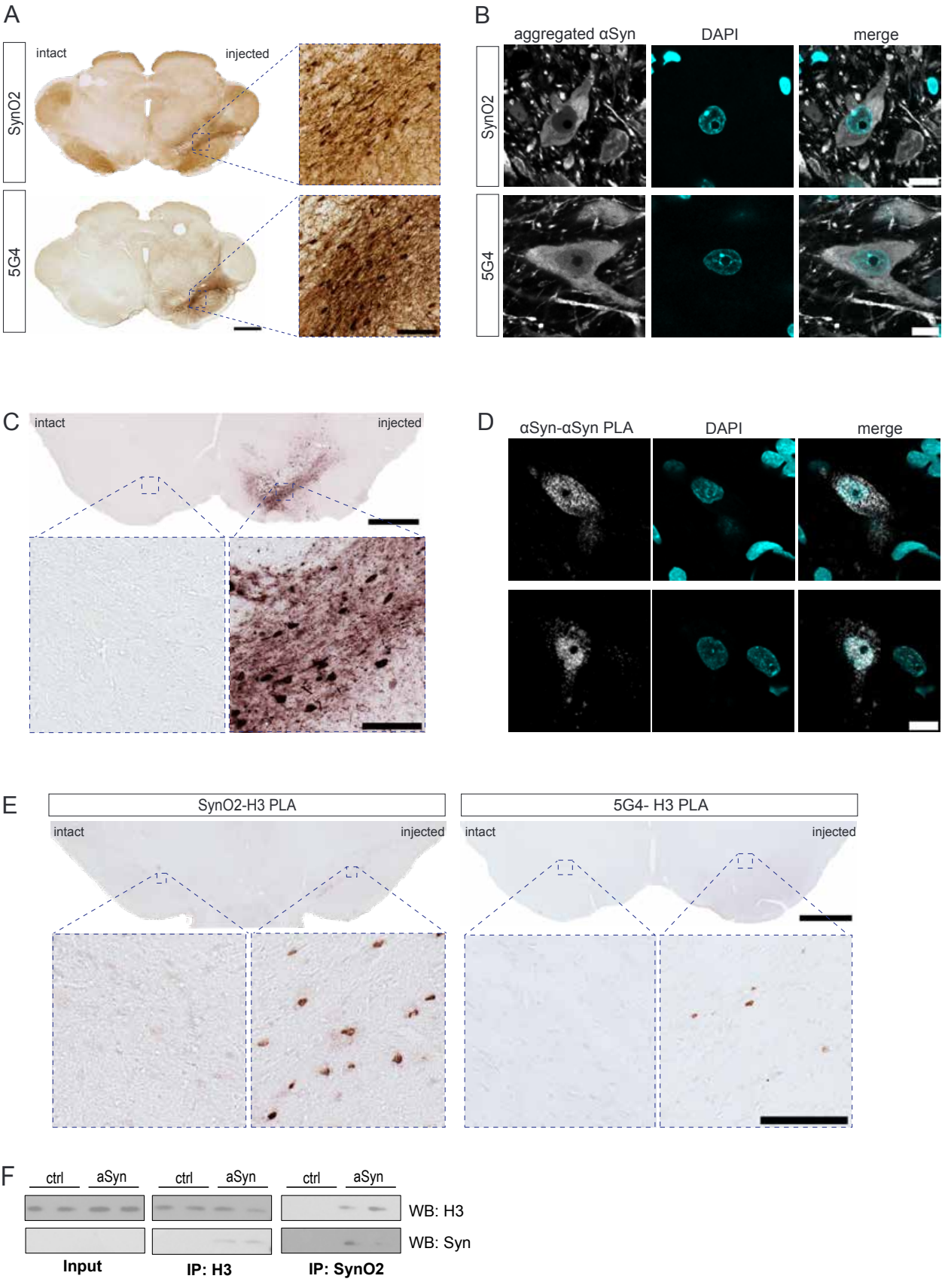
A
intact
injected
SynO2
5G4
B
aggregated αSyn
DAPI
merge
SynO2
5G4
C
intact
injected
D
αSyn-αSyn PLA
DAPI
merge
E
SynO2-H3 PLA
5G4- H3 PLA
intact
injected
intact
injected
F
ctrl
aSyn
ctrl
aSyn
ctrl
aSyn
WB: H3
WB: Syn
Input
IP: H3
IP: SynO2

Fig. 4: Nuclear aggregation of αSyn and association with histones. Rats were unilaterally injected with αSyn-AAV (5e11 gc/ml) into the right ventral midbrain, just dorsal to the SNpc, and sacrificed 4 weeks post-injection. (**A**) Representative images show αSyn aggregates in nigral neurons of the injected hemisphere, detected with SynO2 or 5G4, two conformation-specific antibodies (n = 5 rats/antibody staining). Scale bars, 1000 µm (low magnification), 100 µm (high magnification). (**B**) Nuclear accumulation of aggregated αSyn was visualized with SynO2 and 5G4. Images show co-localization of SynO2 or 5G4 immunoreactivity (white) with DAPI (blue) in neuronal nuclei (n = 5 rats/antibody staining). Scale bar, 10 µm. (**C** and **D**) To further examine αSyn aggregation, midbrain sections were processed for αSyn-αSyn PLA. In (C), chromogenic PLA puncta mark αSyn aggregates specifically in the SNpc of the injected hemisphere (n = 5 rats). Scale bars, 1000 µm for low and 100 µm for high magnification. In (D), fluorescent PLA was used with confocal microscopy to detect αSyn aggregates within neuronal nuclei (n = 5 rats), with the PLA signal (white) co-localizing with DAPI (blue). Scale bar, 10 µm. (**E**) Interactions between aggregated αSyn and histone H3 were assessed using two separate PLAs involving SynO2 / H3 or 5G4 / H3 antibody pairs (n = 5 rats/PLA group). Representative images show chromogenic PLA puncta indicative of aggregated αSyn-H3 proximity within the nuclei of SNpc neurons in the injected hemisphere. Scale bars, 1000 µm and 100 µm in low- and high-magnification images, respectively. (**F**) Two groups of animals were injected with either αSyn-AAVs or GFP-AAVs (5e11 gc/ml) and sacrificed 4 weeks later (n = 2 rats/group). The latter group served as a negative control. Co-immunoprecipitation (IP) of H3 and αSyn confirmed the presence of WB immunoreactivities only in samples from αSyn-AAV-treated rats.

3.5 Nuclear αSyn increases histone acetylation

Data showing nuclear accumulation of αSyn and its interaction with histones raised the question of whether these effects of αSyn overexpression affected histone modifications. Interestingly, altered histone modifications, particularly changes in acetylation of histone H3 at lysine 27 (H3K27), have previously been reported in cell and transgenic fly models of αSyn overexpression (Kontopoulos et al. 2006; Liu et al. 2011; Paiva et al. 2017). To evaluate H3K27 acetylation and trimethylation levels in the AAV-induced αSyn overexpression rat model, midbrain sections were processed with quadruple immunofluorescent staining. This protocol enabled simultaneous detection of (i) total histone H3, (ii) H3K27 acetylation or trimethylation, (iii) human αSyn, and (iv) TH (a marker of dopaminergic neurotransmission) within nigral neurons (Figs. 5A and 5B). Preliminary quantitative analysis of fluorescent intensities, which is currently being replicated, showed a 38.7 % increase in neuronal H3K27 acetylation in midbrain sections from the injected hemisphere compared to sections from the non-injected brain side (Fig 5C). In contrast, H3K27 trimethylation levels remained unchanged irrespective of whether they were quantified in samples from the injected or non-injected hemisphere (Fig. 5D).

These results suggest a selective alteration in H3K27 acetylation in response to αSyn overexpression. αSyn-histone interactions could play an important role in causing this effect, bearing significant pathophysiological consequences, for example, due to changes in chromatin remodeling.

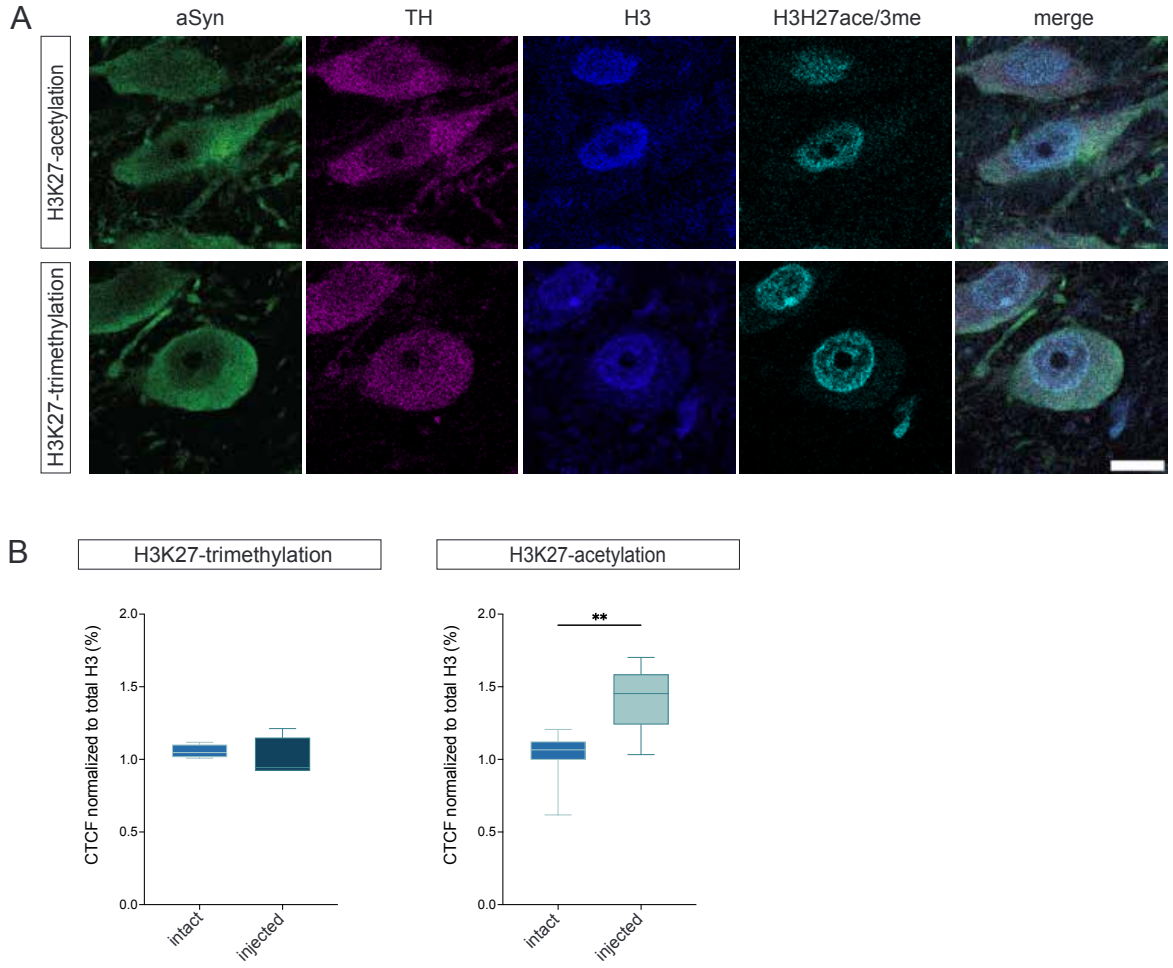

Fig. 5: Histone modifications in midbrain neurons from αSyn-overexpressing rats. (**A** and **B**) Rats received unilateral injections of αSyn-AAV (5e11 gc/ml) into the right ventral midbrain and were sacrificed 4 weeks post-injection. To assess changes in histone modifications, quadruple fluorescent staining was performed using antibodies against (i) αSyn (green), (ii) TH (violet), (iii) H3 (blue), and (iv) either H3K27-acetylation (n = 8 rats) or H3K27– trimethylation (n = 4 rats) (white). Representative confocal images show nigral neurons in the injected hemisphere. Scalebar, 10 µm (A). Corrected total cell fluorescence (CTCF) for H3K27 acetylation or trimethylation was quantified within TH- and human αSyn-positive neurons from the injected hemisphere, as well as in TH-positive neurons from the intact brain side. Approximately 40 neurons were analyzed per animal. CTCF values for each histone modification were normalized to total H3 levels and averaged for each animal (B). Box and whisker plots display median, upper, and lower quartiles, with whiskers indicating maximum and minimum. Statistical significance is denoted as **p* < 0.05, ***p* < 0.01, ****p* < 0.001, and ****p < 0.0001.

3.6 Inducible αSyn-overexpression is achieved by doxycycline treatment

The pathophysiological consequences of nuclear αSyn accumulation and histone-αSyn interactions may vary depending on the duration of nuclear αSyn burden. Very little is known, however, about the reversibility of this burden. It is also unknown whether and to which extent nuclear αSyn accumulation recedes once cytosolic protein levels are normalized after its overexpression. To address these important questions, an *in-vivo* model was developed using the TetOn expression system in combination with doxycycline treatment. This model allowed us to regulate the timing of both induction and cessation of αSyn overexpression, facilitating the study of the relationship between nuclear and cytosolic αSyn accumulation.

The TetOn system utilized in this study permits controlled transcription initiation. Binding of the reverse tetracycline transactivator (rtTA) to the tetracycline-responsive element (TRE) promoter occurs exclusively in the presence of doxycycline, a stable tetracycline analog (Fig. 6A) (Gossen and Bujard 1992). Unilateral stereotactic injections were performed into the right ventral mesencephalon, immediately dorsal to the SNpc, using two AAVs at a 1:2 ratio: one encoding the rtTA transactivator (TetOn-AAV) and the other encoding αSyn under the TRE promoter (αS^{TRE}-AAV, Fig. 6B). Initial experiments were aimed at optimizing doxycycline concentration in the drinking water. Starting 2 weeks post-surgery, rats were given drinking water containing 0, 0.5, 1.0, or 1.5 mg/ml doxycycline for 4 weeks (Fig. 6C). Water intake across all groups showed no significant differences during this 4-week period (Fig. 6D). Immunohistochemical analysis demonstrated robust αSyn expression in the midbrain and striatum of all doxycycline-treated groups, while control animals that received no doxycycline exhibited little αSyn signal within nigral neuronal cell bodies and striatal axonal projections (Figs. 6E and 6F). Analysis of TH-stained sections revealed a moderate loss of nigral dopaminergic neurons and striatal fibers that, in the group of animals treated with the lowest doxycycline dose (0.5 mg/ml), was comparable to the effects observed in rats injected with αSyn-AAV (without TetOn system) (compare Figs. 1E and F with Figs. 6G and H). Treatment of animals with 1.0 and 1.5 mg/ml doxycycline caused more severe nigrostriatal damage (Figs. 6G and 6H). Based on these results, induction of αSyn expression in subsequent experiments using the TetOn model was achieved with administration of doxycycline at a dose of 0.5 mg/ml.

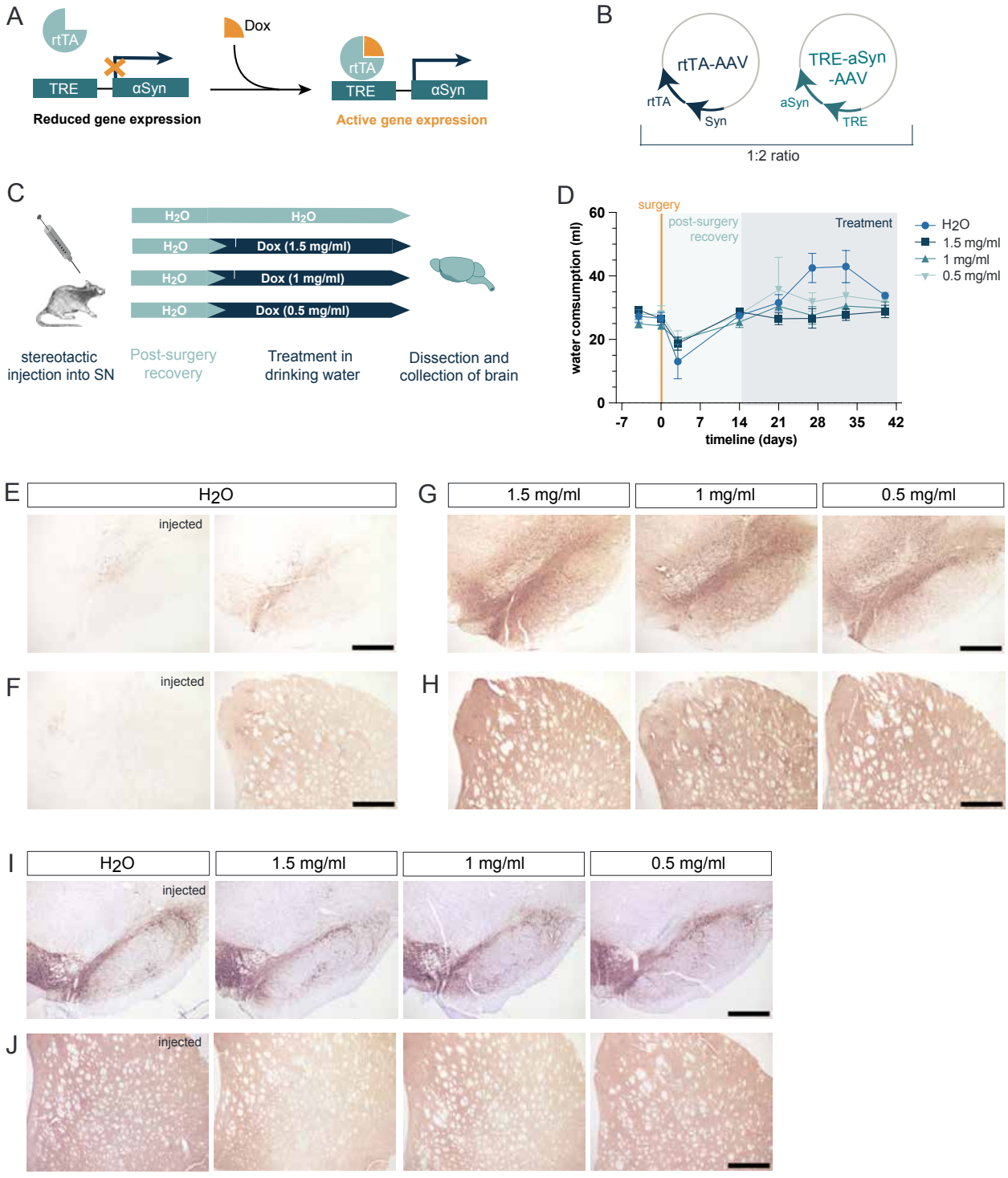

Fig. 6: Inducible αSyn-overexpression mediated by doxycycline treatment. (**A**) Regulation of αSyn transcription by the TetOn system. The reverse tetracycline transactivator (rtTA) binds to the tetracycline response element (TRE) promoter only in the presence of doxycycline (Dox), thus initiating αSyn expression. (**B** and **C**) Rats received unilateral injections of two AAV vectors (1:2 ratio), one encoding the TetOn transactivator (TetOn-AAV) and the other encoding αSyn under the TRE-promoter (αS^{TRE}-AAV) (B), into the right ventral midbrain, just dorsal to the SNpc (C). Starting 2 weeks post-

surgery, rats received drinking water containing varying concentrations of doxycycline (0, 0.5, 1.0, or 1.5 mg/ml); animals were then sacrificed at 4 weeks after initiation of doxycycline treatment (n = 6 rats/treatment group) (C). (**D**) Water consumption was monitored across all treatment groups (n = 3 cages/treatment group). Error bars represent SEM. (**E** and **F**) Representative bright-field images show human αSyn-positive immunoreactivity in the SNpc (E) and striatum (F) of rats (injected hemisphere) that did not receive doxycycline. In some samples (see images on the left), no or minimal immunoreactivity was observed, while, in other tissue sections, human αSyn expression was more evident. Slight transgene expression in control tissue from untreated rats likely reflects "leakage" of αSyn expression caused by non-specific binding of the rtTA. Scale bars, 1000 μm. (**G** and **H**) Representative bright-field images of human αSyn immunoreactivity in the SNpc (G) and striatum (H) of rats (injected hemisphere) treated with different doxycycline doses. As compared to findings in tissue from untreated rats (E and F), treatment with doxycycline induced a marked human αSyn expression. Scale bars, 1000 μm. (**I** and **J**) Neuronal integrity in the SNpc (I) and striatum (J) was assessed by TH immunostaining. Images show a dose-dependent reduction of immunoreactivity, consistent with a loss of neuronal integrity. Scale bars, 1000 μm.

While conducting these initial experiments to optimize the TetOn model of αSyn expression, results showed that, in some instances, low αSyn expression could be detected even in control animals that did not receive doxycycline treatment (Figs. 6E and F). This phenomenon, often referred to as "leakage" of the TetOn systems, is a known effect that can be addressed, at least in part, by adjusting the relative amount of the rtTA (Ali Hosseini Rad et al. 2020; Roney et al. 2016). A set of experiments was therefore designed to determine whether "leaked" αSyn expression could be mitigated by changing the TetOn-AAV / αS^{TRE}-AAV ratio from 1:2 to 1:3, thus effectively reducing the amount of rtTA (Fig. 7A). Two groups of animals received AAV injections at a ratio of 1:3 and were then treated with either 0.5 mg/ml doxycycline or no doxycycline (Fig. 7B). Immunohistochemical staining with anti-αSyn confirmed the induction of robust αSyn expression in the doxycycline-treated group. It also confirmed a slight leakage of αSyn expression in the untreated control group, which could be minimized, however, using the adjusted 1:3 AAV ratio (Figs. 7C and 7D). Leaked αSyn expression using this 1:3 ratio would be unlikely to have any significant effect on the results of subsequent experiments in which the TetOn inducible model was used to investigate the reversibility of nuclear αSyn accumulation and the relationship between cytosolic and nuclear αSyn burden.

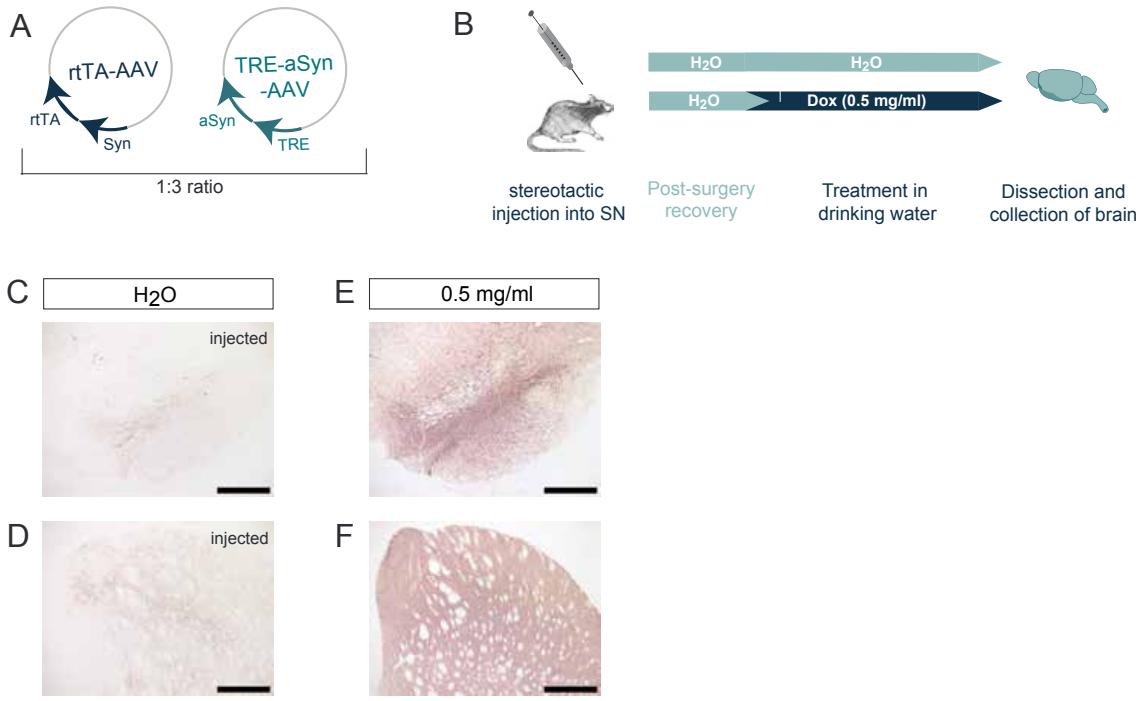

Fig. 7: Refinement of doxycycline-inducible αSyn overexpression. (**A**) Rats received unilateral midbrain co-injections of TetOn-AAV and αS^{TRE}-AAV using a 1:3 rather than a 1:2 ratio (see Fig. 6) of the two vectors. (**B**) Beginning at 2 weeks post-surgery, rats were given drinking water with or without doxycycline (0.5 mg/ml) for 4 weeks; at this time, animals were sacrificed and brains collected (n = 6 rats/treatment group). (**C** and **D**) Representative bright-field images of human αSyn immunoreactivity in the SNpc (C) and striatum (D) of rats that did not receive doxycycline. Please note that these images represent the maximum "leakage" observed under this experimental condition (1:3 rather than 1:2 AAV ratio). Scale bars, 1000 µm. (**E** and **F**) Representative bright-field images of human αSyn immunoreactivity in the SNpc (E) and striatum (F) of rats treated with 0.5 mg/ml doxycycline. Scale bars, 1000 µm.

3.7 Cessation of doxycycline treatment reverses αSyn overexpression

In the TetOn model, αSyn overexpression triggered by doxycycline administration should be reversed after cessation of drug treatment. To test this “off” effect, five groups of rats underwent a combined stereotactic nigral injection of TetOn-AAV and αS^{TRE}-AAV as described above. Starting 2 weeks post-surgery, all animals received doxycycline in their drinking water for a 4-week induction period. Upon doxycycline withdrawal, animals were then sacrificed at intervals of 0, 2, 4, 8, or 12 weeks to monitor intraneuronal αSyn expression (Fig. 8A). Immunohistological analysis of midbrain and forebrain tissue sections stained with anti-αSyn revealed a gradual decline in immunoreactivity within the SNpc and striatum, reflecting progressive αSyn clearance following the withdrawal of doxycycline-induced expression (Figs. 8B and 8C). A marked reduction in αSyn content was already observed in the SNpc at 2 and 4 weeks after doxycycline withdrawal (Fig. 8B). Interestingly, at the same time points, the reduction in αSyn levels was less pronounced in the striatum, suggesting a delayed and slower process of αSyn clearance (Figs. 8C and D). Despite these initial differences, cessation of doxycycline-induced αSyn overexpression was observed in both the SNpc and striatum at 8 weeks post-drug withdrawal (Figs. 8B to 8D).

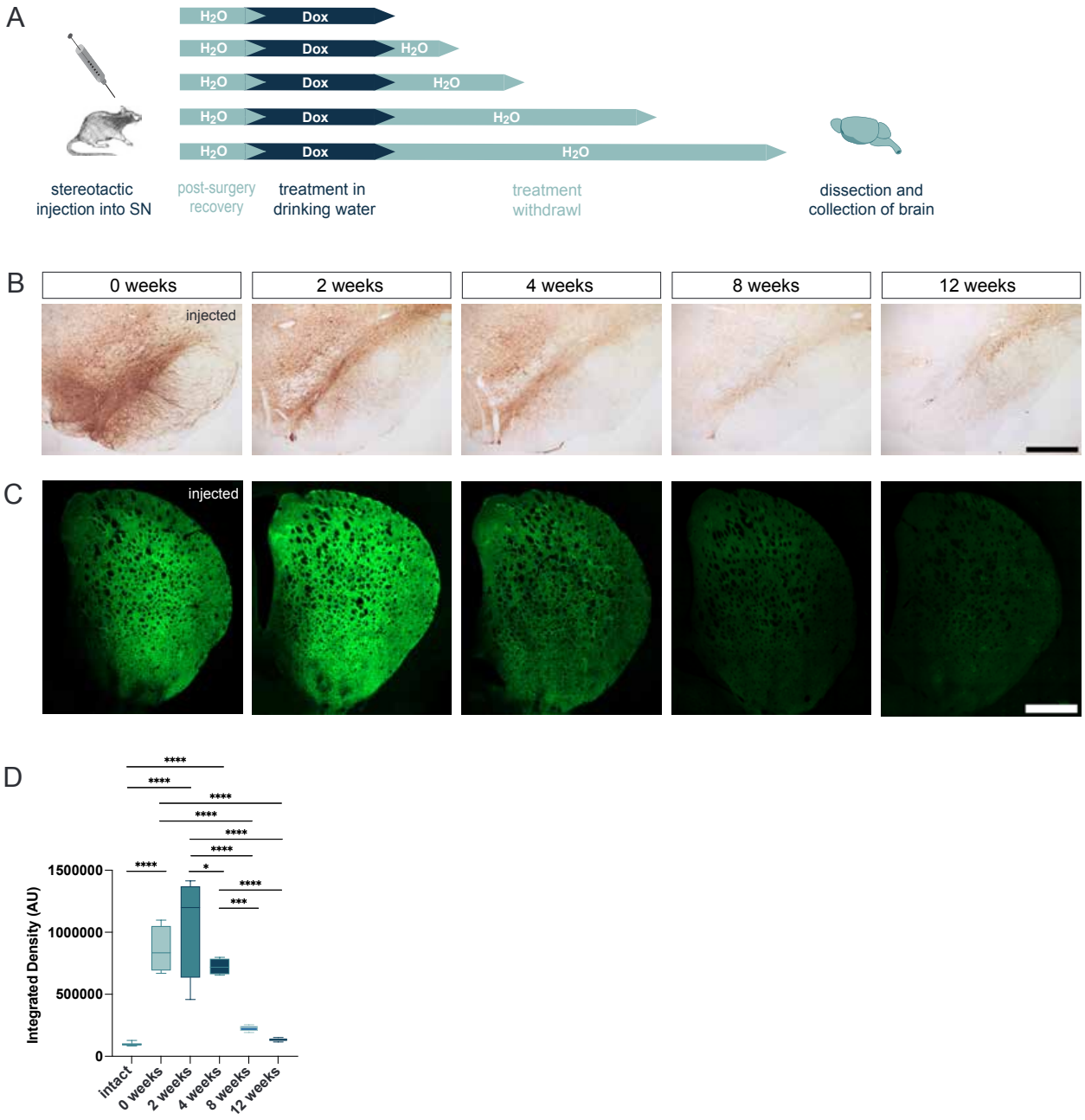

Fig. 8: αSyn clearance following cessation of doxycycline-induced overexpression. (**A**) Rats were injected unilaterally into the right ventral midbrain, using two AAV vectors: TetOn-AAV and αS^{TRE}-AAV. The ratio of the two vectors was 1:3. Beginning 2 weeks post-surgery, rats were treated with doxycycline (0.5 mg/ml) in their drinking water for 4 weeks. At this time point, the doxycycline treatment war terminated, and animals were kept for 0, 2, 4, 8, or 12 weeks before being sacrificed (n = 8 rats/time point). (**B**) Representative bright-field images show SNpc-containing midbrain sections stained with anti-human αSyn. A progressive reduction of protein overexpression occurred after doxycycline withdrawal. Scale bar, 1000 µm. (**C**) Representative fluorescent images of striatal sections show human αSyn (green) expression at different time points after doxycycline withdrawal. Scale bar, 1000 µm. (**D**) Intregrated density of striatal αSyn fluorescent signal was

measured in the intact and injected hemispheres. For each animal, values were collected and averaged from 3 alternating striatal sections. Values from the injected hemisphere were collected and averaged (n = 4 rats/time point). Values from control (intact side) tissue collected at the different time points post-doxycycline were averaged. Box and whisker plots present the median, upper, and lower quartiles, with the whiskers representing maximum and minimum values. Statistical significance is indicated as *$p < 0.05$, **$p < 0.01$, ***$p < 0.001$, and ****$p < 0.0001$.

3.8 αSyn-histones interactions are reversible

To investigate the effect of halting αSyn overexpression on nuclear αSyn accumulation, rats underwent the aforementioned treatment involving doxycycline administration for 4 weeks and subsequent withdrawal. Animals were sacrificed 4 weeks after drug withdrawal, and midbrain sections were processed for PLAs to detect interactions of human αSyn or aggregated αSyn with histones. Analysis of human αSyn-histone interactions revealed a significant reduction in nuclear signal following the doxycycline withdrawal period, with only sparse immunoreactivity puncta detectable within neuronal nuclei (Fig. 9A). Similarly, PLA designed to detect interactions between aggregated αSyn (assessed using the SynO2 antibody) and histones revealed complete ablation of detectable signal after the same clearance period (Fig. 9B). Complementary immunohistochemical analyses corroborated these findings, demonstrating substantially reduced immunoreactivity for human αSyn and diminished prevalence in nigral neurons (Fig. 9C), while the immunoreactivity for aggregated αSyn species returned to baseline levels after the same 4-week clearance period (Fig. 9D).

Collectively, these results indicate that αSyn-histones interactions are reversible, even if they involve aggregated αSyn species. Data are also consistent with the conclusion that, following its overexpression, clearance of αSyn follows a time course similar to that in neuronal perikaryal and neuronal nuclei.

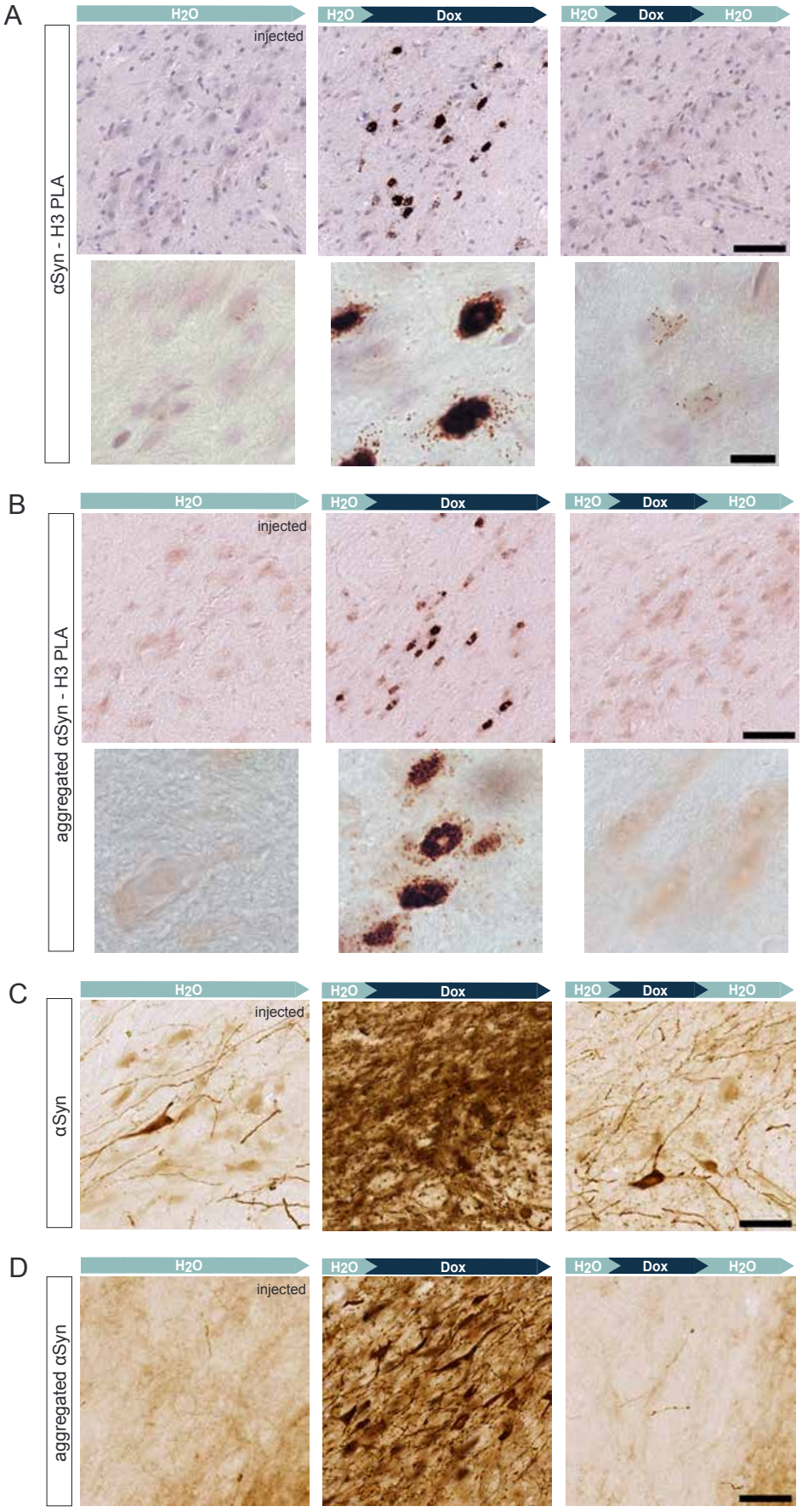
A
H2O
H2O
Dox
H2O
Dox
H2O
injected
αSyn - H3 PLA
B
H2O
H2O
Dox
H2O
Dox
H2O
injected
aggregated αSyn - H3 PLA
C
H2O
H2O
Dox
H2O
Dox
H2O
injected
αSyn
D
H2O
H2O
Dox
H2O
Dox
H2O
injected
aggregated αSyn

Fig. 9: Reversibility of αSyn-histone interactions. Rats were injected unilaterally into the right ventral midbrain using two AAV vectors: TetOn-AAV and αS^{TRE}-AAV (1:3 ratio). Starting 2 weeks post-surgery, one group of rats was treated with doxycycline (0.5 mg/ml) in their drinking water for 4 weeks. At this time point, the doxycycline treatment was terminated, and animals (n = 4 rats) were kept for an additional 4 weeks before being sacrificed (panels on the right). For comparison, a negative control group (n = 4 rats) received only water for 8 weeks (panels on the left). A positive control group (n = 4 rats) was also generated; it consisted of rats treated with doxycycline throughout the 8-week period of the experiment (panels in the middle). (**A**) Representative images of midbrain tissue sections processed for PLA to detect αSyn-histone interactions (αSyn-H3 PLA). High-magnification images show neurons in the SNpc. (**B**) Representative images of midbrain tissue sections processed for PLA to detect interactions between histone H3 and aggregated αSyn (SynO2-H3 PLA). High-magnification images show neurons in the SNpc. Scale bars, 50 μm and 10 μm for low- and high-magnification images, respectively. (**C** and **D**) Midbrain tissue sections from the same animals in the three experimental groups were processed for immunohistochemistry using an antibody detecting human αSyn or an antibody detecting aggregated αSyn. Representative images show neurons in the SNpc of the injected hemisphere. Scale bars, 50 μm.

3.9 Nuclear clearance of αSyn is proteasome-dependent

Data showing an efficient reduction of nuclear αSyn levels and the reversibility of αSyn-histone interactions raise the question of whether specific mechanisms or pathways are involved in nuclear αSyn clearance under conditions of increased αSyn expression. Cellular degradation of αSyn is primarily mediated through lysosomal pathways and the ubiquitin-proteasome system (UPS) (Stefanis et al. 2019). While nuclei are devoid of the autophagic machinery, they contain a UPS capable of degrading nuclear aberrant protein as well as small protein aggregates (Iwata et al. 2009; den Brave et al. 2020). Consequently, the next set of experiments was designed to investigate the role of the nuclear UPS in mediating αSyn degradation in αSyn-overexpressing neurons. Analyses were carried out in midbrain tissue sections from rats injected with empty AAV (Null-AAV), GFP-AAV, or αSyn-AAV and involved the measurement of proteasomal enzymatic activity using a chymotrypsin-like activity assay. This assay employs an AMC-tagged peptide substrate that releases the highly fluorescent AMC molecule upon UPS-mediated cleavage; fluorescence measurements then provide a sensitive quantification of proteasomal activity.

Initially, assay parameters for measuring nuclear proteasome activity were optimized, including fluorescent gain, dilution factor, and time points. SNpc-containing ventral midbrain tissue from naïve rats was dissected, nuclear fractions were isolated, and protein content was quantified. Fluorescent gains of 0, 500, 1000, 2000, and 4000 were tested, with a gain of 1000 yielding the optimal signal; lower gains resulted in indistinct sample separation, while higher gains led to sample saturation (Fig. 10A). Nuclear fraction dilutions of 10 x and 20 x were also tested, with the 20-x dilution providing values within the standard curve range (Fig. 10B). Fluorescent signals were taken every 5 min, starting at 15 min after the beginning of incubation and ending at 75 min. A linear phase occurred between 35 and 65 min and was used to calculate the increase in AMC fluorescence over time and to estimate UPS activity (Fig. 10C).

Using the optimized assay parameters, nuclear fractions from Null-AAV-, GFP-AAV-, or αSyn-AAV-injected rats were analyzed for proteasomal activity. A significant increase in proteasome activity was observed solely in the injected hemisphere of αSyn-AAV-treated animals (Fig. 10D), indicating a relationship between nuclear αSyn accumulation and enhanced UPS-mediated protein degradation. It is conceivable that this effect mitigates

the deleterious consequences of nuclear αSyn burden and may play an important role in reversing this burden after cessation of αSyn overexpression.

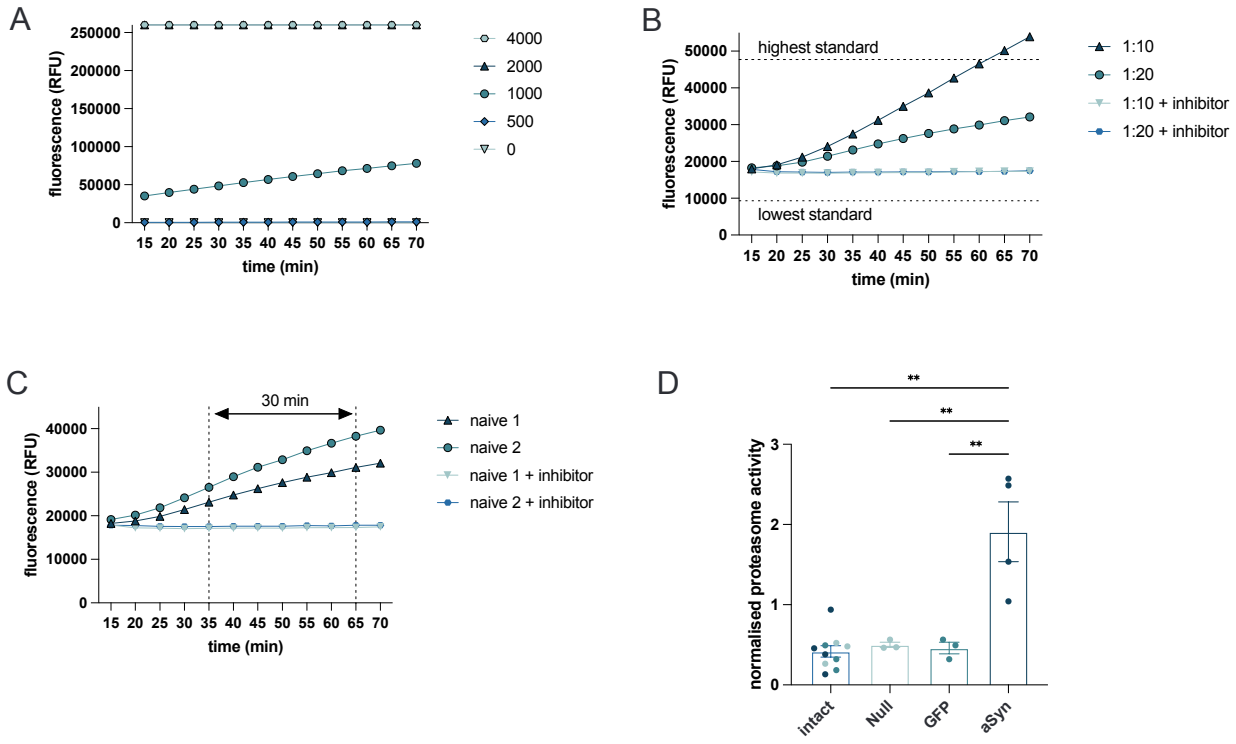

Fig. 10: Proteasome-dependent clearance of αSyn. (**A** to **C**) Nuclear fractions were isolated from ventral midbrain tissue of naïve rats (n = 2 rats), and chymotrypsin-like proteasomal enzymatic activity was assessed using an AMC-tagged peptide substrate. For optimization, fluorescent signal was measured under various gain settings (0, 500, 1000, 2000, 4000) to determine the optimal detection range (A). Different dilutions of the nuclear fractions (1:10, 1:20) were tested (B). Using the 1:20 dilution, fluorescent signals were recorded every 5 min to establish a 30-min window of linear activity increase (C). (**D**) Rats were injected unilaterally with αSyn-AAV (5e11 gc/ml), GFP-AAV (5e11 gc/ml), or Null-AAV (5e11 gc/ml) into the right ventral midbrain and sacrificed 4 weeks post-injection (n = 3 - 4 rats/group). Nuclear fractions were prepared from midbrain tissue of the intact and injected hemispheres. AMC fluorescent signal was measured in these fractions, and normalized proteasome activity calculated. Null, GFP, and aSyn bars show averages of the values detected in tissue from the injected side; symbols show the values in individual animals. The intact bar shows the average of all values measured in tissue from the intact hemisphere; symbols show values in individual rats from the three different experimental groups. Error bars represent SEM. Statistical significance is indicated as *$p < 0.05$, **$p < 0.01$, ***$p < 0.001$, and ****p < 0.0001.

4. Discussion

The nuclear translocation of αSyn likely represents a highly relevant component in the pathophysiology of PD. However, important factors concerning the conditions and mechanisms governing αSyn translocation, the intranuclear consequences of αSyn accumulation, intranuclear αSyn aggregation, and the reversibility and clearance of nuclear αSyn burden remain largely unexplored. Notably, there is a lack of *in-vivo* research investigating these critical issues. Our study aimed to address several of these knowledge gaps by examining five principal aspects of nuclear αSyn pathobiology *in-vivo*.

4.1 The relationship between αSyn accumulation and nuclear translocation

First, we aimed to investigate the relationship between αSyn accumulation and its nuclear translocation. Our study established an AAV-mediated αSyn overexpression model through a unilateral injection of αSyn-delivering AAVs into the rat ventral mesencephalon, demonstrating robust human αSyn expression at the injection site and in anatomically connected regions, particularly the striatum. This pattern aligns with previous research (Kirik, Rosenblad, et al. 2002; Klein et al. 2002; Ulusoy et al. 2010; Ulusoy et al. 2017) and confirms successful viral transduction and protein expression. Importantly, we detected αSyn within the nucleus following the initiation of overexpression.

Although protein overexpression models face criticism for creating artificially exaggerated conditions (M Decressac et al. 2012; Van der Perren et al. 2015; Albert et al. 2019), our approach offers several advantages for investigating nuclear αSyn translocation. The amplification allows for proof-of-concept studies that identify factors governing αSyn's nuclear entry, function, and persistence while simultaneously reflecting a pathophysiological phenomenon frequently observed in PD. The genetic basis for chronically increased αSyn levels in PD is well established. These primarily involve multiplications in the *SNCA* gene (Farrer et al. 2004; Miller et al. 2004) and polymorphisms in the gene promoter regions (Fuchs et al. 2008). Complementing these direct genetic causes, mutations in genes regulating αSyn degradation, such as *GBA1*, *ATP13A2*, and *PRKN,* contribute to increased αSyn accumulation through impaired clearance mechanisms (Shimura et al. 2001; Mazzulli et al. 2011; Usenovic et al. 2012). At the transcriptional level, various factors that interact directly with the αSyn promoter further drive protein upregulation (Yang and Latchman 2008; Duplan et al. 2016).

Beyond these intrinsic genetic factors, environmental triggers can acutely elevate αSyn levels. Exposure to toxins such as MPTP and paraquat induces αSyn accumulation (Manning-Bog et al. 2002; Chorfa et al. 2013; Vila et al. 2000). Similarly, traumatic brain injury (Surgucheva et al. 2014; Acosta et al. 2015), a recognized risk factor for PD development (Ascherio and Schwarzschild 2016; Bellou et al. 2016), has been shown to induce αSyn accumulation. Together, these examples of pathophysiological αSyn accumulation underline the relevance of the AAV-mediated αSyn-overexpression model. However, we acknowledge that the acute nature of the AAV-mediated αSyn overexpression model contrasts with the decades-long elevation of αSyn experienced by genetic PD patients. This suggests a valuable avenue for future research using more chronic models. Another important consideration is that αSyn levels produced in this model may still be higher than in the aforementioned (patho-)physiological cases. Keeping this caveat in mind, we also used an alternative model of paraquat exposure in mice, which is known to moderately, yet detectably, increase αSyn levels (Manning-Bog et al. 2002; Fernagut et al. 2007; Tong et al. 2022). Our experiments demonstrated that paraquat exposure triggers αSyn nuclear entry, providing compelling evidence that nuclear translocation is a consistent consequence of enhanced αSyn expression, regardless of the underlying mechanism. The implications of our findings are particularly intriguing when considering brain regions that have physiologically high levels of αSyn, such as the dorsal motor nucleus of the vagus nerve (Taguchi et al. 2016). This natural accumulation might contribute to the selective vulnerability of specific neuronal populations in PD pathogenesis.

We further designed experiments with varying AAV titers to investigate the relationship between cytosolic αSyn accumulation and nuclear translocation. Our initial hypothesis that higher cytosolic αSyn would proportionally increase nuclear translocation was only partially supported by the results. Unexpectedly, we did not find significant differences in cytosolic αSyn concentration among the three AAV titer groups. Similarly, the extent of αSyn translocation and levels of nuclear αSyn levels were quite comparable in these experimental groups. Thus, data were consistent with a dynamic equilibrium between the cytosolic and nuclear compartments. The specific reason(s) for the lack of titer-dependent effects remain unclear. However, further analyses in our tissue samples from the SNpc and striatum revealed a pronounced compartment-specific accumulation

pattern: while αSyn intensity within SNpc neuronal cell bodies remained relatively consistent despite increasing AAV titers, striatal αSyn-positive axonal fibers exhibited clear titer-dependent increases. This differential accumulation pattern may reflect a fundamentally distinct handling of αSyn between neuronal cell bodies and projections. Given αSyn's primary function in the synapses, preferential anterograde transport and axonal accumulation would be expected; this axonal/synaptic accumulation may be more directly related to the titers of AAV-induced transduction. Alternatively, compartment-specific differences in protein degradation efficiency might explain these observations. The molecular mechanisms underlying this compartmentalized αSyn distribution warrant further investigation, especially since, in our experimental model, the pathological consequences of αSyn overexpression followed a titer-dependent pattern, indicating that αSyn accumulation within projections and synapses (rather than the cell bodies) may be more directly correlated with neuronal demise. These pathological consequences included a significant loss of TH-positive neurons in the SNpc, likely due to αSyn gain of toxic function. αSyn overexpression can trigger protein aggregation, impaired proteostasis, mitochondrial dysfunction, and synaptic deficits, collectively contributing to neuronal death (Nemani et al. 2010; Lehtonen et al. 2019; Lurette et al. 2023). Higher AAV titers likely exacerbate this toxicity by overwhelming cellular degradation pathways, including the ubiquitin-proteasome system and autophagy (Snyder et al. 2003; Winslow et al. 2010; Ebrahimi-Fakhari et al. 2012; McKinnon et al. 2020). While AAV vectors generally exhibit low toxicity, excessive viral loads may provoke mild immune responses or cellular stress. These mechanisms, however, typically do not serve as primary drivers of neurodegeneration in this model (Hinderer et al. 2018; Hudry and Vandenberghe 2019). Notably, αSyn accumulation in presynaptic terminals, a known indicator of synaptic dysfunction, was elevated only in medium and high titer groups, suggesting a threshold effect where αSyn must reach critical expression levels before triggering substantial synaptic pathology.

In conclusion, αSyn overexpression, whether induced by AAVs or paraquat, leads to the αSyn accumulation in the nucleus. Considering the numerous disease-related conditions associated with elevations in cytosolic αSyn, αSyn nuclear translocation is likely to represent a mechanism of pathophysiological relevance in human synucleinopathies.

4.2 Detection of nuclear αSyn

Investigations of nuclear αSyn have relied heavily on αSyn-specific antibodies (Maroteaux et al. 1988; McLean et al. 2000; Vila et al. 2000; Sangchot et al. 2002; Kontopoulos et al. 2006; Koss et al. 2022; Du et al. 2024), yet antibody sensitivity and specificity remain critical challenges in validating nuclear αSyn localization. While the MJFR1 and Syn211 clones exhibit high specificity for human αSyn, they are characterized by relatively low sensitivity (Waxman et al. 2008; Leupold et al. 2022). Reports on the total (rodent and human) αSyn antibody clone Syn1 have been inconsistent, with some studies confirming its specificity, while others document nonspecific binding to a 45 kDa protein (Perrin et al. 2003; Altay et al. 2023). The most concerning case involves the αSyn clone 3D5, where early studies reported strong immunohistochemical signals in the nuclei of rat and mouse tissue (Yu et al. 2007; Zhang et al. 2008; Vivacqua et al. 2011) that were subsequently proven to be non-specific in αSyn knock-out mice (Huang et al. 2011). Antibody reliability issues also extend to antibodies for aggregated or modified αSyn species. For instance, nuclear phosphorylated αSyn (pS129-αSyn) has been reported in multiple studies (Schell et al. 2009; Wakamatsu et al. 2007; Peelaerts et al. 2015; Villar-Piqué, Lopes da Fonseca, Sant'Anna, et al. 2016; Rutherford et al. 2016; Delic et al. 2018; Elfarrash et al. 2021; Kumar et al. 2022). However, recent rigorous subcellular analysis of commonly used pS129 antibodies has revealed strong cross-reactivity in nuclear fractions of both wild-type and knockout neurons, indicating that these signals do not represent genuine αSyn species (Lashuel et al. 2022).

To overcome these methodological limitations of single-antibody immunohistochemical approaches, we developed and validated a highly specific and semiquantitative PLA that enhances the reliability of nuclear αSyn detection while simultaneously confirming its interaction with histones. This approach offers two advantages: first, the inherent signal amplification of PLA significantly boosts the sensitivity of the highly specific Syn211 antibody clone for human αSyn, thereby overcoming the constraints of conventional immunohistochemistry. Secondly, incorporating an antibody against histone H3 enables direct and unambiguous visualization of αSyn-H3 interactions *in-vivo*. Given that histone H3 is an exclusively nuclear protein, the αSyn-H3 PLA signal provides definitive evidence of nuclear αSyn

localization, reinforcing its potential role in nuclear processes described earlier. This methodological advance represents a valuable tool for investigating nuclear αSyn and αSyn-H3 interactions with unprecedented specificity and sensitivity.

4.3 Implications of αSyn-histone interactions

Our preliminary findings suggest that nuclear accumulation of αSyn is associated with selective alterations in histone modifications, specifically an increase in H3K27 acetylation without corresponding changes in H3K27 trimethylation. The observed interaction between αSyn and histones elucidates a potential molecular mechanism through which αSyn may mediate transcriptional dysregulation in PD. Epigenetic modification of histones has been extensively documented across various experimental PD models, yielding conflicting results regarding alterations in histone acetylation and methylation patterns (Kontopoulos et al. 2006; Sugeno et al. 2016; Paiva et al. 2017; Lee et al. 2021). Importantly, our findings align with post-mortem analyses of PD patient brain tissue, which consistently reveal hyperacetylation at multiple histone residues, with H3K27 hyperacetylation being the most pronounced (Gebremedhin and Rademacher 2016; Toker et al. 2021; Huang et al. 2021). While this study did not directly address the functional consequences of H3K27 hyperacetylation, prior research by Toker et al. (2021) indicates that this specific modification is particularly enriched at genomic loci containing PD-associated genes, suggesting a significant role in disease pathogenesis. Furthermore, αSyn overexpression has been implicated in extensive transcriptional alterations affecting pathways governing synaptic dysfunction, neurogenesis, neuronal differentiation, ER-Golgi trafficking, and DNA repair mechanisms (Paiva et al. 2017; Paiva et al. 2018; Schaffner et al. 2023). The molecular mechanism by which αSyn affects histone acetylation is still not fully understood. Whether αSyn directly induces histone hyperacetylation via its interaction with histone H3 or operates through alternative pathways requires further investigation. Several mechanistic possibilities may exist; one hypothesis suggests that impaired autophagy, caused by cellular αSyn accumulation, reduces HDAC activity, consequently enhancing histone acetylation (Park et al. 2016). Additionally, emerging evidence links histones to neuroinflammatory processes, wherein activated microglia contribute to epigenetic modifications characteristic of PD pathology (Harrison et al. 2018).

Our data demonstrate that acute nuclear αSyn accumulation modifies epigenetic markers; however, the comprehensive transcriptional consequences of αSyn-induced epigenetic changes remain to be fully characterized. Critical questions persist regarding cellular adaptation to chronic elevation, specifically whether neurons possess compensatory mechanisms to mitigate acute effects of histone modifications or potentially decouple transcriptional from translational processes under sustained αSyn burden. Furthermore, the reversibility of these epigenetic changes represents a compelling avenue for investigation: do histone modifications persist after nuclear αSyn clearance, or are they reversible? We plan to address this question as a continuation of this project using the inducible αSyn overexpression model discussed later. Elucidating these αSyn-induced epigenetic mechanisms and their transcriptional impacts could provide new information essential for our understanding of disease development and progression.

4.4 αSyn aggregation in the nucleus

Our investigation reveals that αSyn not only accumulates within neuronal nuclei but also forms intranuclear aggregates that directly interact with histones. This formation of nuclear αSyn aggregates supports our hypothesis that protein crowding within the nuclear compartment promotes αSyn assembly. The nuclear environment, characterized by high concentrations of nucleic acids and proteins, provides favorable conditions for αSyn oligomerization and aggregation (Stephens et al. 2019). Furthermore, aggregation of αSyn within neuronal nuclei may be promoted by αSyn-histone interactions since, as shown by an earlier *in-vitro* study, αSyn assembly is significantly enhanced in the presence of histones (Goers et al. 2003; Jiang et al. 2017). Our new *in-vivo* findings are likely to bear translational relevance for PD pathology. In a paper by Roberts and colleagues, small immunoreactive dots can be seen within neuronal nuclei in PLA-processed tissue specimens from PD patients (Roberts et al. 2015); this observation, although not commented on by the authors of the paper, is consistent with the presence of nuclear aggregated αSyn in PD brain. In a separate study, FACS-isolated neuronal nuclei from PD patients revealed the presence of αSyn oligomers (Garcia-Esparcia et al. 2015). The presence of αSyn oligomers within the nucleus also carries significant pathological implications, particularly given the growing recognition that oligomeric αSyn

species may represent especially toxic forms of the protein (Winner et al. 2011; Fusco et al. 2017; Bigi et al. 2023).

Antibody specificity has long posed challenges in detecting aggregated αSyn, particularly in the nuclear compartment. The SynO2 clone was initially reported to be specific to early αSyn oligomers and late amyloid fibrils but not to monomeric αSyn (Vaikath et al. 2015). However, it has more recently been shown to strongly recognize oligomers and fibrils, while also detecting αSyn monomers in a concentration-dependent manner (Kumar et al. 2020). SynO2's specificity toward αSyn aggregates has been revealed to result from avidity rather than structural epitope recognition (Petersen et al. 2023). To address these considerations, we validated our findings using a second conformation-specific antibody, 5G4-αSyn, which exhibits high conformational specificity for αSyn aggregates with minimal signal for monomers (Kumar et al. 2020). 5G4-αSyn has been shown to detect aggregate pathology in synucleinopathic brain regions, while weakly recognizing monomeric protein in Lewy body dementia patient tissue homogenates (Kovacs et al. 2012). Importantly, these antibodies target different regions of the αSyn protein: SynO2's epitope is located within the C-terminal region, while 5G4-αSyn's epitope is situated within the N-terminus (Kovacs et al. 2012; Kumar et al. 2020). This distinction is significant given recent evidence that N-terminus-targeting antibodies exhibit substantial specificity for unique αSyn aggregate morphologies, whereas C-terminus-associated antibodies primarily detect endogenous, non-pathological αSyn (Wiseman et al. 2024).

To overcome the inherent limitations of conformation-specific antibodies, we employed multiple PLA techniques that detect protein interactions through spatial proximity of proteins rather than relying solely on single antibody specificity. First, we used the αSyn-αSyn PLA, which specifically detects αSyn oligomers but not monomers *in-vitro* and can identify small αSyn aggregates in post-mortem brains of PD patients (Roberts et al. 2015; Sekiya et al. 2022). This approach has been extensively validated for investigating αSyn aggregation in numerous studies (Musgrove et al. 2019; Behere et al. 2021; Helwig et al. 2022). Additionally, we established two novel PLAs that combine conformation-specific antibodies (SynO2 and 5G4-αSyn) with the histone H3 antibody to validate the nuclear localization of aggregated αSyn species. Collectively, our complementary approaches provide compelling new evidence that αSyn forms aggregates within the nucleus and that

these aggregates directly interact with histones. This interaction potentially represents a critical link connecting protein aggregation pathology with epigenetic dysregulation.

4.5 Reversibility of αSyn-histone interactions and nuclear clearance mechanisms

We initially proposed a mechanistic model for nuclear accumulation and aggregation based on our findings and the existing literature. The nuclear translocation of αSyn likely occurs primarily through passive diffusion across nuclear pore complexes, facilitated by the protein's relatively small size (16 kDa) and predominantly unfolded structure (Timney et al. 2016). This passive diffusion normally operates bidirectionally, maintaining equilibrium between nuclear and cytoplasmic αSyn pools. αSyn aggregation may disrupt this balance, however, since the increased size of αSyn aggregate species (e.g., oligomers) within the nucleus would prevent their diffusion through the nuclear pores (30-60 kDa threshold), possibly resulting in their progressive, persistent accumulation. We hypothesized that this "trapping" effect may represent a primary mechanism underlying nuclear αSyn retention and give rise to a self-perpetuating cycle of αSyn nuclear translocation, aggregation, and accumulation that would contribute to neuronal dysfunction in synucleinopathies.

To test this hypothesis, we developed a TetOn-inducible system that provides precise temporal control over αSyn overexpression, allowing us to monitor the dynamics of cytosolic and nuclear αSyn accumulation during both the initiation and termination of overexpression. Our doxycycline-inducible AAV-mediated αSyn overexpression rat model successfully regulated protein expression *in-vivo*, with doxycycline withdrawal resulting in a progressive normalization of αSyn levels. Notably, we immediately observed distinct compartment-specific clearance kinetics, with αSyn immunoreactivity diminishing substantially more rapidly in the SNpc (cell bodies) compared to the striatum (projections and synapses) following doxycycline withdrawal. This difference likely reflects at least two underlying mechanisms. First, αSyn undergoes axonal transport and accumulates at presynaptic terminals where it regulates synaptic vesicle trafficking (Burré et al. 2010). Given that αSyn exists in both cytosolic and membrane-associated states (Fortin et al. 2010; Ramalingam and Dettmer 2021), its enrichment at presynaptic terminals may increase the proportion of membrane-bound protein, thereby extending the timeframe required for complete clearance from these regions. Second, regional differences in the

expression and activity of protein degradation machinery between cell bodies in the SNpc and terminals/synapses in the striatum might influence the rate of αSyn clearance, making it relatively more efficient within the perikarya of nigral dopaminergic neurons (Frampton et al. 2012; Farfel-Becker et al. 2020).

Contrary to our initial hypothesis that αSyn, especially in its aggregated form, would remain sequestered within the nucleus following cessation of overexpression, our findings revealed that both monomeric and aggregated nuclear αSyn levels decline in parallel with the cytosolic levels of the protein. Nuclear αSyn-histone interactions, including those involving aggregated αSyn species, were completely reversed within four weeks of halting αSyn overexpression. The marked reduction in human αSyn-histone PLA signals and complete normalization of aggregated αSyn-histone PLA signals suggest robust clearance mechanisms capable of removing various αSyn species from the nuclear compartment. This efficient removal may occur through multiple pathways. One possibility is nucleo-cytoplasmic transport, which would export αSyn from the nucleus for subsequent degradation. However, the diameter of nuclear pores theoretically precludes the passive diffusion of larger αSyn aggregates (Timney et al. 2016). Investigations into active transport mechanisms for nuclear αSyn export remain notably limited, highlighting a critical area that requires further research.

Alternatively, or in addition, it is possible that specialized protein degradation pathways within the nucleus itself may play a crucial role in clearing nuclear αSyn. Two primary mechanisms, the UPS and the autophagy-lysosome pathway, typically degrade αSyn under pathophysiological conditions (Stefanis et al. 2019). However, only a few studies have investigated their relative contribution *in-vivo*. Particularly relevant are the results of one study, in which mechanisms of αSyn degradation were compared in αSyn-overexpressing transgenic mice vs. wild-type controls. These results showed that proteasomal inhibition led to accumulation of both endogenous (in wild-type mice) and overexpressed (in transgenic mice) αSyn, while lysosomal inhibition induced accumulation only in the transgenic overexpression setting (Ebrahimi-Fakhari et al. 2011). This suggests the autophagy-lysosomal pathway is more specifically involved in the degradation of accumulated (overexpressed) αSyn that may be present in the form of misfolded and/or aggregated protein (Ebrahimi-Fakhari et al. 2011).

Nuclei lack autophagic machinery but maintain functional UPS components capable of degrading aberrant proteins and small aggregates (Iwata et al. 2009; den Brave et al. 2020). Based on this consideration, we measured nuclear proteasomal activity under our experimental condition of *in-vivo* αSyn overexpression. Results of this analysis support UPS-mediated nuclear αSyn clearance, demonstrating an efficient mechanism for reducing nuclear αSyn levels and reversing αSyn-histone interactions. Notably, enhanced proteasomal activity was detected specifically in the αSyn-overexpressing hemisphere, indicating a targeted response to nuclear αSyn accumulation. Furthermore, this targeted upregulation was exclusive to αSyn-overexpressing animals, with no comparable response in rats treated with GFP-AAV or Null-AAV. Taken together, these findings indicate that nuclear UPS activation represents a precise, localized mechanism responding to nuclear αSyn accumulation, rather than a generalized consequence of viral exposure or non-nuclear protein overexpression.

The reversibility of αSyn accumulation, as shown using our TetOn-inducible system, bears important implications for our understanding of pathophysiological conditions that are accompanied by enhanced levels of neuronal αSyn and may play a role in PD pathogenic processes (e.g., traumatic brain injury). In general, our observations support strategies targeting αSyn production, such as RNA interference or antisense oligonucleotide approaches, that may effectively reduce αSyn burden even following substantial accumulation. It is noteworthy, however, that the tissue-specific (striatum vs. SN) differences in clearance kinetics identified in our study indicate that such therapeutic interventions may require prolonged treatment periods to achieve complete αSyn reduction across all neuronal compartments (projections vs. cell bodies). Novel, important translational implications are also highlighted by our findings showing the reversal of αSyn-histone interactions and the role of the UPS in clearing nuclear αSyn. These findings underscore the relevance of therapeutic interventions that may effectively mitigate nuclear αSyn accumulation. In particular, they suggest that pharmacological enhancement of nuclear UPS might represent a novel complementary therapeutic approach for synucleinopathies, which could accelerate the clearance of nuclear αSyn and thereby prevent nuclear dysfunction and associated transcriptional dysregulation.

4.6 Conclusion and future outlook

Our study provides compelling evidence for a role of αSyn in the nucleus during PD pathogenesis. We demonstrate that increased αSyn burden, whether induced by AAV-mediated overexpression or paraquat exposure, promotes nuclear translocation of αSyn. Our *in-vivo* data further reveal that nuclear αSyn directly interacts with histones, establishing a mechanistic link between nuclear αSyn and potential transcriptional dysregulation through altered epigenetic modifications. Notably, we show that nuclear αSyn forms aggregates that interact with histone, underscoring a potential pathological mechanism underlying disease progression. Perhaps as significantly, we establish that nuclear αSyn accumulation, aggregation, and αSyn-histone interactions represent reversible processes, with the UPS mediating nuclear αSyn clearance.

While fostering our knowledge of nuclear αSyn pathophysiology, these findings also raise several questions that warrant further investigation.

First, a comprehensive characterization of the transcriptional alterations resulting from nuclear αSyn accumulation would enhance our understanding of downstream pathological cascades. Specifically, genome-wide analyses of chromatin accessibility, histone modifications, and transcriptional profiles in response to αSyn burden could reveal dysregulated gene networks contributing to neurodegenerative processes. Determining whether specific genomic regions are particularly vulnerable to αSyn-mediated disruption might also identify selective cellular vulnerabilities in synucleinopathies.

Second, while we have established reversibility of nuclear αSyn accumulation, the potential persistence of transcriptional dysregulation after αSyn clearance remains unexplored. Epigenetic modifications induced during periods of αSyn nuclear accumulation might persist after protein clearance, creating a “molecular memory” of pathological insult. Determining the temporal relationship between αSyn clearance and epigenetic and transcriptional normalization would provide crucial insights into potential long-term effects of nuclear αSyn accumulation.

Third, age-related alterations in nuclear translocation and clearance mechanisms warrant detailed examination, particularly considering the age-related prevalence of PD and potential age-related impairments of neuronal protein degradation activity. Evidence suggests that intraneuronal αSyn expression is enhanced with age, particularly within

neuronal populations susceptible to PD pathology (Li et al. 2004; Chu and Kordower 2007; Alladi et al. 2010). It is conceivable, therefore, that aging neurons become more susceptible to αSyn nuclear accumulation. This nuclear burden may be exacerbated by age-associated changes in nuclear pore complex integrity, nucleo-cytoplasmic transport efficiency, and nuclear proteasomal activity. Investigations into these processes in aged animal models would more accurately recapitulate pathological processes underlying PD development and progression in humans.

Fourth, a variety of factors could modulate nuclear αSyn dynamics, enhancing or alleviating the deleterious consequences of nuclear αSyn burden. Other environmental stressors beyond paraquat may influence αSyn nuclear translocation. For example, traumatic brain injury is a known PD risk factor capable of affecting neuronal αSyn expression (Uryu et al. 2003) and, therefore, potentially associated with enhanced αSyn nuclear translocation. Future studies elucidating the relationship between PD environmental risk factors and nuclear αSyn burden bear important public health implications since they may point to specific preventive strategies and policies. Other factors that could modulate PD pathology include nutrition and exercise. In a recent study, intermittent fasting has been shown to significantly affect αSyn pathology in an animal model of PD (Szegő et al. 2025). It remains unknown, however, if dietary changes (as well as other lifestyle practices such as physical activity) impact on cellular αSyn levels and disposition. Studies examining the effects of specific dietary or exercise interventions on nuclear αSyn expression and nuclear αSyn accumulation/clearance could identify modifiable lifestyle factors relevant to disease prevention and/or progression.

Fifth, comparative analysis of clearance mechanisms operating under different αSyn accumulation conditions (e.g., AAV-induced overexpression vs. paraquat exposure vs aging) would likely provide valuable insights into context-dependent nuclear clearance responses. Another important focus of future investigations should be to determine whether chronic αSyn accumulation eventually overwhelms nuclear clearance mechanisms. Impairment of these mechanisms could not only exacerbate the toxic consequences of αSyn burden but may also negatively affect nuclear function and cytoplasmic-nuclear interactions.

Finally, our findings support a role of nuclear αSyn as a significant contributor to PD pathogenetic processes while identifying its clearance as a promising therapeutic

target. The reversibility of nuclear αSyn accumulation and αSyn-histone interactions demonstrated in our study requires further investigation to determine whether αSyn clearance fully reverses its epigenetic effects or if certain modifications persist. If so, changes in nuclear αSyn could influence disease development and progression over a longer period, even after protein levels are normalized.

5. Abstract

Pathological accumulation of alpha-synuclein (αSyn) is a hallmark of Parkinson's disease (PD). While αSyn primarily localizes at synaptic terminals under physiological conditions, emerging evidence suggests translocation to the nucleus may contribute to PD pathophysiology. Despite growing interest in nuclear αSyn, previous detection methods have lacked reliability, and critical questions regarding the mechanisms of nuclear translocation, intranuclear αSyn behavior, and potential reversibility of nuclear accumulation remain unanswered. This study aimed to establish robust methodologies for detecting nuclear αSyn, to elucidate conditions prompting nuclear αSyn translocation, and to assess intranuclear consequences and clearance dynamics following αSyn nuclear accumulation.

We utilized three complementary *in-vivo* models: constitutive αSyn overexpression via intraparenchymal injections of adeno-associated viral vectors in the rat substantia nigra; a doxycycline-inducible system allowing for controlled initiation and cessation of αSyn overexpression; and nigrostriatal pathology triggered by systemic paraquat injections. Comprehensive analyses included immunohistochemistry, multiple proximity ligation assays (PLAs), co-immunoprecipitation (Co-IP), and proteasome activity assays.

Across all models, increased neuronal αSyn expression promoted its nuclear translocation. Once it gained access into the nuclei, αSyn directly interacted with histones, as demonstrated by our novel PLA approach and confirmed by Co-IP. αSyn overexpression altered epigenetic modifications, indicating a potential mechanistic link to transcriptional dysregulation. Moreover, our data revealed that nuclear αSyn formed aggregates that also interact with histones. Finally, using the doxycycline-regulated model, we demonstrated for the first time that nuclear αSyn accumulation, aggregation, and αSyn-histone interactions were reversible upon cessation of αSyn overexpression. This reversibility was due, at least in part, to αSyn clearance facilitated by the nuclear ubiquitin-proteasome system.

In summary, using multiple *in-vivo* approaches and analytical techniques, we provide compelling new evidence for conditions and mechanisms associated with αSyn nuclear translocation and accumulation that may play a role in pathogenic processes in PD and other synucleinopathies. Our findings support the conclusion that nuclear αSyn and αSyn-histone interactions should be considered important therapeutic targets. One strategy for

therapeutic intervention could be to reverse the deleterious effects of nuclear αSyn accumulation by promoting specific mechanisms involved in nuclear αSyn clearance.

6. List of figures

7. List of tables

8. References

Abdelmotilib, H., Maltbie, T., Delic, V., et al. 2017. α-Synuclein fibril-induced inclusion spread in rats and mice correlates with dopaminergic Neurodegeneration. *Neurobiology of Disease* 105, pp. 84–98.

Abounit, S., Bousset, L., Loria, F., et al. 2016. Tunneling nanotubes spread fibrillar α-synuclein by intercellular trafficking of lysosomes. *The EMBO Journal* 35(19), pp. 2120–2138.

Acosta, S.A., Tajiri, N., de la Pena, I., et al. 2015. Alpha-synuclein as a pathological link between chronic traumatic brain injury and Parkinson's disease. *Journal of Cellular Physiology* 230(5), pp. 1024–1032.

Adler, C.H. and Beach, T.G. 2016. Neuropathological basis of nonmotor manifestations of Parkinson's disease. *Movement Disorders* 31(8), pp. 1114–1119.

Ahn, K.J., Paik, S.R., Chung, K.C. and Kim, J. 2006. Amino acid sequence motifs and mechanistic features of the membrane translocation of alpha-synuclein. *Journal of Neurochemistry* 97(1), pp. 265–279.

Alam, P., Bousset, L., Melki, R. and Otzen, D.E. 2019. α-synuclein oligomers and fibrils: a spectrum of species, a spectrum of toxicities. *Journal of Neurochemistry* 150(5), pp. 522–534.

Albert, K., Voutilainen, M.H., Domanskyi, A., et al. 2019. Downregulation of tyrosine hydroxylase phenotype after AAV injection above substantia nigra: Caution in experimental models of Parkinson's disease. *Journal of Neuroscience Research* 97(3), pp. 346–361.

Ali Hosseini Rad, S.M., Poudel, A., Tan, G.M.Y. and McLellan, A.D. 2020. Optimisation of Tet-On inducible systems for Sleeping Beauty-based chimeric antigen receptor (CAR) applications. *Scientific Reports* 10(1), p. 13125.

Alladi, P.A., Mahadevan, A., Vijayalakshmi, K., Muthane, U., Shankar, S.K. and Raju, T.R. 2010. Ageing enhances alpha-synuclein, ubiquitin and endoplasmic reticular stress protein expression in the nigral neurons of Asian Indians. *Neurochemistry International* 57(5), pp. 530–539.

Altay, M.F., Kumar, S.T., Burtscher, J., et al. 2023. Development and validation of an expanded antibody toolset that captures alpha-synuclein pathological diversity in Lewy body diseases. *npj Parkinson's Disease* 9(1), p. 161.

Alvarez-Erviti, L., Seow, Y., Schapira, A.H., et al. 2011. Lysosomal dysfunction increases exosome-mediated alpha-synuclein release and transmission. *Neurobiology of Disease* 42(3), pp. 360–367.

Armstrong, M.J. and Okun, M.S. 2020. Diagnosis and treatment of parkinson disease: A review. *The Journal of the American Medical Association* 323(6), pp. 548–560.

Ascherio, A. and Schwarzschild, M.A. 2016. The epidemiology of Parkinson's disease: risk factors and prevention. *Lancet Neurology* 15(12), pp. 1257–1272.

Bakhit, Y., Schmitt, I., Hamed, A., et al. 2022. Methylation of alpha-synuclein in a Sudanese cohort. *Parkinsonism & Related Disorders* 101, pp. 6–8.

Bandres-Ciga, S., Diez-Fairen, M., Kim, J.J. and Singleton, A.B. 2020. Genetics of Parkinson's disease: An introspection of its journey towards precision medicine. *Neurobiology of Disease* 137, p. 104782.

Behere, A., Thörnqvist, P.-O., Winberg, S., Ingelsson, M., Bergström, J. and Ekmark-Lewén, S. 2021. Visualization of early oligomeric α-synuclein pathology and its impact on the dopaminergic system in the (Thy-1)-h[A30P]α-syn transgenic mouse model. *Journal of Neuroscience Research* 99(10), pp. 2525–2539.

Bellou, V., Belbasis, L., Tzoulaki, I., Evangelou, E. and Ioannidis, J.P.A. 2016. Environmental risk factors and Parkinson's disease: An umbrella review of meta-analyses. *Parkinsonism & Related Disorders* 23, pp. 1–9.

Ben Gedalya, T., Loeb, V., Israeli, E., Altschuler, Y., Selkoe, D.J. and Sharon, R. 2009. Alpha-synuclein and polyunsaturated fatty acids promote clathrin-mediated endocytosis and synaptic vesicle recycling. *Traffic* 10(2), pp. 218–234.

Betarbet, R., Sherer, T.B., MacKenzie, G., Garcia-Osuna, M., Panov, A.V. and Greenamyre, J.T. 2000. Chronic systemic pesticide exposure reproduces features of Parkinson's disease. *Nature Neuroscience* 3(12), pp. 1301–1306.

Bigi, A., Cascella, R. and Cecchi, C. 2023. α-Synuclein oligomers and fibrils: partners in crime in synucleinopathies. *Neural regeneration research* 18(11), pp. 2332–2342.

Blauwendraat, C., Nalls, M.A. and Singleton, A.B. 2020. The genetic architecture of Parkinson's disease. *Lancet Neurology* 19(2), pp. 170–178.

Bloem, B.R., Okun, M.S. and Klein, C. 2021. Parkinson's disease. *The Lancet* 397(10291), pp. 2284–2303.

Braak, H., Del Tredici, K., Rüb, U., de Vos, R.A.I., Jansen Steur, E.N.H. and Braak, E. 2003. Staging of brain pathology related to sporadic Parkinson's disease. *Neurobiology of Aging* 24(2), pp. 197–211.

Braak, H., Rüb, U., Jansen Steur, E.N.H., Del Tredici, K. and de Vos, R.A.I. 2005. Cognitive status correlates with neuropathologic stage in Parkinson disease. *Neurology* 64(8), pp. 1404–1410.

den Brave, F., Cairo, L.V., Jagadeesan, C., et al. 2020. Chaperone-Mediated Protein Disaggregation Triggers Proteolytic Clearance of Intra-nuclear Protein Inclusions. *Cell reports* 31(9), p. 107680.

Brown, D.R. 2007. Interactions between metals and alpha-synuclein--function or artefact? *The FEBS Journal* 274(15), pp. 3766–3774.

Burbulla, L.F., Song, P., Mazzulli, J.R., et al. 2017. Dopamine oxidation mediates mitochondrial and lysosomal dysfunction in Parkinson's disease. *Science* 357(6357), pp. 1255–1261.

Burré, J., Sharma, M., Tsetsenis, T., Buchman, V., Etherton, M.R. and Südhof, T.C. 2010. Alpha-synuclein promotes SNARE-complex assembly in vivo and in vitro. *Science* 329(5999), pp. 1663–1667.

Cavalli, G. and Heard, E. 2019. Advances in epigenetics link genetics to the environment and disease. *Nature* 571(7766), pp. 489–499.

Chandra, S., Chen, X., Rizo, J., Jahn, R. and Südhof, T.C. 2003. A broken alpha -helix in folded alpha -Synuclein. *The Journal of Biological Chemistry* 278(17), pp. 15313–15318.

Chartier-Harlin, M.-C., Kachergus, J., Roumier, C., et al. 2004. Alpha-synuclein locus duplication as a cause of familial Parkinson's disease. *The Lancet* 364(9440), pp. 1167–1169.

Chaudhuri, K.R. and Schapira, A.H.V. 2009. Non-motor symptoms of Parkinson's disease: dopaminergic pathophysiology and treatment. *Lancet Neurology* 8(5), pp. 464–474.

Chen, K., Bennett, S.A., Rana, N., et al. 2018. Neurodegenerative Disease Proteinopathies Are Connected to Distinct Histone Post-translational Modification Landscapes. *ACS Chemical Neuroscience* 9(4), pp. 838–848.

Chen, V., Moncalvo, M., Tringali, D., et al. 2020. The mechanistic role of alpha-synuclein in the nucleus: impaired nuclear function caused by familial Parkinson's disease SNCA mutations. *Human Molecular Genetics* 29(18), pp. 3107–3121.

Cherny, D., Hoyer, W., Subramaniam, V. and Jovin, T.M. 2004. Double-stranded DNA stimulates the fibrillation of alpha-synuclein in vitro and is associated with the mature fibrils: an electron microscopy study. *Journal of Molecular Biology* 344(4), pp. 929–938.

Chinta, S.J., Mallajosyula, J.K., Rane, A. and Andersen, J.K. 2010. Mitochondrial α-synuclein accumulation impairs complex I function in dopaminergic neurons and results in increased mitophagy in vivo. *Neuroscience Letters* 486(3), pp. 235–239.

Choi, B.-K., Choi, M.-G., Kim, J.-Y., et al. 2013. Large α-synuclein oligomers inhibit neuronal SNARE-mediated vesicle docking. *Proceedings of the National Academy of Sciences of the United States of America* 110(10), pp. 4087–4092.

Chorfa, A., Bétemps, D., Morignat, E., et al. 2013. Specific pesticide-dependent increases in α-synuclein levels in human neuroblastoma (SH-SY5Y) and melanoma (SK-MEL-2) cell lines. *Toxicological Sciences* 133(2), pp. 289–297.

Chu, Y. and Kordower, J.H. 2007. Age-associated increases of alpha-synuclein in monkeys and humans are associated with nigrostriatal dopamine depletion: Is this the target for Parkinson's disease? *Neurobiology of Disease* 25(1), pp. 134–149.

Chung, C.Y., Khurana, V., Yi, S., et al. 2017. In Situ Peroxidase Labeling and Mass-Spectrometry Connects Alpha-Synuclein Directly to Endocytic Trafficking and mRNA Metabolism in Neurons. *Cell Systems* 4(2), p. 242–250.e4.

Chung, H.K., Ho, H.-A., Pérez-Acuña, D. and Lee, S.-J. 2019. Modeling α-Synuclein Propagation with Preformed Fibril Injections. *Journal of movement disorders* 12(3), pp. 139–151.

Colla, E., Jensen, P.H., Pletnikova, O., Troncoso, J.C., Glabe, C. and Lee, M.K. 2012. Accumulation of toxic α-synuclein oligomer within endoplasmic reticulum occurs in α-synucleinopathy in vivo. *The Journal of Neuroscience* 32(10), pp. 3301–3305.

Corasaniti, M.T., Bagetta, G., Rodinò, P., Gratteri, S. and Nisticò, G. 1992. Neurotoxic effects induced by intracerebral and systemic injection of paraquat in rats. *Human & Experimental Toxicology* 11(6), pp. 535–539.

Costello, S., Cockburn, M., Bronstein, J., Zhang, X. and Ritz, B. 2009. Parkinson's disease and residential exposure to maneb and paraquat from agricultural applications in the central valley of California. *American Journal of Epidemiology* 169(8), pp. 919–926.

Danzer, K.M., Haasen, D., Karow, A.R., et al. 2007. Different species of alpha-synuclein oligomers induce calcium influx and seeding. *The Journal of Neuroscience* 27(34), pp. 9220–9232.

Danzer, K.M., Ruf, W.P., Putcha, P., et al. 2011. Heat-shock protein 70 modulates toxic extracellular α-synuclein oligomers and rescues trans-synaptic toxicity. *The FASEB Journal* 25(1), pp. 326–336.

Das, A.T., Tenenbaum, L. and Berkhout, B. 2016. Tet-On Systems For Doxycycline-inducible Gene Expression. *Current Gene Therapy* 16(3), pp. 156–167.

Davidi, D., Schechter, M., Elhadi, S.A., Matatov, A., Nathanson, L. and Sharon, R. 2020. α-Synuclein Translocates to the Nucleus to Activate Retinoic-Acid-Dependent Gene Transcription. *iScience* 23(3), p. 100910.

Davidson, W.S., Jonas, A., Clayton, D.F. and George, J.M. 1998. Stabilization of alpha-synuclein secondary structure upon binding to synthetic membranes. *The Journal of Biological Chemistry* 273(16), pp. 9443–9449.

Decressac, Mickael, Kadkhodaei, B., Mattsson, B., Laguna, A., Perlmann, T. and Björklund, A. 2012. α-Synuclein-induced down-regulation of Nurr1 disrupts GDNF signaling in nigral dopamine neurons. *Science Translational Medicine* 4(163), p. 163ra156.

Decressac, M, Mattsson, B., Lundblad, M., Weikop, P. and Björklund, A. 2012. Progressive neurodegenerative and behavioural changes induced by AAV-mediated overexpression of α-synuclein in midbrain dopamine neurons. *Neurobiology of Disease* 45(3), pp. 939–953.

Delic, V., Chandra, S., Abdelmotilib, H., et al. 2018. Sensitivity and specificity of phospho-Ser129 α-synuclein monoclonal antibodies. *The Journal of Comparative Neurology* 526(12), pp. 1978–1990.

Deliz, J.R., Tanner, C.M. and Gonzalez-Latapi, P. 2024. Epidemiology of parkinson's disease: an update. *Current Neurology and Neuroscience Reports* 24(6), pp. 163–179.

Dent, S.E., King, D.P., Osterberg, V.R., et al. 2022. Phosphorylation of the aggregate-forming protein alpha-synuclein on serine-129 inhibits its DNA-bending properties. *The Journal of Biological Chemistry* 298(2), p. 101552.

Desplats, P., Lee, H.-J., Bae, E.-J., et al. 2009. Inclusion formation and neuronal cell death through neuron-to-neuron transmission of alpha-synuclein. *Proceedings of the National Academy of Sciences of the United States of America* 106(31), pp. 13010–13015.

Desplats, P., Spencer, B., Coffee, E., et al. 2011. Alpha-synuclein sequesters Dnmt1 from the nucleus: a novel mechanism for epigenetic alterations in Lewy body diseases. *The Journal of Biological Chemistry* 286(11), pp. 9031–9037.

Desplats, P., Spencer, B., Crews, L., et al. 2012. α-Synuclein induces alterations in adult neurogenesis in Parkinson disease models via p53-mediated repression of Notch1. *The Journal of Biological Chemistry* 287(38), pp. 31691–31702.

Devi, L., Raghavendran, V., Prabhu, B.M., Avadhani, N.G. and Anandatheerthavarada, H.K. 2008. Mitochondrial import and accumulation of alpha-synuclein impair complex I in human dopaminergic neuronal cultures and Parkinson disease brain. *The Journal of Biological Chemistry* 283(14), pp. 9089–9100.

Dhillon, A.S., Tarbutton, G.L., Levin, J.L., et al. 2008. Pesticide/environmental exposures and Parkinson's disease in East Texas. *Journal of agromedicine* 13(1), pp. 37–48.

Di Nisio, E., Lupo, G., Licursi, V. and Negri, R. 2021. The role of histone lysine methylation in the response of mammalian cells to ionizing radiation. *Frontiers in genetics* 12, p. 639602.

Dickson, D.W., Braak, H., Duda, J.E., et al. 2009. Neuropathological assessment of Parkinson's disease: refining the diagnostic criteria. *Lancet Neurology* 8(12), pp. 1150–1157.

Dieriks, B.V., Park, T.I.-H., Fourie, C., Faull, R.L.M., Dragunow, M. and Curtis, M.A. 2017. α-synuclein transfer through tunneling nanotubes occurs in SH-SY5Y cells and primary brain pericytes from Parkinson's disease patients. *Scientific Reports* 7, p. 42984.

Ding, H., Fineberg, N.S., Gray, M. and Yacoubian, T.A. 2013. α-Synuclein Overexpression Represses 14-3-3θ Transcription. *Journal of Molecular Neuroscience*.

Domenger, C. and Grimm, D. 2019. Next-generation AAV vectors-do not judge a virus (only) by its cover. *Human Molecular Genetics* 28(R1), pp. R3–R14.

Dorsey, E.R., Sherer, T., Okun, M.S. and Bloem, B.R. 2018. The emerging evidence of the parkinson pandemic. *Journal of Parkinson's disease* 8(s1), pp. S3–S8.

Doxakis, E. 2010. Post-transcriptional regulation of alpha-synuclein expression by mir-7 and mir-153. *The Journal of Biological Chemistry* 285(17), pp. 12726–12734.

Du, T., Li, G., Zong, Q., Luo, H., Pan, Y. and Ma, K. 2024. Nuclear alpha-synuclein accelerates cell senescence and neurodegeneration. *Immunity & ageing : I & A* 21(1), p. 47.

Duffy, M.F., Collier, T.J., Patterson, J.R., et al. 2018. Lewy body-like alpha-synuclein inclusions trigger reactive microgliosis prior to nigral degeneration. *Journal of Neuroinflammation* 15(1), p. 129.

Duplan, E., Giordano, C., Checler, F. and Alves da Costa, C. 2016. Direct α-synuclein promoter transactivation by the tumor suppressor p53. *Molecular Neurodegeneration* 11(1), p. 13.

Ebrahimi-Fakhari, D., Cantuti-Castelvetri, I., Fan, Z., et al. 2011. Distinct roles in vivo for the ubiquitin-proteasome system and the autophagy-lysosomal pathway in the degradation of α-synuclein. *The Journal of Neuroscience* 31(41), pp. 14508–14520.

Ebrahimi-Fakhari, D., McLean, P.J. and Unni, V.K. 2012. Alpha-synuclein's degradation in vivo: opening a new (cranial) window on the roles of degradation pathways in Parkinson disease. *Autophagy* 8(2), pp. 281–283.

Elfarrash, S., Jensen, N.M., Ferreira, N., et al. 2021. Polo-like kinase 2 inhibition reduces serine-129 phosphorylation of physiological nuclear alpha-synuclein but not of the aggregated alpha-synuclein. *Plos One* 16(10), p. e0252635.

Eliezer, D., Kutluay, E., Bussell, R. and Browne, G. 2001. Conformational properties of alpha-synuclein in its free and lipid-associated states. *Journal of Molecular Biology* 307(4), pp. 1061–1073.

Emmanouilidou, E., Melachroinou, K., Roumeliotis, T., et al. 2010. Cell-produced alpha-synuclein is secreted in a calcium-dependent manner by exosomes and impacts neuronal survival. *The Journal of Neuroscience* 30(20), pp. 6838–6851.

Eschbach, J., von Einem, B., Müller, K., et al. 2015. Mutual exacerbation of peroxisome proliferator-activated receptor γ coactivator 1α deregulation and α-synuclein oligomerization. *Annals of Neurology* 77(1), pp. 15–32.

Fares, M.-B., Ait-Bouziad, N., Dikiy, I., et al. 2014. The novel Parkinson's disease linked mutation G51D attenuates in vitro aggregation and membrane binding of α-synuclein, and enhances its secretion and nuclear localization in cells. *Human Molecular Genetics* 23(17), pp. 4491–4509.

Farfel-Becker, T., Roney, J.C., Cheng, X.-T., Li, S., Cuddy, S.R. and Sheng, Z.-H. 2020. The secret life of degradative lysosomes in axons: delivery from the soma, enzymatic activity, and local autophagic clearance. *Autophagy* 16(1), pp. 167–168.

Farrelly, L.A., Thompson, R.E., Zhao, S., et al. 2019. Histone serotonylation is a permissive modification that enhances TFIID binding to H3K4me3. *Nature* 567(7749), pp. 535–539.

Farrer, M., Kachergus, J., Forno, L., et al. 2004. Comparison of kindreds with parkinsonism and alpha-synuclein genomic multiplications. *Annals of Neurology* 55(2), pp. 174–179.

Fernagut, P.O., Hutson, C.B., Fleming, S.M., et al. 2007. Behavioral and histopathological consequences of paraquat intoxication in mice: effects of alpha-synuclein over-expression. *Synapse* 61(12), pp. 991–1001.

Forno, L.S. and Norville, R.L. 1976. Ultrastructure of Lewy bodies in the stellate ganglion. *Acta Neuropathologica* 34(3), pp. 183–197.

Fortin, D.L., Nemani, V.M., Nakamura, K. and Edwards, R.H. 2010. The behavior of alpha-synuclein in neurons. *Movement Disorders* 25 Suppl 1, pp. S21-6.

Fox, S.H. and Brotchie, J.M. 2010. The MPTP-lesioned non-human primate models of Parkinson's disease. Past, present, and future. In: *Recent Advances in Parkinson'S Disease - Translational and Clinical Research*. Progress in brain research. Elsevier, pp. 133–157.

Fox, S.H., Katzenschlager, R., Lim, S.-Y., et al. 2018. International Parkinson and movement disorder society evidence-based medicine review: Update on treatments for the motor symptoms of Parkinson's disease. *Movement Disorders* 33(8), pp. 1248–1266.

Frampton, J.P., Guo, C. and Pierchala, B.A. 2012. Expression of axonal protein degradation machinery in sympathetic neurons is regulated by nerve growth factor. *Journal of Neuroscience Research* 90(8), pp. 1533–1546.

Fuchs, J., Tichopad, A., Golub, Y., et al. 2008. Genetic variability in the SNCA gene influences alpha-synuclein levels in the blood and brain. *The FASEB Journal* 22(5), pp. 1327–1334.

Fusco, G., Chen, S.W., Williamson, P.T.F., et al. 2017. Structural basis of membrane disruption and cellular toxicity by α-synuclein oligomers. *Science* 358(6369), pp. 1440–1443.

Garcia-Esparcia, P., Hernández-Ortega, K., Koneti, A., et al. 2015. Altered machinery of protein synthesis is region- and stage-dependent and is associated with α-synuclein oligomers in Parkinson's disease. *Acta neuropathologica communications* 3, p. 76.

Garcia-Reitböck, P., Anichtchik, O., Bellucci, A., et al. 2010. SNARE protein redistribution and synaptic failure in a transgenic mouse model of Parkinson's disease. *Brain: A Journal of Neurology* 133(Pt 7), pp. 2032–2044.

Gebremedhin, K.G. and Rademacher, D.J. 2016. Histone H3 acetylation in the postmortem Parkinson's disease primary motor cortex. *Neuroscience Letters* 627, pp. 121–125.

George, J.M., Jin, H., Woods, W.S. and Clayton, D.F. 1995. Characterization of a novel protein regulated during the critical period for song learning in the zebra finch. *Neuron* 15(2), pp. 361–372.

Giasson, B.I., Murray, I.V., Trojanowski, J.Q. and Lee, V.M. 2001. A hydrophobic stretch of 12 amino acid residues in the middle of alpha-synuclein is essential for filament assembly. *The Journal of Biological Chemistry* 276(4), pp. 2380–2386.

Gillam, J.E. and MacPhee, C.E. 2013. Modelling amyloid fibril formation kinetics: mechanisms of nucleation and growth. *Journal of Physics. Condensed Matter* 25(37), p. 373101.

Goers, J., Manning-Bog, A.B., McCormack, A.L., et al. 2003. Nuclear localization of alpha-synuclein and its interaction with histones. *Biochemistry* 42(28), pp. 8465–8471.

Goldman, S.M., Marek, K., Ottman, R., et al. 2019. Concordance for Parkinson's disease in twins: A 20-year update. *Annals of Neurology* 85(4), pp. 600–605.

Goldman, S.M., Weaver, F.M., Gonzalez, B., et al. 2024. Parkinson's disease progression and exposure to contaminated water at camp lejeune. *Movement Disorders*.

Gonçalves, S. and Outeiro, T.F. 2013. Assessing the subcellular dynamics of alpha-synuclein using photoactivation microscopy. *Molecular Neurobiology* 47(3), pp. 1081–1092.

Gossen, M. and Bujard, H. 1992. Tight control of gene expression in mammalian cells by tetracycline-responsive promoters. *Proceedings of the National Academy of Sciences of the United States of America* 89(12), pp. 5547–5551.

Grotewold, N. and Albin, R.L. 2024. Update: Protective and risk factors for Parkinson disease. *Parkinsonism & Related Disorders* 125, p. 107026.

Grozdanov, V. and Danzer, K.M. 2018. Release and uptake of pathologic alpha-synuclein. *Cell and Tissue Research* 373(1), pp. 175–182.

Grünblatt, E., Mandel, S., Jacob-Hirsch, J., et al. 2004. Gene expression profiling of parkinsonian substantia nigra pars compacta; alterations in ubiquitin-proteasome, heat shock protein, iron and oxidative stress regulated proteins, cell adhesion/cellular matrix and vesicle trafficking genes. *Journal of Neural Transmission* 111(12), pp. 1543–1573.

Gundersen, H.J. and Jensen, E.B. 1987. The efficiency of systematic sampling in stereology and its prediction. *Journal of Microscopy* 147(Pt 3), pp. 229–263.

Halliday, G.M., Holton, J.L., Revesz, T. and Dickson, D.W. 2011. Neuropathology underlying clinical variability in patients with synucleinopathies. *Acta Neuropathologica* 122(2), pp. 187–204.

Halliday, G.M., Ophof, A., Broe, M., et al. 2005. Alpha-synuclein redistributes to neuromelanin lipid in the substantia nigra early in Parkinson's disease. *Brain: A Journal of Neurology* 128(Pt 11), pp. 2654–2664.

Harrison, I.F., Smith, A.D. and Dexter, D.T. 2018. Pathological histone acetylation in Parkinson's disease: Neuroprotection and inhibition of microglial activation through SIRT 2 inhibition. *Neuroscience Letters* 666, pp. 48–57.

Hashimoto, M., Takenouchi, T., Rockenstein, E. and Masliah, E. 2003. Alpha-synuclein up-regulates expression of caveolin-1 and down-regulates extracellular signal-regulated kinase activity in B103 neuroblastoma cells: role in the pathogenesis of Parkinson's disease. *Journal of Neurochemistry* 85(6), pp. 1468–1479.

Hegde, M.L. and Rao, K.S.J. 2007. DNA induces folding in alpha-synuclein: understanding the mechanism using chaperone property of osmolytes. *Archives of Biochemistry and Biophysics* 464(1), pp. 57–69.

Heikkila, R.E., Cabbat, F.S., Manzino, L. and Duvoisin, R.C. 1984. Effects of 1-methyl-4-phenyl-1,2,5,6-tetrahydropyridine on neostriatal dopamine in mice. *Neuropharmacology* 23(6), pp. 711–713.

Helwig, M., Klinkenberg, M., Rusconi, R., et al. 2016. Brain propagation of transduced α-synuclein involves non-fibrillar protein species and is enhanced in α-synuclein null mice. *Brain: A Journal of Neurology* 139(Pt 3), pp. 856–870.

Helwig, M., Ulusoy, A., Rollar, A., et al. 2022. Neuronal hyperactivity-induced oxidant stress promotes in vivo α-synuclein brain spreading. *Science Advances* 8(35), p. eabn0356.

Hinderer, C., Katz, N., Buza, E.L., et al. 2018. Severe Toxicity in Nonhuman Primates and Piglets Following High-Dose Intravenous Administration of an Adeno-Associated Virus Vector Expressing Human SMN. *Human Gene Therapy* 29(3), pp. 285–298.

Hinnell, C., Hurt, C.S., Landau, S., Brown, R.G., Samuel, M. and PROMS-PD Study Group 2012. Nonmotor versus motor symptoms: how much do they matter to health status in Parkinson's disease? *Movement Disorders* 27(2), pp. 236–241.

Hoyer, W., Cherny, D., Subramaniam, V. and Jovin, T.M. 2004. Impact of the acidic C-terminal region comprising amino acids 109-140 on alpha-synuclein aggregation in vitro. *Biochemistry* 43(51), pp. 16233–16242.

Huang, M., Lou, D., Charli, A., et al. 2021. Mitochondrial dysfunction–induced H3K27 hyperacetylation perturbs enhancers in Parkinson's disease. *JCI Insight*.

Huang, Z., Xu, Z., Wu, Y. and Zhou, Y. 2011. Determining nuclear localization of alpha-synuclein in mouse brains. *Neuroscience* 199, pp. 318–332.

Hudry, E. and Vandenberghe, L.H. 2019. Therapeutic AAV gene transfer to the nervous system: A clinical reality. *Neuron* 101(5), pp. 839–862.

Ilijic, E., Guzman, J.N. and Surmeier, D.J. 2011. The L-type channel antagonist isradipine is neuroprotective in a mouse model of Parkinson's disease. *Neurobiology of Disease* 43(2), pp. 364–371.

Ingelsson, M. 2016. Alpha-Synuclein Oligomers-Neurotoxic Molecules in Parkinson's Disease and Other Lewy Body Disorders. *Frontiers in Neuroscience* 10, p. 408.

Iwai, A., Masliah, E., Yoshimoto, M., et al. 1995. The precursor protein of non-A beta component of Alzheimer's disease amyloid is a presynaptic protein of the central nervous system. *Neuron* 14(2), pp. 467–475.

Iwata, A., Miura, S., Kanazawa, I., Sawada, M. and Nukina, N. 2001. alpha-Synuclein forms a complex with transcription factor Elk-1. *Journal of Neurochemistry* 77(1), pp. 239–252.

Iwata, A., Nagashima, Y., Matsumoto, L., et al. 2009. Intranuclear degradation of polyglutamine aggregates by the ubiquitin-proteasome system. *The Journal of Biological Chemistry* 284(15), pp. 9796–9803.

Jakes, R., Spillantini, M.G. and Goedert, M. 1994. Identification of two distinct synucleins from human brain. *FEBS Letters* 345(1), pp. 27–32.

Jang, A., Lee, H.-J., Suk, J.-E., Jung, J.-W., Kim, K.-P. and Lee, S.-J. 2010. Non-classical exocytosis of alpha-synuclein is sensitive to folding states and promoted under stress conditions. *Journal of Neurochemistry* 113(5), pp. 1263–1274.

Jellinger, K.A. 2011. Synuclein deposition and non-motor symptoms in Parkinson disease. *Journal of the Neurological Sciences* 310(1–2), pp. 107–111.

Jensen, P.H., Li, J.Y., Dahlström, A. and Dotti, C.G. 1999. Axonal transport of synucleins is mediated by all rate components. *The European Journal of Neuroscience* 11(10), pp. 3369–3376.

Jiang, H., Jackson-Lewis, V., Muthane, U., et al. 1993. Adenosine receptor antagonists potentiate dopamine receptor agonist-induced rotational behavior in 6-hydroxydopamine-lesioned rats. *Brain Research* 613(2), pp. 347–351.

Jiang, P., Gan, M. and Dickson, D.W. 2021. Apoptotic Neuron-Derived Histone Amyloid Fibrils Induce α-Synuclein Aggregation. *Molecular Neurobiology* 58(2), pp. 867–876.

Jiang, P., Gan, M., Yen, S.-H., McLean, P.J. and Dickson, D.W. 2017. Histones facilitate α-synuclein aggregation during neuronal apoptosis. *Acta Neuropathologica* 133(4), pp. 547–558.

Jiang, P., Gan, M., Yen, S.-H., Moussaud, S., McLean, P.J. and Dickson, D.W. 2016. Proaggregant nuclear factor(s) trigger rapid formation of α-synuclein aggregates in apoptotic neurons. *Acta Neuropathologica* 132(1), pp. 77–91.

Jin, H., Kanthasamy, A., Ghosh, A., Yang, Y., Anantharam, V. and Kanthasamy, A.G. 2011. α-Synuclein negatively regulates protein kinase Cδ expression to suppress apoptosis in dopaminergic neurons by reducing p300 histone acetyltransferase activity. *The Journal of Neuroscience* 31(6), pp. 2035–2051.

Jos, S., Gogoi, H., Prasad, T.K., et al. 2021. Molecular insights into α-synuclein interaction with individual human core histones, linker histone, and dsDNA. *Protein Science* 30(10), pp. 2121–2131.

Jowaed, A., Schmitt, I., Kaut, O. and Wüllner, U. 2010. Methylation regulates alpha-synuclein expression and is decreased in Parkinson's disease patients' brains. *The Journal of Neuroscience* 30(18), pp. 6355–6359.

Junn, E., Lee, K.-W., Jeong, B.S., Chan, T.W., Im, J.-Y. and Mouradian, M.M. 2009. Repression of alpha-synuclein expression and toxicity by microRNA-7. *Proceedings of the National Academy of Sciences of the United States of America* 106(31), pp. 13052–13057.

Kabaria, S., Choi, D.C., Chaudhuri, A.D., Mouradian, M.M. and Junn, E. 2015. Inhibition of miR-34b and miR-34c enhances α-synuclein expression in Parkinson's disease. *FEBS Letters* 589(3), pp. 319–325.

Kalia, L.V. and Lang, A.E. 2015. Parkinson's disease. *The Lancet* 386(9996), pp. 896–912.

Karampetsou, M., Ardah, M.T., Semitekolou, M., et al. 2017. Phosphorylated exogenous alpha-synuclein fibrils exacerbate pathology and induce neuronal dysfunction in mice. *Scientific Reports* 7(1), p. 16533.

Khan, E., Hasan, I. and Haque, M.E. 2023. Parkinson's disease: exploring different animal model systems. *International Journal of Molecular Sciences* 24(10).

Kim, J.J., Vitale, D., Otani, D.V., et al. 2024. Multi-ancestry genome-wide association meta-analysis of Parkinson's disease. *Nature Genetics* 56(1), pp. 27–36.

Kim, T., Mehta, S.L., Kaimal, B., Lyons, K., Dempsey, R.J. and Vemuganti, R. 2016. Poststroke Induction of α-Synuclein Mediates Ischemic Brain Damage. *The Journal of Neuroscience* 36(26), pp. 7055–7065.

Kirik, D., Georgievska, B., Burger, C., et al. 2002. Reversal of motor impairments in parkinsonian rats by continuous intrastriatal delivery of L-dopa using rAAV-mediated gene transfer. *Proceedings of the National Academy of Sciences of the United States of America* 99(7), pp. 4708–4713.

Kirik, D., Rosenblad, C., Burger, C., et al. 2002. Parkinson-like neurodegeneration induced by targeted overexpression of alpha-synuclein in the nigrostriatal system. *The Journal of Neuroscience* 22(7), pp. 2780–2791.

Klein, R.L., King, M.A., Hamby, M.E. and Meyer, E.M. 2002. Dopaminergic cell loss induced by human A30P alpha-synuclein gene transfer to the rat substantia nigra. *Human Gene Therapy* 13(5), pp. 605–612.

Klokkaris, A. and Migdalska-Richards, A. 2024. An overview of epigenetic changes in the parkinson's disease brain. *International Journal of Molecular Sciences* 25(11).

Kontopoulos, E., Parvin, J.D. and Feany, M.B. 2006. Alpha-synuclein acts in the nucleus to inhibit histone acetylation and promote neurotoxicity. *Human Molecular Genetics* 15(20), pp. 3012–3023.

Kordower, J.H., Chu, Y., Hauser, R.A., Freeman, T.B. and Olanow, C.W. 2008. Lewy body-like pathology in long-term embryonic nigral transplants in Parkinson's disease. *Nature Medicine* 14(5), pp. 504–506.

Koss, D.J., Erskine, D., Porter, A., et al. 2022. Nuclear alpha-synuclein is present in the human brain and is modified in dementia with Lewy bodies. *Acta neuropathologica communications* 10(1), p. 98.

Kovacs, G.G., Wagner, U., Dumont, B., et al. 2012. An antibody with high reactivity for disease-associated α-synuclein reveals extensive brain pathology. *Acta Neuropathologica* 124(1), pp. 37–50.

Krüger, R., Kuhn, W., Müller, T., et al. 1998. Ala30Pro mutation in the gene encoding alpha-synuclein in Parkinson's disease. *Nature Genetics* 18(2), pp. 106–108.

Kumar, S.T., Jagannath, S., Francois, C., Vanderstichele, H., Stoops, E. and Lashuel, H.A. 2020. How specific are the conformation-specific α-synuclein antibodies? Characterization and validation of 16 α-synuclein conformation-specific antibodies using well-characterized preparations of α-synuclein monomers, fibrils and oligomers with distinct structures and morphology. *Neurobiology of Disease* 146, p. 105086.

Kumar, S.T., Mahul-Mellier, A.-L., Hegde, R.N., et al. 2022. A NAC domain mutation (E83Q) unlocks the pathogenicity of human alpha-synuclein and recapitulates its pathological diversity. *Science Advances* 8(17), p. eabn0044.

Lama, J., Buhidma, Y., Fletcher, E.J.R. and Duty, S. 2021. Animal models of Parkinson's disease: a guide to selecting the optimal model for your research. *Neuronal Signaling* 5(4), p. NS20210026.

Lang, A.E. and Lozano, A.M. 1998. Parkinson's disease. First of two parts. *The New England Journal of Medicine* 339(15), pp. 1044–1053.

Lang, Y., Zhang, H., Yu, H., Li, Y., Liu, X. and Li, M. 2022. Long non-coding RNA myocardial infarction-associated transcript promotes 1-Methyl-4-phenylpyridinium ion-induced neuronal inflammation and oxidative stress in Parkinson's disease through regulating microRNA-221-3p/ transforming growth factor /nuclear factor E2-related factor 2 axis. *Bioengineered* 13(1), pp. 930–940.

Lange, L.M., Gonzalez-Latapi, P., Rajalingam, R., et al. 2022. Nomenclature of Genetic Movement Disorders: Recommendations of the International Parkinson and Movement Disorder Society Task Force - An Update. *Movement Disorders* 37(5), pp. 905–935.

Langston, J.W. 2017. The MPTP Story. *Journal of Parkinson's disease* 7(s1), pp. S11–S19.

Lashuel, H.A., Mahul-Mellier, A.-L., Novello, S., et al. 2022. Revisiting the specificity and ability of phospho-S129 antibodies to capture alpha-synuclein biochemical and pathological diversity. *npj Parkinson's Disease* 8(1), p. 136.

Le Guiner, C., Stieger, K., Toromanoff, A., et al. 2014. Transgene regulation using the tetracycline-inducible TetR-KRAB system after AAV-mediated gene transfer in rodents and nonhuman primates. *Plos One* 9(9), p. e102538.

Lee, H.-J., Patel, S. and Lee, S.-J. 2005. Intravesicular localization and exocytosis of alpha-synuclein and its aggregates. *The Journal of Neuroscience* 25(25), pp. 6016–6024.

Lee, H.-J., Suk, J.-E., Bae, E.-J., Lee, J.-H., Paik, S.R. and Lee, S.-J. 2008. Assembly-dependent endocytosis and clearance of extracellular alpha-synuclein. *The International Journal of Biochemistry & Cell Biology* 40(9), pp. 1835–1849.

Lee, J.-Y., Kim, H., Jo, A., et al. 2021. α-Synuclein A53T Binds to Transcriptional Adapter 2-Alpha and Blocks Histone H3 Acetylation. *International Journal of Molecular Sciences* 22(10).

Lee, S.S., Kim, Y.M., Junn, E., et al. 2003. Cell cycle aberrations by alpha-synuclein over-expression and cyclin B immunoreactivity in Lewy bodies. *Neurobiology of Aging* 24(5), pp. 687–696.

Lehtonen, Š., Sonninen, T.-M., Wojciechowski, S., Goldsteins, G. and Koistinaho, J. 2019. Dysfunction of cellular proteostasis in parkinson's disease. *Frontiers in Neuroscience* 13, p. 457.

Lepack, A.E., Werner, C.T., Stewart, A.F., et al. 2020. Dopaminylation of histone H3 in ventral tegmental area regulates cocaine seeking. *Science* 368(6487), pp. 197–201.

Lesage, S., Anheim, M., Letournel, F., et al. 2013. G51D α-synuclein mutation causes a novel parkinsonian-pyramidal syndrome. *Annals of Neurology* 73(4), pp. 459–471.

Lesage, S. and Brice, A. 2009. Parkinson's disease: from monogenic forms to genetic susceptibility factors. *Human Molecular Genetics* 18(R1), pp. R48-59.

Leupold, L., Sigutova, V., Gerasimova, E., et al. 2022. The Quest for Anti-α-Synuclein Antibody Specificity-Lessons Learnt From Flow Cytometry Analysis. *Frontiers in neurology* 13, p. 869103.

Lewy, F. 1912. Paralysis agitans. In: Lewandowsky, M. and Abelsdorff, G. eds. *Handbuch der Neurologie*. I. Pathologische Anatomie. Springer Verlag, pp. 920–930.

Li, J.-Y., Englund, E., Holton, J.L., et al. 2008. Lewy bodies in grafted neurons in subjects with Parkinson's disease suggest host-to-graft disease propagation. *Nature Medicine* 14(5), pp. 501–503.

Li, W., Lesuisse, C., Xu, Y., Troncoso, J.C., Price, D.L. and Lee, M.K. 2004. Stabilization of alpha-synuclein protein with aging and familial parkinson's disease-linked A53T mutation. *The Journal of Neuroscience* 24(33), pp. 7400–7409.

Li, X., Li, W., Liu, G., Shen, X. and Tang, Y. 2015. Association between cigarette smoking and Parkinson's disease: A meta-analysis. *Archives of Gerontology and Geriatrics* 61(3), pp. 510–516.

Li, X., Yin, J., Cheng, C., Sun, J., Li, Z. and Wu, Y. 2005. Paraquat induces selective dopaminergic nigrostriatal degeneration in aging C57BL/6 mice. *Chinese Medical Journal* 118(16), pp. 1357–1361.

Li, Y. 2021. Modern epigenetics methods in biological research. *Methods* 187, pp. 104–113.

Li, Y., Fang, J., Zhou, Z., et al. 2020. Downregulation of lncRNA BACE1-AS improves dopamine-dependent oxidative stress in rats with Parkinson's disease by upregulating microRNA-34b-5p and downregulating BACE1. *Cell Cycle* 19(10), pp. 1158–1171.

Lin, W.-L., DeLucia, M.W. and Dickson, D.W. 2004. Alpha-synuclein immunoreactivity in neuronal nuclear inclusions and neurites in multiple system atrophy. *Neuroscience Letters* 354(2), pp. 99–102.

Lin, X., Parisiadou, L., Sgobio, C., et al. 2012. Conditional expression of Parkinson's disease-related mutant α-synuclein in the midbrain dopaminergic neurons causes progressive neurodegeneration and degradation of transcription factor nuclear receptor related 1. *The Journal of Neuroscience* 32(27), pp. 9248–9264.

Lindersson, E., Beedholm, R., Højrup, P., et al. 2004. Proteasomal inhibition by alpha-synuclein filaments and oligomers. *The Journal of Biological Chemistry* 279(13), pp. 12924–12934.

Lindström, V., Fagerqvist, T., Nordström, E., et al. 2014. Immunotherapy targeting α-synuclein protofibrils reduced pathology in (Thy-1)-h[A30P] α-synuclein mice. *Neurobiology of Disease* 69, pp. 134–143.

Liu, A.K.L., Chau, T.W., Lim, E.J., et al. 2019. Hippocampal CA2 Lewy pathology is associated with cholinergic degeneration in Parkinson's disease with cognitive decline. *Acta neuropathologica communications* 7(1), p. 61.

Liu, C., Zhao, Y., Xi, H., Jiang, J., Yu, Y. and Dong, W. 2021. The Membrane Interaction of Alpha-Synuclein. *Frontiers in Cellular Neuroscience* 15, p. 633727.

Liu, X., Lee, Y.J., Liou, L.-C., et al. 2011. Alpha-synuclein functions in the nucleus to protect against hydroxyurea-induced replication stress in yeast. *Human Molecular Genetics* 20(17), pp. 3401–3414.

Livingston, C. and Monroe-Duprey, L. 2024. A review of levodopa formulations for the treatment of parkinson's disease available in the united states. *Journal of pharmacy practice* 37(2), pp. 485–494.

Lo Bianco, C., Ridet, J.L., Schneider, B.L., Deglon, N. and Aebischer, P. 2002. alpha -Synucleinopathy and selective dopaminergic neuron loss in a rat lentiviral-based model of Parkinson's disease. *Proceedings of the National Academy of Sciences of the United States of America* 99(16), pp. 10813–10818.

Luger, K., Dechassa, M.L. and Tremethick, D.J. 2012. New insights into nucleosome and chromatin structure: an ordered state or a disordered affair? *Nature Reviews. Molecular Cell Biology* 13(7), pp. 436–447.

Luk, K.C., Kehm, V., Carroll, J., et al. 2012. Pathological α-synuclein transmission initiates Parkinson-like neurodegeneration in nontransgenic mice. *Science* 338(6109), pp. 949–953.

Luo, Y., Qiao, L., Li, M., Wen, X., Zhang, W. and Li, X. 2024. Global, regional, national epidemiology and trends of Parkinson's disease from 1990 to 2021: findings from the Global Burden of Disease Study 2021. *Frontiers in aging neuroscience* 16, p. 1498756.

Lurette, O., Martín-Jiménez, R., Khan, M., et al. 2023. Aggregation of alpha-synuclein disrupts mitochondrial metabolism and induce mitophagy via cardiolipin externalization. *Cell death & disease* 14(11), p. 729.

Ma, K.-L., Song, L.-K., Yuan, Y.-H., Zhang, Y., Han, N., et al. 2014. The nuclear accumulation of alpha-synuclein is mediated by importin alpha and promotes neurotoxicity by accelerating the cell cycle. *Neuropharmacology* 82, pp. 132–142.

Ma, K.-L., Song, L.-K., Yuan, Y.-H., Zhang, Y., Yang, J.-L., et al. 2014. α-Synuclein is prone to interaction with the GC-box-like sequence in vitro. *Cellular and Molecular Neurobiology* 34(4), pp. 603–609.

Maingay, M., Romero-Ramos, M., Carta, M. and Kirik, D. 2006. Ventral tegmental area dopamine neurons are resistant to human mutant alpha-synuclein overexpression. *Neurobiology of Disease* 23(3), pp. 522–532.

Manning-Bog, A.B., McCormack, A.L., Li, J., Uversky, V.N., Fink, A.L. and Di Monte, D.A. 2002. The herbicide paraquat causes up-regulation and aggregation of alpha-synuclein in mice: paraquat and alpha-synuclein. *The Journal of Biological Chemistry* 277(3), pp. 1641–1644.

Maroteaux, L., Campanelli, J.T. and Scheller, R.H. 1988. Synuclein: a neuron-specific protein localized to the nucleus and presynaptic nerve terminal. *The Journal of Neuroscience* 8(8), pp. 2804–2815.

Maroteaux, L. and Scheller, R.H. 1991. The rat brain synucleins; family of proteins transiently associated with neuronal membrane. *Brain research. Molecular brain research* 11(3–4), pp. 335–343.

Martinez, J., Moeller, I., Erdjument-Bromage, H., Tempst, P. and Lauring, B. 2003. Parkinson's disease-associated alpha-synuclein is a calmodulin substrate. *The Journal of Biological Chemistry* 278(19), pp. 17379–17387.

Masliah, E., Rockenstein, E., Veinbergs, I., et al. 2000. Dopaminergic loss and inclusion body formation in alpha-synuclein mice: implications for neurodegenerative disorders. *Science* 287(5456), pp. 1265–1269.

Matsumoto, L., Takuma, H., Tamaoka, A., et al. 2010. CpG demethylation enhances alpha-synuclein expression and affects the pathogenesis of Parkinson's disease. *Plos One* 5(11), p. e15522.

Maurano, M.T., Humbert, R., Rynes, E., et al. 2012. Systematic localization of common disease-associated variation in regulatory DNA. *Science* 337(6099), pp. 1190–1195.

Mazzocchi, M., Wyatt, S.L., Mercatelli, D., et al. 2019. Gene Co-expression Analysis Identifies Histone Deacetylase 5 and 9 Expression in Midbrain Dopamine Neurons and as Regulators of Neurite Growth via Bone Morphogenetic Protein Signaling. *Frontiers in cell and developmental biology* 7, p. 191.

Mazzulli, J.R., Xu, Y.-H., Sun, Y., et al. 2011. Gaucher disease glucocerebrosidase and α-synuclein form a bidirectional pathogenic loop in synucleinopathies. *Cell* 146(1), pp. 37–52.

Mazzulli, J.R., Zunke, F., Isacson, O., Studer, L. and Krainc, D. 2016. α-Synuclein-induced lysosomal dysfunction occurs through disruptions in protein trafficking in human midbrain synucleinopathy models. *Proceedings of the National Academy of Sciences of the United States of America* 113(7), pp. 1931–1936.

McFarland, N.R., Lee, J.-S., Hyman, B.T. and McLean, P.J. 2009. Comparison of transduction efficiency of recombinant AAV serotypes 1, 2, 5, and 8 in the rat nigrostriatal system. *Journal of Neurochemistry* 109(3), pp. 838–845.

McKinnon, C., De Snoo, M.L., Gondard, E., et al. 2020. Early-onset impairment of the ubiquitin-proteasome system in dopaminergic neurons caused by α-synuclein. *Acta neuropathologica communications* 8(1), p. 17.

McLean, P.J., Ribich, S. and Hyman, B.T. 2000. Subcellular localization of alpha-synuclein in primary neuronal cultures: effect of missense mutations. *Journal of Neural Transmission. Supplementum* (58), pp. 53–63.

Milanese, C., Cerri, S., Ulusoy, A., et al. 2018. Activation of the DNA damage response in vivo in synucleinopathy models of Parkinson's disease. *Cell death & disease* 9(8), p. 818.

Miller, D.W., Hague, S.M., Clarimon, J., et al. 2004. Alpha-synuclein in blood and brain from familial Parkinson disease with SNCA locus triplication. *Neurology* 62(10), pp. 1835–1838.

Miller, R.M., Kiser, G.L., Kaysser-Kranich, T., et al. 2007. Wild-type and mutant alpha-synuclein induce a multi-component gene expression profile consistent with shared pathophysiology in different transgenic mouse models of PD. *Experimental Neurology* 204(1), pp. 421–432.

Miranda-Morales, E., Meier, K., Sandoval-Carrillo, A., Salas-Pacheco, J., Vázquez-Cárdenas, P. and Arias-Carrión, O. 2017. Implications of DNA methylation in parkinson's disease. *Frontiers in Molecular Neuroscience* 10, p. 225.

Monti, B., Gatta, V., Piretti, F., Raffaelli, S.S., Virgili, M. and Contestabile, A. 2010. Valproic acid is neuroprotective in the rotenone rat model of Parkinson's disease: involvement of alpha-synuclein. *Neurotoxicity Research* 17(2), pp. 130–141.

Monti, B., Polazzi, E., Batti, L., Crochemore, C., Virgili, M. and Contestabile, A. 2007. Alpha-synuclein protects cerebellar granule neurons against 6-hydroxydopamine-induced death. *Journal of Neurochemistry* 103(2), pp. 518–530.

Mosharov, E.V., Larsen, K.E., Kanter, E., et al. 2009. Interplay between cytosolic dopamine, calcium, and alpha-synuclein causes selective death of substantia nigra neurons. *Neuron* 62(2), pp. 218–229.

Murata, H., Barnhill, L.M. and Bronstein, J.M. 2022. Air pollution and the risk of parkinson's disease: A review. *Movement Disorders* 37(5), pp. 894–904.

Musgrove, R.E., Helwig, M., Bae, E.-J., et al. 2019. Oxidative stress in vagal neurons promotes parkinsonian pathology and intercellular α-synuclein transfer. *The Journal of Clinical Investigation* 129(9), pp. 3738–3753.

Nalls, M.A., Blauwendraat, C., Vallerga, C.L., et al. 2019. Identification of novel risk loci, causal insights, and heritable risk for Parkinson's disease: a meta-analysis of genome-wide association studies. *Lancet Neurology* 18(12), pp. 1091–1102.

Nemani, V.M., Lu, W., Berge, V., et al. 2010. Increased expression of alpha-synuclein reduces neurotransmitter release by inhibiting synaptic vesicle reclustering after endocytosis. *Neuron* 65(1), pp. 66–79.

Nielsen, M.S., Vorum, H., Lindersson, E. and Jensen, P.H. 2001. Ca2+ binding to alpha-synuclein regulates ligand binding and oligomerization. *The Journal of Biological Chemistry* 276(25), pp. 22680–22684.

Nishie, M., Mori, F., Yoshimoto, M., Takahashi, H. and Wakabayashi, K. 2004. A quantitative investigation of neuronal cytoplasmic and intranuclear inclusions in the pontine and inferior olivary nuclei in multiple system atrophy. *Neuropathology and Applied Neurobiology* 30(5), pp. 546–554.

Nitsch, S., Zorro Shahidian, L. and Schneider, R. 2021. Histone acylations and chromatin dynamics: concepts, challenges, and links to metabolism. *EMBO Reports* 22(7), p. e52774.

Nonnekes, J., Post, B., Tetrud, J.W., Langston, J.W. and Bloem, B.R. 2018. MPTP-induced parkinsonism: an historical case series. *Lancet Neurology* 17(4), pp. 300–301.

Oaks, A.W., Marsh-Armstrong, N., Jones, J.M., Credle, J.J. and Sidhu, A. 2013. Synucleins antagonize endoplasmic reticulum function to modulate dopamine transporter trafficking. *Plos One* 8(8), p. e70872.

Oueslati, A., Fournier, M. and Lashuel, H.A. 2010. Role of post-translational modifications in modulating the structure, function and toxicity of α-synuclein. In: *Recent advances in parkinson's disease: basic research*. Progress in brain research. Elsevier, pp. 115–145.

Padmaraju, V., Bhaskar, J.J., Prasada Rao, U.J.S., Salimath, P.V. and Rao, K.S. 2011. Role of advanced glycation on aggregation and DNA binding properties of α-synuclein. *Journal of Alzheimer's Disease* 24 Suppl 2, pp. 211–221.

Paiva, I., Jain, G., Lázaro, D.F., et al. 2018. Alpha-synuclein deregulates the expression of COL4A2 and impairs ER-Golgi function. *Neurobiology of Disease* 119, pp. 121–135.

Paiva, I., Pinho, R., Pavlou, M.A., et al. 2017. Sodium butyrate rescues dopaminergic cells from alpha-synuclein-induced transcriptional deregulation and DNA damage. *Human Molecular Genetics* 26(12), pp. 2231–2246.

Panicker, N., Ge, P., Dawson, V.L. and Dawson, T.M. 2021. The cell biology of Parkinson's disease. *The Journal of Cell Biology* 220(4).

Parihar, M.S., Parihar, A., Fujita, M., Hashimoto, M. and Ghafourifar, P. 2009. Alpha-synuclein overexpression and aggregation exacerbates impairment of mitochondrial functions by augmenting oxidative stress in human neuroblastoma cells. *The International Journal of Biochemistry & Cell Biology* 41(10), pp. 2015–2024.

Park, G., Tan, J., Garcia, G., Kang, Y., Salvesen, G. and Zhang, Z. 2016. Regulation of histone acetylation by autophagy in parkinson disease. *The Journal of Biological Chemistry* 291(7), pp. 3531–3540.

Park, J., Lee, K., Kim, K. and Yi, S.-J. 2022. The role of histone modifications: from neurodevelopment to neurodiseases. *Signal transduction and targeted therapy* 7(1), p. 217.

Parkinson, J. 2002. An essay on the shaking palsy. 1817. *The Journal of Neuropsychiatry and Clinical Neurosciences* 14(2), p. 223–36; discussion 222.

Pasanen, P., Myllykangas, L., Siitonen, M., et al. 2014. Novel α-synuclein mutation A53E associated with atypical multiple system atrophy and Parkinson's disease-type pathology. *Neurobiology of Aging* 35(9), p. 2180.e1-5.

Pavlou, M.A.S. and Outeiro, T.F. 2017. Epigenetics in parkinson's disease. *Advances in Experimental Medicine and Biology* 978, pp. 363–390.

Peelaerts, W., Bousset, L., Van der Perren, A., et al. 2015. α-Synuclein strains cause distinct synucleinopathies after local and systemic administration. *Nature* 522(7556), pp. 340–344.

Pellicano, C., Benincasa, D., Pisani, V., Buttarelli, F.R., Giovannelli, M. and Pontieri, F.E. 2007. Prodromal non-motor symptoms of Parkinson's disease. *Neuropsychiatric Disease and Treatment* 3(1), pp. 145–152.

Perrin, R.J., Payton, J.E., Barnett, D.H., et al. 2003. Epitope mapping and specificity of the anti-alpha-synuclein monoclonal antibody Syn-1 in mouse brain and cultured cell lines. *Neuroscience Letters* 349(2), pp. 133–135.

Petersen, I., Ali, M.I., Petrovic, A., et al. 2023. Multivalent design of the monoclonal SynO2 antibody improves binding strength to soluble α-Synuclein aggregates. *MAbs* 15(1), p. 2256668.

Phan, J.-A., Stokholm, K., Zareba-Paslawska, J., et al. 2017. Early synaptic dysfunction induced by α-synuclein in a rat model of Parkinson's disease. *Scientific Reports* 7(1), p. 6363.

Pichard, V., Aubert, D., Boni, S., et al. 2012. Specific micro RNA-regulated TetR-KRAB transcriptional control of transgene expression in viral vector-transduced cells. *Plos One* 7(12), p. e51952.

Pieger, K., Schmitt, V., Gauer, C., et al. 2022. Translocation of Distinct Alpha Synuclein Species from the Nucleus to Neuronal Processes during Neuronal Differentiation. *Biomolecules* 12(8).

Pinho, R., Guedes, L.C., Soreq, L., et al. 2016. Gene Expression Differences in Peripheral Blood of Parkinson's Disease Patients with Distinct Progression Profiles. *Plos One* 11(6), p. e0157852.

Pinho, R., Paiva, I., Jercic, K.G., et al. 2019. Nuclear localization and phosphorylation modulate pathological effects of alpha-synuclein. *Human Molecular Genetics* 28(1), pp. 31–50.

Pissadaki, E.K. and Bolam, J.P. 2013. The energy cost of action potential propagation in dopamine neurons: clues to susceptibility in Parkinson's disease. *Frontiers in Computational Neuroscience* 7, p. 13.

Pitz, V., Makarious, M.B., Bandres-Ciga, S., et al. 2024. Analysis of rare Parkinson's disease variants in millions of people. *npj Parkinson's Disease* 10(1), p. 11.

Poewe, W., Seppi, K., Tanner, C.M., et al. 2017. Parkinson disease. *Nature reviews. Disease primers* 3, p. 17013.

Polymeropoulos, M.H., Lavedan, C., Leroy, E., et al. 1997. Mutation in the alpha-synuclein gene identified in families with Parkinson's disease. *Science* 276(5321), pp. 2045–2047.

Popova, B., Wang, D., Pätz, C., et al. 2021. DEAD-box RNA helicase Dbp4/DDX10 is an enhancer of α-synuclein toxicity and oligomerization. *PLoS Genetics* 17(3), p. e1009407.

Qamhawi, Z., Towey, D., Shah, B., et al. 2015. Clinical correlates of raphe serotonergic dysfunction in early Parkinson's disease. *Brain: A Journal of Neurology* 138(Pt 10), pp. 2964–2973.

Ramalingam, N. and Dettmer, U. 2021. Temperature is a key determinant of alpha- and beta-synuclein membrane interactions in neurons. *The Journal of Biological Chemistry* 296, p. 100271.

Recasens, A., Dehay, B., Bové, J., et al. 2014. Lewy body extracts from Parkinson disease brains trigger α-synuclein pathology and neurodegeneration in mice and monkeys. *Annals of Neurology* 75(3), pp. 351–362.

Ritz, B., Ascherio, A., Checkoway, H., et al. 2007. Pooled analysis of tobacco use and risk of Parkinson disease. *Archives of Neurology* 64(7), pp. 990–997.

Roberts, R.F., Wade-Martins, R. and Alegre-Abarrategui, J. 2015. Direct visualization of alpha-synuclein oligomers reveals previously undetected pathology in Parkinson's disease brain. *Brain: A Journal of Neurology* 138(Pt 6), pp. 1642–1657.

Roney, I.J., Rudner, A.D., Couture, J.-F. and Kærn, M. 2016. Improvement of the reverse tetracycline transactivator by single amino acid substitutions that reduce leaky target gene expression to undetectable levels. *Scientific Reports* 6, p. 27697.

Rousseaux, M.W., de Haro, M., Lasagna-Reeves, C.A., et al. 2016. TRIM28 regulates the nuclear accumulation and toxicity of both alpha-synuclein and tau. *eLife* 5.

Rutherford, N.J., Brooks, M. and Giasson, B.I. 2016. Novel antibodies to phosphorylated α-synuclein serine 129 and NFL serine 473 demonstrate the close molecular homology of these epitopes. *Acta neuropathologica communications* 4(1), p. 80.

Ryan, E., Seehra, G., Sharma, P. and Sidransky, E. 2019. GBA1-associated parkinsonism: new insights and therapeutic opportunities. *Current Opinion in Neurology* 32(4), pp. 589–596.

Ryu, S., Baek, I. and Liew, H. 2019. Sumoylated α-synuclein translocates into the nucleus by karyopherin α6. *Molecular & Cellular Toxicology* 15(1), pp. 103–109.

Sangchot, P., Sharma, S., Chetsawang, B., Porter, J., Govitrapong, P. and Ebadi, M. 2002. Deferoxamine attenuates iron-induced oxidative stress and prevents mitochondrial aggregation and alpha-synuclein translocation in SK-N-SH cells in culture. *Developmental Neuroscience* 24(2–3), pp. 143–153.

Savica, R., Rocca, W.A. and Ahlskog, J.E. 2010. When does Parkinson disease start? *Archives of Neurology* 67(7), pp. 798–801.

Schaffner, S.L. and Kobor, M.S. 2022. DNA methylation as a mediator of genetic and environmental influences on Parkinson's disease susceptibility: Impacts of alpha-Synuclein, physical activity, and pesticide exposure on the epigenome. *Frontiers in genetics* 13, p. 971298.

Schaffner, S.L., Wassouf, Z., Hentrich, T., Nuesch-Germano, M., Kobor, M.S. and Schulze-Hentrich, J.M. 2023. Distinct impacts of alpha-synuclein overexpression on the hippocampal epigenome of mice in standard and enriched environments. *Neurobiology of Disease* 186, p. 106274.

Schaser, A.J., Osterberg, V.R., Dent, S.E., et al. 2019. Alpha-synuclein is a DNA binding protein that modulates DNA repair with implications for Lewy body disorders. *Scientific Reports* 9(1), p. 10919.

Scheiblich, H., Eikens, F., Wischhof, L., et al. 2024. Microglia rescue neurons from aggregate-induced neuronal dysfunction and death through tunneling nanotubes. *Neuron* 112(18), p. 3106–3125.e8.

Schell, H., Hasegawa, T., Neumann, M. and Kahle, P.J. 2009. Nuclear and neuritic distribution of serine-129 phosphorylated alpha-synuclein in transgenic mice. *Neuroscience* 160(4), pp. 796–804.

Schneider, B.L., Seehus, C.R., Capowski, E.E., Aebischer, P., Zhang, S.-C. and Svendsen, C.N. 2007. Over-expression of alpha-synuclein in human neural progenitors leads to specific changes in fate and differentiation. *Human Molecular Genetics* 16(6), pp. 651–666.

Sekiya, H., Tsuji, A., Hashimoto, Y., et al. 2022. Discrepancy between distribution of alpha-synuclein oligomers and Lewy-related pathology in Parkinson's disease. *Acta neuropathologica communications* 10(1), p. 133.

Sevcsik, E., Trexler, A.J., Dunn, J.M. and Rhoades, E. 2011. Allostery in a disordered protein: oxidative modifications to α-synuclein act distally to regulate membrane binding. *Journal of the American Chemical Society* 133(18), pp. 7152–7158.

Shahi, G.S., Das, N.P. and Moochhala, S.M. 1991. 1-Methyl-4-phenyl-1,2,3,6-tetrahydropyridine-induced neurotoxicity: partial protection against striato-nigral dopamine depletion in C57BL/6J mice by cigarette smoke exposure and by β-naphthoflavone-pretreatment. *Neuroscience Letters* 127(2), pp. 247–250.

Shahmoradian, S.H., Lewis, A.J., Genoud, C., et al. 2019. Lewy pathology in Parkinson's disease consists of crowded organelles and lipid membranes. *Nature Neuroscience* 22(7), pp. 1099–1109.

Sharma, R., Bisht, P., Kesharwani, A., Murti, K. and Kumar, N. 2024. Epigenetic modifications in Parkinson's disease: A critical review. *European Journal of Pharmacology* 975, p. 176641.

Sherer, T.B., Kim, J.H., Betarbet, R. and Greenamyre, J.T. 2003. Subcutaneous rotenone exposure causes highly selective dopaminergic degeneration and alpha-synuclein aggregation. *Experimental Neurology* 179(1), pp. 9–16.

Shi, X., Sun, Y., Wang, P., et al. 2018. The interaction between calcineurin and α-synuclein is regulated by calcium and calmodulin. *Biochemical and Biophysical Research Communications* 496(4), pp. 1109–1114.

Shibayama-Imazu, T., Okahashi, I., Omata, K., et al. 1993. Cell and tissue distribution and developmental change of neuron specific 14 kDa protein (phosphoneuroprotein 14). *Brain Research* 622(1–2), pp. 17–25.

Shimura, H., Schlossmacher, M.G., Hattori, N., et al. 2001. Ubiquitination of a new form of alpha-synuclein by parkin from human brain: implications for Parkinson's disease. *Science* 293(5528), pp. 263–269.

Siddiqui, A., Chinta, S.J., Mallajosyula, J.K., et al. 2012. Selective binding of nuclear alpha-synuclein to the PGC1alpha promoter under conditions of oxidative stress may contribute to losses in mitochondrial function: implications for Parkinson's disease. *Free Radical Biology & Medicine* 53(4), pp. 993–1003.

Singleton, A.B., Farrer, M., Johnson, J., et al. 2003. alpha-Synuclein locus triplication causes Parkinson's disease. *Science* 302(5646), p. 841.

Snyder, H., Mensah, K., Theisler, C., Lee, J., Matouschek, A. and Wolozin, B. 2003. Aggregated and monomeric alpha-synuclein bind to the S6' proteasomal protein and inhibit proteasomal function. *The Journal of Biological Chemistry* 278(14), pp. 11753–11759.

Sohn, J., Takahashi, M., Okamoto, S., Ishida, Y., Furuta, T. and Hioki, H. 2017. A Single Vector Platform for High-Level Gene Transduction of Central Neurons: Adeno-Associated Virus Vector Equipped with the Tet-Off System. *Plos One* 12(1), p. e0169611.

de Solis, C.A., Ho, A., Holehonnur, R. and Ploski, J.E. 2016. The Development of a Viral Mediated CRISPR/Cas9 System with Doxycycline Dependent gRNA Expression for Inducible In vitro and In vivo Genome Editing. *Frontiers in Molecular Neuroscience* 9, p. 70.

Somayaji, M., Lanseur, Z., Choi, S.J., Sulzer, D. and Mosharov, E.V. 2021. Roles for α-Synuclein in Gene Expression. *Genes* 12(8).

Song, H., Chen, J., Huang, J., et al. 2023. Epigenetic modification in Parkinson's disease. *Frontiers in cell and developmental biology* 11, p. 1123621.

Soreq, L., Ben-Shaul, Y., Israel, Z., Bergman, H. and Soreq, H. 2012. Meta-analysis of genetic and environmental Parkinson's disease models reveals a common role of mitochondrial protection pathways. *Neurobiology of Disease* 45(3), pp. 1018–1030.

Specht, C.G., Tigaret, C.M., Rast, G.F., Thalhammer, A., Rudhard, Y. and Schoepfer, R. 2005. Subcellular localisation of recombinant alpha- and gamma-synuclein. *Molecular and Cellular Neurosciences* 28(2), pp. 326–334.

Spillantini, M.G., Schmidt, M.L., Lee, V.M., Trojanowski, J.Q., Jakes, R. and Goedert, M. 1997. Alpha-synuclein in Lewy bodies. *Nature* 388(6645), pp. 839–840.

Stefanis, L., Emmanouilidou, E., Pantazopoulou, M., Kirik, D., Vekrellis, K. and Tofaris, G.K. 2019. How is alpha-synuclein cleared from the cell? *Journal of Neurochemistry* 150(5), pp. 577–590.

Stephens, A.D., Zacharopoulou, M. and Kaminski Schierle, G.S. 2019. The Cellular Environment Affects Monomeric α-Synuclein Structure. *Trends in Biochemical Sciences* 44(5), pp. 453–466.

Sugeno, N., Jäckel, S., Voigt, A., Wassouf, Z., Schulze-Hentrich, J. and Kahle, P.J. 2016. α-Synuclein enhances histone H3 lysine-9 dimethylation and H3K9me2-dependent transcriptional responses. *Scientific Reports* 6, p. 36328.

Sulzer, D. and Surmeier, D.J. 2013. Neuronal vulnerability, pathogenesis, and Parkinson's disease. *Movement Disorders* 28(6), pp. 715–724.

Sung, J.Y., Kim, J., Paik, S.R., Park, J.H., Ahn, Y.S. and Chung, K.C. 2001. Induction of neuronal cell death by Rab5A-dependent endocytosis of alpha-synuclein. *The Journal of Biological Chemistry* 276(29), pp. 27441–27448.

Surgucheva, I., He, S., Rich, M.C., et al. 2014. Role of synucleins in traumatic brain injury — an experimental in vitro and in vivo study in mice. *Molecular and Cellular Neurosciences* 63, pp. 114–123.

Surmeier, D.J., Guzman, J.N., Sanchez-Padilla, J. and Schumacker, P.T. 2011. The role of calcium and mitochondrial oxidant stress in the loss of substantia nigra pars compacta dopaminergic neurons in Parkinson's disease. *Neuroscience* 198, pp. 221–231.

Szegő, É.M., Höfs, L., Antoniou, A., et al. 2025. Intermittent fasting reduces alpha-synuclein pathology and functional decline in a mouse model of Parkinson's disease. *Nature Communications* 16(1), p. 4470.

Tagliafierro, L., Zamora, M.E. and Chiba-Falek, O. 2019. Multiplication of the SNCA locus exacerbates neuronal nuclear aging. *Human Molecular Genetics* 28(3), pp. 407–421.

Taguchi, K., Watanabe, Y., Tsujimura, A. and Tanaka, M. 2016. Brain region-dependent differential expression of alpha-synuclein. *The Journal of Comparative Neurology* 524(6), pp. 1236–1258.

Tanik, S.A., Schultheiss, C.E., Volpicelli-Daley, L.A., Brunden, K.R. and Lee, V.M.Y. 2013. Lewy body-like α-synuclein aggregates resist degradation and impair macroautophagy. *The Journal of Biological Chemistry* 288(21), pp. 15194–15210.

Tanner, C.M., Kamel, F., Ross, G.W., et al. 2011. Rotenone, paraquat, and Parkinson's disease. *Environmental Health Perspectives* 119(6), pp. 866–872.

Timney, B.L., Raveh, B., Mironska, R., et al. 2016. Simple rules for passive diffusion through the nuclear pore complex. *The Journal of Cell Biology* 215(1), pp. 57–76.

Toker, L., Tran, G.T., Sundaresan, J., et al. 2021. Genome-wide histone acetylation analysis reveals altered transcriptional regulation in the Parkinson's disease brain. *Molecular Neurodegeneration* 16(1), p. 31.

Tong, T., Duan, W., Xu, Y., et al. 2022. Paraquat exposure induces Parkinsonism by altering lipid profile and evoking neuroinflammation in the midbrain. *Environment International* 169, p. 107512.

Tretiakoff, C. 1919. Con-tribution a l'Etude de L'Anatomie pathologique du Locus Ni-ger de Soemmering avec quelques de´ductions relatives a` lapathoge´nie des troubles du tonus musculaire et De La Maladiede Parkinson. *These de Paris*.

Tuttle, M.D., Comellas, G., Nieuwkoop, A.J., et al. 2016. Solid-state NMR structure of a pathogenic fibril of full-length human α-synuclein. *Nature Structural & Molecular Biology* 23(5), pp. 409–415.

Ulmer, T.S., Bax, A., Cole, N.B. and Nussbaum, R.L. 2005. Structure and dynamics of micelle-bound human alpha-synuclein. *The Journal of Biological Chemistry* 280(10), pp. 9595–9603.

Ulusoy, A., Febbraro, F., Jensen, P.H., Kirik, D. and Romero-Ramos, M. 2010. Co-expression of C-terminal truncated alpha-synuclein enhances full-length alpha-synuclein-induced pathology. *The European Journal of Neuroscience* 32(3), pp. 409–422.

Ulusoy, A., Phillips, R.J., Helwig, M., Klinkenberg, M., Powley, T.L. and Di Monte, D.A. 2017. Brain-to-stomach transfer of α-synuclein via vagal preganglionic projections. *Acta Neuropathologica* 133(3), pp. 381–393.

Ulusoy, A., Rusconi, R., Pérez-Revuelta, B.I., et al. 2013. Caudo-rostral brain spreading of α-synuclein through vagal connections. *EMBO Molecular Medicine* 5(7), pp. 1119–1127.

Ungerstedt, U., Ljungberg, T. and Steg, G. 1974. Behavioral, physiological, and neurochemical changes after 6-hydroxydopamine-induced degeneration of the nigro-striatal dopamine neurons. *Advances in neurology* 5, pp. 421–426.

Uryu, K., Giasson, B.I., Longhi, L., et al. 2003. Age-dependent synuclein pathology following traumatic brain injury in mice. *Experimental Neurology* 184(1), pp. 214–224.

Usenovic, M., Tresse, E., Mazzulli, J.R., Taylor, J.P. and Krainc, D. 2012. Deficiency of ATP13A2 leads to lysosomal dysfunction, α-synuclein accumulation, and neurotoxicity. *The Journal of Neuroscience* 32(12), pp. 4240–4246.

Utton, M.A., Noble, W.J., Hill, J.E., Anderton, B.H. and Hanger, D.P. 2005. Molecular motors implicated in the axonal transport of tau and alpha-synuclein. *Journal of Cell Science* 118(Pt 20), pp. 4645–4654.

Uversky, V.N., Li, J. and Fink, A.L. 2001. Pesticides directly accelerate the rate of alpha-synuclein fibril formation: a possible factor in Parkinson's disease. *FEBS Letters* 500(3), pp. 105–108.

Vaikath, N.N., Majbour, N.K., Paleologou, K.E., et al. 2015. Generation and characterization of novel conformation-specific monoclonal antibodies for α-synuclein pathology. *Neurobiology of Disease* 79, pp. 81–99.

Van der Perren, A., Toelen, J., Carlon, M., et al. 2011. Efficient and stable transduction of dopaminergic neurons in rat substantia nigra by rAAV 2/1, 2/2, 2/5, 2/6.2, 2/7, 2/8 and 2/9. *Gene Therapy* 18(5), pp. 517–527.

Van der Perren, A., Van den Haute, C. and Baekelandt, V. 2015. Viral vector-based models of Parkinson's disease. *Current topics in behavioral neurosciences* 22, pp. 271–301.

Varkey, J., Isas, J.M., Mizuno, N., et al. 2010. Membrane curvature induction and tubulation are common features of synucleins and apolipoproteins. *The Journal of Biological Chemistry* 285(42), pp. 32486–32493.

Vasquez, V., Mitra, J., Hegde, P.M., et al. 2017. Chromatin-Bound Oxidized α-Synuclein Causes Strand Breaks in Neuronal Genomes in in vitro Models of Parkinson's Disease. *Journal of Alzheimer's Disease* 60(s1), pp. S133–S150.

Vasudevaraju, P., Guerrero, E., Hegde, M.L., Collen, T.B., Britton, G.B. and Rao, K.S. 2012. New evidence on α-synuclein and Tau binding to conformation and sequence specific GC* rich DNA: Relevance to neurological disorders. *Journal of pharmacy & bioallied sciences* 4(2), pp. 112–117.

Vila, M., Vukosavic, S., Jackson-Lewis, V., Neystat, M., Jakowec, M. and Przedborski, S. 2000. Alpha-synuclein up-regulation in substantia nigra dopaminergic neurons following administration of the parkinsonian toxin MPTP. *Journal of Neurochemistry* 74(2), pp. 721–729.

Villar-Piqué, A., Lopes da Fonseca, T. and Outeiro, T.F. 2016. Structure, function and toxicity of alpha-synuclein: the Bermuda triangle in synucleinopathies. *Journal of Neurochemistry* 139 Suppl 1, pp. 240–255.

Villar-Piqué, A., Lopes da Fonseca, T., Sant'Anna, R., et al. 2016. Environmental and genetic factors support the dissociation between α-synuclein aggregation and toxicity. *Proceedings of the National Academy of Sciences of the United States of America* 113(42), pp. E6506–E6515.

Vivacqua, G., Casini, A., Vaccaro, R., Fornai, F., Yu, S. and D'Este, L. 2011. Different sub-cellular localization of alpha-synuclein in the C57BL\6J mouse's central nervous system by two novel monoclonal antibodies. *Journal of chemical neuroanatomy* 41(2), pp. 97–110.

Volles, M.J. and Lansbury, P.T. 2002. Vesicle permeabilization by protofibrillar alpha-synuclein is sensitive to Parkinson's disease-linked mutations and occurs by a pore-like mechanism. *Biochemistry* 41(14), pp. 4595–4602.

Volpicelli-Daley, L.A., Gamble, K.L., Schultheiss, C.E., Riddle, D.M., West, A.B. and Lee, V.M.-Y. 2014. Formation of α-synuclein Lewy neurite-like aggregates in axons impedes the transport of distinct endosomes. *Molecular Biology of the Cell* 25(25), pp. 4010–4023.

Wakabayashi, K. and Takahashi, H. 1997. Neuropathology of autonomic nervous system in Parkinson's disease. *European Neurology* 38 Suppl 2, pp. 2–7.

Wakamatsu, M., Ishii, A., Ukai, Y., et al. 2007. Accumulation of phosphorylated alpha-synuclein in dopaminergic neurons of transgenic mice that express human alpha-synuclein. *Journal of Neuroscience Research* 85(8), pp. 1819–1825.

Waxman, E.A., Duda, J.E. and Giasson, B.I. 2008. Characterization of antibodies that selectively detect alpha-synuclein in pathological inclusions. *Acta Neuropathologica* 116(1), pp. 37–46.

Weinreb, P.H., Zhen, W., Poon, A.W., Conway, K.A. and Lansbury, P.T. 1996. NACP, a protein implicated in Alzheimer's disease and learning, is natively unfolded. *Biochemistry* 35(43), pp. 13709–13715.

Whone, A.L., Watts, R.L., Stoessl, A.J., et al. 2003. Slower progression of Parkinson's disease with ropinirole versus levodopa: The REAL-PET study. *Annals of Neurology* 54(1), pp. 93–101.

Winner, B., Jappelli, R., Maji, S.K., et al. 2011. In vivo demonstration that alpha-synuclein oligomers are toxic. *Proceedings of the National Academy of Sciences of the United States of America* 108(10), pp. 4194–4199.

Winslow, A.R., Chen, C.-W., Corrochano, S., et al. 2010. α-Synuclein impairs macroautophagy: implications for Parkinson's disease. *The Journal of Cell Biology* 190(6), pp. 1023–1037.

Wiseman, J.A., Murray, H.C., Faull, R.L.M.F., et al. 2024. Aggregate-prone brain regions in Parkinson's disease are rich in unique N-terminus α-synuclein conformers with high proteolysis susceptibility. *npj Parkinson's Disease* 10(1), p. 1.

Xilouri, M., Brekk, O.R. and Stefanis, L. 2016. Autophagy and Alpha-Synuclein: Relevance to Parkinson's Disease and Related Synucleopathies. *Movement Disorders* 31(2), pp. 178–192.

Yacoubian, T.A., Cantuti-Castelvetri, I., Bouzou, B., et al. 2008. Transcriptional dysregulation in a transgenic model of Parkinson disease. *Neurobiology of Disease* 29(3), pp. 515–528.

Yakunin, E., Kisos, H., Kulik, W., Grigoletto, J., Wanders, R.J.A. and Sharon, R. 2014. The regulation of catalase activity by PPAR γ is affected by α-synuclein. *Annals of clinical and translational neurology* 1(3), pp. 145–159.

Yang, Y.X. and Latchman, D.S. 2008. Nurr1 transcriptionally regulates the expression of alpha-synuclein. *Neuroreport* 19(8), pp. 867–871.

Yu, S., Li, X., Liu, G., et al. 2007. Extensive nuclear localization of alpha-synuclein in normal rat brain neurons revealed by a novel monoclonal antibody. *Neuroscience* 145(2), pp. 539–555.

Zarranz, J.J., Alegre, J., Gómez-Esteban, J.C., et al. 2004. The new mutation, E46K, of alpha-synuclein causes Parkinson and Lewy body dementia. *Annals of Neurology* 55(2), pp. 164–173.

Zhang, F., Wang, F., Li, C.-H., et al. 2022. Therapeutic effects of subthalamic nucleus deep brain stimulation on anxiety and depression in Parkinson's disease patients. *Journal of Neurorestoratology* 10(1), pp. 31–42.

Zhang, L., Zhang, C., Zhu, Y., et al. 2008. Semi-quantitative analysis of alpha-synuclein in subcellular pools of rat brain neurons: an immunogold electron microscopic study using a C-terminal specific monoclonal antibody. *Brain Research* 1244, pp. 40–52.

Zhang, Z. and Cheng, Y. 2014. miR-16-1 promotes the aberrant α-synuclein accumulation in parkinson disease via targeting heat shock protein 70. *Thescientificworldjournal* 2014, p. 938348.

Zhong, S., Luo, X., Chen, Xing-shu, et al. 2010. Expression and subcellular location of alpha-synuclein during mouse-embryonic development. *Cellular and Molecular Neurobiology* 30(3), pp. 469–482.

9. Statement on own contribution

The work presented in this thesis was carried out at the German Center for Neurodegenerative Diseases (DZNE) under the supervision of Prof. Dr. Donato Di Monte. The overall research question was developed by Prof. Dr. Donato Di Monte and further refined by me in consultation with him. Experimental planning was carried out by me in collaboration with Prof. Dr. Di Monte.

Unless stated otherwise below, all experiments described in this thesis were performed by me. This includes animal procedures, tissue collection and processing, histological and biochemical analyses, microscopy, image acquisition, image analysis, data processing, and data visualization. Perfusions and tissue processing were performed by me, in some cases with technical assistance from members of the laboratory.

Specific parts of the experimental work and analyses were conducted by members of the Di Monte Lab as follows: In the first experiment, stereological quantification of dopaminergic neurons was performed by Priv.-Doz. Dr. Ayse Ulusoy. Animal procedures, tissue collection and processing, staining, data integration, and interpretation of these data in the context of the thesis were carried out by me.

For the co-immunoprecipitation experiments, I performed the animal procedures and collected the tissue. Co-immunoprecipitation assays and the subsequent Western blot analyses were performed by Dr. Eva Szegö. These experiments were used to validate the interaction between histones and α-synuclein. Processing and presentation of the resulting Western blot data, as well as their interpretation in the context of the thesis, were carried out by me.

The animal cohort used for the quadruple staining experiments was initiated by Priv.-Doz. Dr. Ayse Ulusoy and Shirley So-Ling Lee. I contributed to tissue collection and tissue processing. Quadruple staining and fluorescence imaging were performed by Shirley So-Ling Lee. These data were used to assess alterations in histone marks. Further processing, statistical analysis, and interpretation of these data in the context of the thesis were carried out by me.

Statistical analyses, where applicable, were performed by me independently. The interpretation of the results and the preparation of the thesis manuscript were carried out by me under the supervision of Prof. Dr. Di Monte.

In preparing this work, I used ChatGPT to improve language clarity, readability, and phrasing. After using this tool, I reviewed and edited the relevant passages and take full responsibility for the content of the published dissertation.
I confirm that I have written this thesis independently and have not used any sources or aids other than those specified by me.
I hereby confirm that my thesis complies with the Statement by the Executive Committee of the Deutsche Forschungsgemeinschaft (DFG, German Research Foundation) on the Influence of Generative Models of Text and Image Creation on Science and the Humanities and on the DFG's Funding Activities.

10. Acknowledgements

First and foremost, I want to express my deepest gratitude to my supervisor and PI, Dino, Prof. Dr. Donato Di Monte, for providing me the opportunity to pursue my PhD and for his unwavering support and guidance throughout this journey.

I am sincerely grateful to my thesis committee members, Priv.-Doz. Dr. Dan Ehninger, Prof. Dr. Harald Neumann, and Prof. Dr. Ina Vorberg, for their valuable time, expertise, and constructive feedback during the TAC meetings throughout my PhD.

And to all the current and former members of the Di Monte lab, thank you for our collaborative work, research discussions, feedback, and suggestions that have enriched my research experience. A special thanks goes Laura, Shirley, Anushka, Camilla, and Zoe, who assisted me with the labor-intensive animal and tissue work - without your help, I could never have managed the workload. I would like to extend my heartfelt appreciation to Ayse and Sinéad, who, as senior scientists throughout nearly all of my time in the lab, provided mentoring and advice on both scientific matters and other areas. To Laura and Shirley, thank you for teaching me and for our joint learning about what it means to organize a lab, refine experimental procedures, and achieve effective teamwork. I am indebted to Ayse, Michael H., Michael K., Céline, Helia, and Ben for teaching me the procedures and skills I have extensively used during my project. My sincere thanks to Bettina, Bianca, Yvonne, and Katherina for their support in navigating the complex landscape of German bureaucracy.

I would also like to express my gratitude to those who shaped my path to neuroscience during my earlier academic journey. I thank Prof. Dr. Yanai for hosting me in his laboratory, and Prof. Dr. Yoshikawa, Prof. Dr. Nakamura, and Dr. Naganuma for their supervision during that time. I also greatly appreciate Prof. Dr. Steinbusch and the whole organizing team of the EURON Neuroscience double master's program for this excellent opportunity. I am particularly grateful to my first research host lab, where I became excited about collaborative neuroscientific research: thanks to Prof. Dr. Bert Joosten, Dr. Nynke van den Hooge, and the entire team. Many thanks to my high-school biology teacher, Marc Brandenburg, who laid a solid foundation and first inspired me to pursue this path.

Finally, I would like to thank my family and friends for their unwavering support, patience, and encouragement throughout my academic journey.

11. Curriculum vitae

Publications

La Vitola, P., Szegö, E. M., Pinto-Costa, R., **Rollar, A.**, Harbachova, E., Schapira, A. H., Ulusoy, A., & Di Monte, D. A. (2024). Mitochondrial oxidant stress promotes α-synuclein aggregation and spreading in mice with mutated glucocerebrosidase. *NPJ Parkinson's disease*, *10*(1), 233. https://doi.org/10.1038/s41531-024-00842-8

Klinkenberg, M., Helwig, M., Pinto-Costa, R., **Rollar, A.**, Rusconi, R., Di Monte, D. A., & Ulusoy, A. (2023). Interneuronal In Vivo Transfer of Synaptic Proteins. *Cells*, *12*(4), 569. https://doi.org/10.3390/cells12040569

Helwig, M., Ulusoy, A., **Rollar, A.**, O'Sullivan, S. A., Lee, S. S. L., Aboutalebi, H., Pinto-Costa, R., Jevans, B., Klinkenberg, M., & Di Monte, D. A. (2022). Neuronal hyperactivity-induced oxidant stress promotes in vivo α-synuclein brain spreading. Science advances, 8(35), eabn0356. https://doi.org/10.1126/sciadv.abn0356